Naval Research Laboratory
Monterey, CA 93943-5006

NRL/FR/7541-92-9403

A Synoptic Comparison of Special Sensor Microwave/Imager Displays with Numerical Products

THOMAS F. LEE
JAMES S. BOYLE

Marine Meteorology Division

January 1993

REPORT DOCUMENTATION PAGE

Form Approved
OBM No. 0704-0188

1. AGENCY USE ONLY *(Leave blank)*	2. REPORT DATE	3. REPORT TYPE AND DATES COVERED
	January 1993	Final

4. TITLE AND SUBTITLE

A Synoptic Comparison of Special Sensor Microwave/Imager Displays with Numerical Products

5. FUNDING NUMBERS

Job Order No. 94411B
Program Element No. 0603704N
Project No. X1596
Task No.
Accession No. DN658753

6. AUTHOR(S)

Thomas F. Lee and Dr. James S. Boyle

7. PERFORMING ORGANIZATION NAME(S) AND ADDRESS(ES)

Naval Research Laboratory Detachment
Marine Meteorology Division
Monterey, CA 93943-5006

8. PERFORMING ORGANIZATION REPORT NUMBER

Formal Report 9403
NOARL Report 34

9. SPONSORING/MONITORING AGENCY NAME(S) AND ADDRESS(ES)

Space and Naval Warfare Systems Command
(PMW-141)
Washington, DC 20363-5100

10. SPONSORING/MONITORING AGENCY REPORT NUMBER

11. SUPPLEMENTARY NOTES

This research was performed by the Naval Oceanographic and Atmospheric Research Laboratory (NOARL), recently designated the Naval Research Laboratory. Formerly NOARL Report 34.

12a. DISTRIBUTION/AVAILABILITY STATEMENT

Approved for public release; distribution is unlimited. Naval Research Laboratory, Washington, DC 20376-5320.

12b. DISTRIBUTION CODE

13. ABSTRACT *(Maximum 200 words)*

Marine environmental products from the Special Sensor Microwave/Imager (SSM/I) are compared with analyses from an operational numerical forecast system. The SSM/I products considered are windspeed, precipitable water, and precipitation. The SSM/I products give a finer representation of spatial detail than the forecast system products. In particular, the SSM/I windspeeds can be used to examine continental influences on marine windspeeds. Such mesoscale effects are not analyzed well by global numerical models.

However, the output from the numerical forecast system can provide parameters not available from the SSM/I products, such as wind direction. In addition, forecast system output can provide information between satellite passes and in regions contaminated by precipitation on SSM/I products.

14. SUBJECT TERMS

Special Sensor Microwave/Imager, microwave radiometry, Defense Meteorological Satellite Program, Navy Operational Global Atmospheric Prediction System, remote sensing

15. NUMBER OF PAGES

125

16. PRICE CODE

17. SECURITY CLASSIFICATION OF REPORT	18. SECURITY CLASSIFICATION OF THIS PAGE	19. SECURITY CLASSIFICATION OF ABSTRACT	20. LIMITATION OF ABSTRACT
Unclassified	Unclassified	Unclassified	Same as report

Contents

Acknowledgments

This support of the sponsor, Space and Naval Warfare Systems Command (PMW-141), CAPT C. Hoffman, USN, Program Element 0603704N, is gratefully acknowledged for making this effort possible.

We would like to thank the staff of the Naval Environmental Operational Nowcasting System at our Monterey, CA facility. James Goerss, Paul Tag, Robert Fett, Mary Alice Rennick, and Edward Barker also gave valuable suggestions.

The mention of commercial products or the use of company names does not in any way imply endorsement by the U.S. Navy or NOARL.

A Synoptic Comparison of Special Sensor Microwave/Imager Displays with Numerical Products

1.0 Introduction

Marine forecasters have learned to depend on visible and infrared satellite images as real-time "snapshots" of large ocean expanses. Years of experience and a variety of training materials help forecasters interpret these images correctly. Increasingly, satellite microwave images and displays are becoming available to forecasters in real time, prompting the need for new documentation. For example, using images from the Scanning Multichannel Microwave Radiometer, Katsaros et al. (1989) demonstrated that synoptic-scale fronts correspond to steep gradients of precipitable water.

Data from the Special Sensor Microwave/Imager (SSM/I) aboard the Defense Meteorological Satellite Program (DMSP) satellite can yield environmental products over the oceans at a nominal 25-km horizontal resolution (Hollinger, 1991). The SSM/I is a passive microwave radiometer that collects radiation naturally emitted by the sea surface and intervening atmosphere. In this report we will discuss displays of three environmental parameters available from the SSM/I: precipitable water, windspeed, and precipitation. To give these displays added meaning, we will compare them with displays of numerical products.

2.0 Background and Data

2.1 Windspeed

Displays of microwave surface windspeed represent a radical departure from traditional depictions of windspeed on weather maps (i.e., using isotachs or wind barbs). While these new displays contain unprecedented detail, their interpretation is not straightforward, since the satellite retrievals do not include wind direction information. Anticipating the operational forecaster's needs from the product, we present several examples of SSM/I windspeed displays juxtaposed with winds from a state-of-the-art forecast system.

Measurement of oceanic windspeed from space is a multifaceted problem (Pierson, 1983; Ulaby et al., 1986). The magnitude of the emitted microwave radiation sensed by the SSM/I is a partial function of surface roughness. Surface roughness, in turn, is an excellent indicator of windspeed, except when high winds induce foam and multiple wave forms. Much of the emphasis thus far has been on the development of statistical windspeed algorithms based on brightness temperatures. Using SSM/I data, Goodberlet et al. (1990) developed a multichannel regression algorithm that estimates surface windspeeds within 2 m/s of in situ buoy observations, an accuracy anticipated by Wentz and Mattox (1986). The Goodberlet et al. global algorithm performs consistently in

Table 1. Windspeed accuracy flags.*

FLAG	STANDARD DEVIATION (m/s)
0	<2
1	2–5
2	5–10
3	>10

*(from Goodberlet et al., 1990)

a variety of climatic regions and becomes unusable only in narrow zones adjacent to ice or land masses. In addition to windspeed, the algorithm outputs "accuracy flags," sometimes referred to as "rain flags," associated with various degrees of degradation to the windspeed analysis due to precipitation (Table 1).

In this presentation we do not consider windspeed values flagged with values of 2 or 3 because of the persistent high bias of these retrievals (Goodberlet et al., 1990). Flagged regions, which we generally "white out," serve a secondary purpose of delineating areas of probable precipitation. For more discussion see, for example, Spencer et al. (1989) or Petty and Katsaros (1990).

2.2 Precipitable Water

The precipitable water displays represent a pixel-by-pixel application of the nonlinear regression equation derived by Alishouse et al. (1990). Valid for all the unfrozen oceans of the world, the equation uses a combination of the 19-, 22-, and 37-GHz channels. While precipitable water represents a vertical integration, its magnitude is strongly correlated with absolute humidity in the marine boundary layer (Liu, 1986; Hsu et al., 1989). Thus, the synoptic evolution of the precipitable water field strongly depends on vapor advection within the boundary layer.

2.3 Precipitation

The precipitation rate algorithm used here was adapted from Hollinger (1991). The 85-GHz channel, normally used in the formulation of rain rate, was missing during the period of data collection used for the products we present. Thus, the oceanic algorithm used a combination of the lower frequency channels of the SSM/I instrument.

2.4 Forecast System Output

The forecast system products used here result from the Navy Operational Global Atmospheric Prediction System (NOGAPS) generated at the Fleet Numerical Oceanographic Center (FNOC), Monterey, California. NOGAPS consists of a multivariate optimum interpolation analysis (Barker et al., 1988), nonlinear normal model initialization, and a T79 spectral forecast model.

For comparison to SSM/I winds, we use a derivative of NOGAPS termed the "marine winds." To compute the marine winds, a nonlinear variational analysis is performed to assimilate low-level cloud-track winds and surface wind observations into the first-guess field based on NOGAPS. The resulting analysis is heavily weighted toward ship observations, buoys, and coastal observations. The height of the analysis is given as 19.5 m above the sea surface, corresponding to the nominal height of most ship observations and the reference level used by the Goodberlet et al., (1990) algorithm. The forecast marine winds are computed from NOGAPS boundary layer winds using a combination of boundary layer theory and ad hoc adjustments.

Global comparison from September, October, and November of 1990 indicate the marine winds analysis has a root-mean-square speed error of 2 m/s with respect to fixed buoys. With respect to SSM/I speeds, the marine winds analysis is slower on average by 0.5 m/s. The

root-mean-square speed discrepancy between the SSM/I and the marine analysis is 5 m/s.

2.5 Comparison Methodology

In our comparisons of the marine winds to SSM/I winds, we illustrate two scenarios. In the first, we interpolate the two nearest analyses to the time of the DMSP overpass. This procedure creates the best case scenario, suited for post-analysis applications. In the second scenario, we interpolate an analysis and a 12-hour forecast to the overpass time, illustrating a more realistic forecast situation.

The SSM/I instrument (Spencer et al., 1989) has a swath width of only 1400 km; thus, there are significant gaps in coverage between successive passes. Near the poles the coverage problem improves, and poleward of about 58° N or S, the SSM/I will image a given region at least once per 12-hour period. The SSM/I data will be received aboard U.S. Navy ships via direct satellite readout by the Tactical Environmental Support System (TESS), a shipboard computer system designed to support nowcasting at sea. Because of the SSM/I coverage limitations, shipboard forecasters will need to supplement gaps in high-resolution SSM/I windspeeds with lower resolution forecast system winds. Where the two data sets coincide, as in the following case studies, forecasters will benefit from the advantages of both.

3.0 Case Studies

3.1 Fair Weather Over the Northeast Atlantic and Adjacent Seas

Relatively light SSM/I windspeeds appear over most of the study area on 29 November 1989 (Fig. 1a). Level 1 accuracy flags (within dotted outlines on Fig. 1a between the British Isles and Iceland) indicate isolated regions of degradation, but the retrievals from within the degraded areas are consistent with those from the surrounding regions. Overall, the windspeed patterns generally agree with the corresponding marine winds display (Fig. 1b). For example, the marine winds product and the SSM/I winds show a similar increase in windspeed from the northern coast of Spain to about 50°N. The two data sets generally also agree over the North Sea, east of the British Isles, where the low SSM/I windspeeds correspond well to the broad minimum of the marine winds product. Nevertheless, the SSM/I data show details not resolved by the coarser marine winds product, e.g., slight variations in windspeed to the north and the east of the British Isles.

The relative minimum in SSM/I windspeed northeast of Iceland (red patch on Fig. 1a) results from the disruption of strong southwesterly flow by the rugged Icelandic terrain. Surface observations also suggest this pattern (Fig. 2). Strong wind observations appear on the southwestern coast of Iceland, but a nearly calm wind appears in the ocean to the east-northeast. The windspeed minimum off Iceland is a prevalent feature, recurring often in the SSM/I windspeed displays we examined. The minimum also appears in conventional climatological summaries (Commander Naval Oceanography Command, 1981).

The marine winds field (Fig. 1b) places this lee minimum to a position more directly to the north of the island. This misplacement stems from

the assimilation by the marine winds algorithm of southerly surface observations (Fig. 2) on the southern coast of Iceland. These observations represent flow that has recently backed from southwest over the ocean to southerly over the island because of increased friction. The marine winds field extends the influence of these observations to the offshore waters, analyzing southerly flow. Thus, it places the lee minimum directly to the north of the island.

To the east of the lee minimum in windspeed, the SSM/I data depict a region of much greater windspeeds (green with embedded blue, indicating speeds in the range of 16 m/s or 32 kt). A ship observation of 35 kts in this region (Fig. 2) tends to corroborate these SSM/I windspeeds. The marine winds field (Fig. 1b) shows a broad region of relatively high windspeeds in this region (greater than 12 m/s) but does not depict the higher windspeeds shown by the SSM/I.

3.2 Deep Occlusion in North Pacific

A deep, occluded low in the northeast Pacific Ocean produced widespread cloudiness and high windspeeds on 1 December 1989 (Fig. 3). A precipitable water display (Alishouse et al., 1990) overlaid with marine wind streamlines (Fig. 4) shows the advection of very moist air (dark gray) northward along the western edge of the pass. The occluded nature of the cyclone is suggested by the "wrapping around" of the moist air on the periphery of the system. Near the center of the cyclone, the streamlines somewhat conform with the circulation suggested by the SSM/I precipitable water field. However, improved agreement would result if the streamline field were shifted by the amount indicated by the black arrow (Fig. 4).

Unlike the previous case, precipitation significantly degrades the quality of the windspeed display (Fig. 5) such that much of the scene is accuracy-flagged (Fig. 6). (Accuracy-flagged regions are "whited-out" on Fig. 5 and appear in gray shades on Fig. 6). Even within the nonflagged regions, there are important local discrepancies between the SSM/I winds and the marine winds product. For example, a distinct minimum in windspeed appears at 48°N, 150°W in the SSM/I analysis but at 49°N, 152°W in the marine winds analysis. The discrepancy is the same as given by the black arrow in Figure 4. This difference in placement between the two products, though small, leads to large local differences within the windspeed gradient region surrounding the circulation center. Thus, a forecaster would have little confidence in the marine winds product just southeast of the center where the SSM/I winds are not displayed (accuracy-flagged region.). In contrast, the following case illustrates a situation in which a forecaster would have a high degree of confidence in the conventional wind product within an SSM/I accuracy-flagged region.

3.3 Frontal System Off the U.S. West Coast

Northerly flow pushed a frontal system southward along the California-Oregon coast on 3 September 1990. An SSM/I precipitable water display shows a "comma" pattern associated with this system, separating relatively

dry air to the north from relatively moist air to the south (Fig. 7). The strong gradient appearing between the two air masses indicates the frontal position (Katsaros et al., 1989)

The SSM/I windspeed display (Fig. 8) places a band of accuracy flags along the frontal position. To the south of the front SSM/I, windspeeds are relatively low, but a sharp increase appears just to the north of the front, marking the leading edge of the advancing air mass. The marine winds product (Fig. 8) does not capture the frontal windspeed increase well, showing only a gradual increase in windspeed from southwest to northwest through the front. The marine winds product and the SSM/I agree well, however, concerning the position of the wind maximum off the Oregon-Washington coast. This agreement would enable a forecaster to be confident of the marine winds product within the accuracy-flagged region (shaped like the head of a "comma"), which appears within the wind maximum.

Both conventional and satellite products (Fig. 8) also depict a low windspeed feature to the northwest of the high windspeed region. The reversal of flow on either side of this elongated feature is consistent with the corresponding precipitable water product. Poleward flow on the western side of this feature brings moist air northward (dark region); equatorward flow on the eastern side brings dry air southward (bright region) from continental sources (Fig. 7).

3.4 Strong Winds Off California

This case demonstrates how successive passes of the SSM/I over a region shift slowly to the east. This is caused by the natural precession of the DMSP satellite over time. It also illustrates how the orientation of the ascending pass differs from the orientation of the descending pass.

A surface pressure analysis shows a 1028-mb high off the West Coast of the United States on 27 April 1990 (Fig. 9). A pressure gradient suggesting northerly flow lies over the West Coast. Figure 10 shows a swath of the windspeed product off the west coast of the United States. On the southeastern edge of the pass (west of California) high windspeeds (dark gray) appear. The accompanying marine isotachs (black lines) suggest that most of the high-wind area is to the east of the SSM/I pass edge. (Note that the 14.2-m/s maximum is to the east of the SSM/I pass.) To the west of the high-speed area lies a region of low windspeeds. This low-speed region is well covered by the SSM/I pass. The SSM/I data suggest completely calm winds in the middle of the high-pressure area. The calm area agrees well with the position of the high given in the surface pressure analysis.

Figure 11 shows the same region 12 hours later. Note that the different orientation of this ascending pass changes the pattern of data coverage as shown in Figure 10. The meteorological situation is relatively unchanged at this later time off the California coast. Low windspeeds associated with the center of the anticyclone still dominate the southern half of the pass in Figure 11, but the southeast edge of the pass indicates faster winds associated with the edge of the high windspeed region. As in

Figure 10, the marine winds product indicates that the high-speed area lies mainly to the east of the SSM/I coverage.

Figure 12 is the descending pass imaged 24 hours after Figure 10 and 12 hours after Figure 11. Notice that its geographical orientation is identical to Figure 10, the previous descending pass, but because of satellite precession the pass coverage is shifted several degrees to the east. Although the synoptic situation has changed little in the southern half of the study region, the eastward shift of the satellite has sharply improved the coverage of the high windspeed region. However, the SSM/I coverage of the lowest windspeeds associated with the high-pressure area is partially cut off on the far western edge of the pass.

3.5 Pacific Water Vapor Advection Over the Eastern Pacific

This example illustrates how model low-level streamlines and SSM/I precipitable water displays can be used to trace the advection of moisture within oceanic systems. The examples show that two SSM/I passes can appear on the same display to provide better spatial coverage. In such situations the user must be aware that the observation time for the two passes is about 100 minutes apart.

From 7 through 9 April 1990 a large low-pressure area dominated the eastern Pacific Ocean (Figs. 13–14). Figure 15 shows precipitable water over two ascending SSM/I passes. Within the western pass, streamlines suggest the cyclonic flow of the developing cyclone. Southerly flow is advecting an elongated stream of moist air from the subtropics northward toward the Aleutian Islands. In the northern portion of the eastern pass of Figure 15, offshore flow from western Canada is advecting dry air into the northwest Pacific Ocean. In the southern portion of the eastern pass, a small-scale cyclone is advecting another stream of moist air northward from the subtropics.

Figure 16 is the same scene a day later. The northern portion of both passes is now dominated by dry, offshore flow. In the eastern pass, the streamlines help trace the cyclonic advection of the moisture around the low center, indicating that the system is in the early occlusion process. Figure 17 is the final scene in the 3-day sequence. Advected in by strong northerly winds, the dry air originating in Alaska and western Canada is now wrapping around the western edge of the cyclone. In Figure 17 the cyclone is cut off from its supply of moist air to the south and is dying.

3.6 Effects of Alaskan Terrain on Marine Windspeed

On 29 November 1989, a small-scale cyclone prevails in the northwest Gulf of Alaska. The marine wind field (Fig. 18) indicates a windspeed minimum near Kodiak Island (Fig. 19). The SSM/I also indicates a minimum in this vicinity. Of more interest, however, are the differences in the two products within the offshore flow near the Aleutian Peninsula. Northerly flow is common here in late fall and represents a combination of synoptic forcing by the semipermanent Aleutian low and cold air drainage from the frigid Alaskan land mass. Figure 18 shows two terrain induced minima in SSM/I windspeed (marked on Fig. 19). One

minimum lies just downwind of the Ahklun Mountains, the other lies just downwind of the Veniaminof Volcano. The shielding effect in this region also appeared in the SSM/I displays on 28 and 30 November (not shown) due the persistence of northerly flow. The shielding effect cast by the Ahklun Mountains is also supported by wind climatologies from surface stations in the region (Brower et al., 1988). The marine winds product (Fig. 18) has a much coarser resolution than the SSM/I and fails to show either of the terrain-induced minimums.

3.7 Aleutian Cyclone

In the previous case topographic features explained a significant portion of the windflow. This example illustrates a case in the same region where synoptic factors are the most influential. On 3 April a cyclone is centered over the Aleutian Islands (Fig. 20). A water vapor (Fig. 21) image shows dry air (light gray) being advected southward on the western portion of the image, while moist air (darker gray) is advected northward on the adjacent pass to the east. The black areas indicate ice pack. Nearly calm flow in the middle of the cyclone appears in Bristol Bay and very strong flow occurs to the southwest (Fig. 22). The concentric isotach overlay (black lines on Fig. 22) illustrates the same pattern: the lowest winds occur within Bristol Bay with much stronger winds to the southwest.

3.8 Cyclone Over the Black Sea

Tactical operations often require the nowcasting of weather conditions within relatively small, enclosed water bodies. In particular, the SSM/I can show small-scale variations which numerical models might not depict adequately. The disadvantage is that the surrounding land areas create side-lobe effects, which contaminate the data near the coastlines. The SSM/I windspeed product is especially sensitive to coastal contamination. Also, research continues on whether the SSM/I windspeed algorithm, developed and validated for open ocean, is valid for inland water bodies. Thus, while the product can be used qualitatively over enclosed water bodies as in the following example, the user cannot strictly rely on the quantitative windspeeds.

Figure 23, a surface chart of the Black Sea region for 28 November 1989, shows the absence of a significant windspeed gradient over the region. Thus, Figure 24, a windspeed image of the Black Sea, shows only light speeds over the eastern two-thirds of the water area. (Disregard higher windspeed areas near the coastline; these represent shoreline contamination.) The accompanying marine wind streamlines (Fig. 24) indicate westerly winds in the western portion of the Black Sea, shifting to more southerly in the eastern half.

Twenty-four hours later a strong high-pressure area has advanced into the region, creating a stronger pressure gradient (Fig. 25). Thus, the marine winds product now develops northerly winds over the western portion of the sea (see streamlines and isotachs on Fig. 26). The winds are particularly strong in the northwest corner of the Black Sea. A

cyclonic circulation appears over the northeastern portion of the Black Sea.

The SSM/I display (Fig. 26) clearly shows that the strongest winds are in the northwest corner of the Black Sea in agreement with the marine winds isotachs. Speeds are in the vicinity of 20 m/s (approximately 40 kt). In the Sea of Azov, east-northeast of the high-speed region, windspeeds are much lower, around 6 m/s (12 kt). The precipitable water image (Fig. 27) is consistent with the windspeed display: low (dry) values on the western side of the image represent a cool, continental air mass advected in from the north. High (moist) values on the eastern side represent moister air with origins in the Mediterranean Sea. The gradient in precipitable water, along with the windshift (indicated by the streamlines), suggests a cold front which divides the Black Sea approximately in half, north to south (Fig. 27). A rain display (Fig. 28) shows that precipitation is falling in the moist southerly flow ahead of the front.

3.9 Frontal Systems in the Western Atlantic Ocean

10 April 1990 at 1200 GMT. On 10 April 1990 high-pressure dominates the western Atlantic Ocean (Fig. 29) with a low-pressure region approaching from the United States. Figure 30, precipitable water, shows that the anticyclonic streamflow pattern is advecting a dry, continental air mass into most of the study area. The southern and eastern edges of this air mass are bounded by a rapid increase in precipitable water. This strong gradient marks the frontal position (marked on Fig. 30), dividing the dry, continental air from moist, subtropical air to the south.

The SSM/I windspeed display (Fig. 31) shows light speeds near the center of the anticyclone. The model streamline center is offset slightly from the SSM/I windspeed minimum. To the south of the center lies a "whited-out" band, indicating a precipitation band associated with the cold front. To the south of this band, windspeeds are relatively light. To the north, windspeeds are much greater.

Figure 32 shows the precipitation rates associated with the frontal band. The central portion of the band lies in the coverage gap between the two passes; thus, two fragments of the same band appear on the display. The northeastern portion of the band contains significant precipitation with embedded values of 5 mm per hour. The southern portion contains only light precipitation with amounts around 1 mm per hour. The omega (vertical motion) field (Fig. 33) supports the precipitation intensity observed on Figure 32. Negative values on this chart indicate rising air at 700 mb; positive values indicate sinking air. The maximum vertical motion of –6.25 microbars/second on the extreme eastern edge of the display corresponds with the region of significant precipitation as observed by the SSM/I display. On the other hand, the center of the anticyclone is represented by an omega value of +3.91 microbars/second, indicating sinking motion.

10 April 1990 at 22 GMT. Ten hours later the high-pressure area has moved slightly toward the northeast (Fig. 34). Figure 35, an SSM/I

swath of precipitable water overlayed with marine level streamlines, shows a large anticyclone distributing dry air throughout a large portion of the study area. The SSM/I precipitable water gradient, marking the frontal zone, has become stationary in the southern portion of Figure 35.

Figure 36 again shows SSM/I precipitable water as in Figure 35 but now overlayed with NOGAPS isopleths of precipitable water. Note that NOGAPS agrees with the SSM/I concerning the uniform dryness of the air mass in the northern two-thirds of the scene (values on the order of 10 kg/m^2). The increasing NOGAPS gradient of precipitable water in the southern portion of the scene agrees well with the darker gray shades shown by the SSM/I. The SSM/I windspeed display shows the ridge line (elongated region of light winds) running through the middle of the image (Fig. 37).

April 1990 at 12 GMT. Fourteen hours later the high-pressure area still dominates the eastern portion of the study area (Fig. 38). However, a 998-mb cyclone over Maine has begun to move into the study region. The precipitable water product shows moist air wrapping around the remaining dry air mass (Fig. 39). Model precipitable water isopleths support this pattern (Fig. 40), indicating the advection of a narrow stream of moist air northward along the East Coast of the United States. The windspeed display (Fig. 41) shows an elongated belt of light winds associated with the anticyclone to the east.

April 1990 at 22 GMT. On 11 April at 22 GMT a pressure trough associated with the East Coast cyclone has begun to move offshore (Fig. 42). The western pass of the precipitable water product (Fig. 43) shows the edge of a tongue of moist air moving up from the south in converging southerly flow. Dry air just to the rear of this tongue marks an advancing dry air mass. A cold front marks the transition between the two air masses. The eastern pass of Figure 43 continues to show anticyclonic rotation of moist air around the retreating high-pressure region. Much of the western pass of the windspeed product (Fig. 44) is rain-flagged, making interpretation difficult. In the eastern pass of Figure 44, lower windspeeds correspond to the ridge line of the anticyclone.

12 April 1990 at 12 GMT. The trough line of 14 hours earlier has pushed off the Atlantic coast (Fig. 45). The precipitable water product (Fig. 46) indicates the associated cold front distinctly as the boundary between dry air over the Atlantic nearshore waters and the tongue of moisture farther offshore. Figure 47 shows that precipitation is falling within the frontal band with embedded values as high as 5 mm per hour. The precipitation is consistent with the omega (vertical motion) product (Fig. 48), which shows a large band of negative values (rising air) off the coast. Figure 49 again shows the precipitable water product but now overlayed with model isopleths of precipitable water. The model isopleths generally agree with the SSM/I precipitable water, except that the gradients depicted by the model are much coarser than depicted by the SSM/I.

The SSM/I windspeed product (Fig. 50) indicates generally light winds in the southern and eastern portions of the study area, with stronger winds in the northwest associated with the frontal system.

3.10 Winds in the Persian Gulf and the Arabian Sea

During a 2-day period (2–3 October 1990) windflow remained fairly uniform over the Persian Gulf and the northeastern Indian Ocean (Fig. 51). The marine winds streamlines show north to northeast winds over the Persian Gulf but south to southwest winds over the Indian Ocean. A convergence zone lies between (Figs. 52–55) the two wind regimes.

The SSM/I displays, placed 12 hours apart, show persistent terrain effects on the wind fields. For example, three of the four passes cover the island of Socotra (Figs. 52, 54, 55). In each instance the SSM/I data clearly show a small region of reduced windspeed to the lee of the island. The overlay of the streamlines on the SSM/I product makes interpretation of this effect much easier. Since the prevailing wind is from the south-southwest, it is easy to conclude that these relatively calm regions are lee effects.

Other lee effects also appear in the series. For example, reduced winds appear, especially in Figures 52, 53 and 55, in the Gulf of Aden downwind of mountainous terrain to the south. Reduced windspeeds also appear south of the Zagros Mountains in the Persian Gulf (Figs. 52–54).

4.0 Discussion and Conclusions

The preceding case studies illustrate that the juxtaposition of SSM/I and NOGAPS products can provide better nowcasting support than either product by itself. This juxtaposition is perhaps most useful in the nowcasting of marine winds. As a complement to the SSM/I display, the marine winds product provides wind direction and consistency in time and space. It also serves as a check on the SSM/I windspeeds in areas of significant precipitation. As a complement to the marine winds products, the SSM/I displays provide timely and detailed spatial variations of surface windspeed. The SSM/I can be especially valuable in areas affected by continental influences, such as the seas northeast of Iceland (Fig. 1a), the Alaskan coastal waters (Fig. 18–19), and the Indian Ocean/Persian Gulf (Figs. 52–55).

Work is underway to assimilate SSM/I windspeed retrievals directly into numerical forecast systems (Goerss, 1989). Nevertheless, even when SSM/I data are routinely assimilated, the integrated approach outlined here still has advantages. First, real-time satellite readout will always be more timely than forecast system output. Second, the high resolution of the SSM/I enables the display of detail not possible using numerical model output. Third, assimilation of SSM/I windspeeds into a forecast system may suffer where the corresponding model wind directions are

in error (e.g., Fig. 1b, off the coast of Iceland). Comparison of the resulting numerical product and real-time SSM/I windspeeds can identify regions where inappropriate assimilation of data has taken place.

Goodberlet et al. (1990) anticipate that the high bias of accuracy flags 2 and 3 will be eliminated in a future statistical algorithm. Such an improvement would help eliminate large gaps in windspeed coverage (e.g., Fig. 5), enhancing the usefulness of the product in regions affected by precipitation.

The juxtaposition of low-level streamlines on SSM/I precipitable water displays is a useful combination. To a significant degree, the SSM/I precipitable water displays we examined conformed to the advection suggested by the marine wind streamlines, but with finer detail. This is not surprising, since atmospheric water over the oceans tends to be concentrated near the surface. Low-level trajectories would offer even better tracers of water vapor advection than surface streamlines. Nevertheless, surface streamlines give an adequate approximation, especially for steady-state systems which are not moving quickly with respect to the windspeed (Holton, 1979).

The SSM/I precipitation product is a reliable indicator of the location of major precipitation systems at sea. We found that SSM/I precipitation signatures corresponded well to other SSM/I signatures (precipitable water and windspeed) and to signatures on NOGAPS products. For example, precipitation tends to fall along frontal boundaries indicated by sharp discontinuities in the SSM/I precipitable water product. Also, precipitation tends to correspond to upward vertical motion in the NOGAPS omega field.

The rainfall rates given by the SSM/I precipitation product, though useful as a relative indicator of intensity, should not be relied upon as accurate estimates. First, precipitation coverage often occurs over a relatively small portion of a 25-km SSM/I footprint. In these circumstances, SSM/I retrievals will be an underestimate of the true intensity. Second, the nature of precipitation systems varies widely from one region to the next. Thus, the assumptions made in a global algorithm, such as in the Calval scheme used here, are valid only in a very general sense. To the extent that these assumptions are not valid in a particular situation, erroneous estimates of precipitation intensity will result.

5.0 References

Alishouse, J. C., S. A. Snyder, J. Vongsathorn, and R. R. Ferraro (1990). Determination of oceanic total precipitable water from the SSM/I. *IEEE Transactions on Geoscience and Remote Sensing* 28:811–816.

Barker, E., J. Goerss, and N. Baker (1988). The Navy's operational multivariate optimum interpolation analysis method. Preprints, *Eighth Conference on Numerical Weather Prediction*, Baltimore, MD,

American Meteorological Society, 45 Beacon St., Boston MA 02018, pp. 161–163.

Brower, W. A., R. G. Baldwin, C. N. Williams, J. L. Wise, and L. D. Leslie (1988). Climatic Atlas of the Outer Continental Shelf Waters and Coastal Regions of Alaska, Volume II Bering Sea. National Climatic Data Center (Asheville, North Carolina); National Environmental Satellite, Data, and Information Service; National Oceanic and Atmospheric Administration; and Arctic Environmental Information and Data Center, University of Alaska (Anchorage, Alaska), pp. 284–285.

Commander Naval Oceanography Command (1981). U. S. Navy Marine Climatic Atlas of the World, Volume IX: World-Wide Means and Standard Deviations, NSTL Station, Bay St. Louis, MS 39529.

Goerss, J. S. (1989). Global data assimilation of SSM/I windspeed measurements. Preprints *Fourth Conference on Satellite Meteorology and Oceanography*, San Diego, CA, American Meteorological Society, 45 Beacon St., Boston MA, 02018, pp. 238–241.

Goodberlet, M. A., C. T. Swift, and J. C. Wilkerson (1990). Ocean surface windspeed measurements of the Special Sensor Microwave/Imager (SSM/I). *IEEE Transactions on Geoscience and 73 Remote Sensing* 28:823–827.

Hollinger, J. P. (ed.) (1991). DMSP Special Sensor Microwave/ Imager Calibration/Validation, Volume II. Naval Research Laboratory, Washington D.C.

Holton, J. R. (1979). *An Introduction to Dynamic Meteorology*. 2nd Edition, International Geophysics Series (v. 23), Academic Press, New York, pp. 64–67.

Hsu, S. A. and B. W. Blanchard (1989). The relationship between total precipitable water and surface-level humidity over the sea surface: a further examination. *J. Geophys. Res.* 94 (c10):14539–14545.

Katsaros, K. B., B. Iftekhar, L. A. McMurdie, and G. W. Petty (1989). Identification of atmospheric fronts over the ocean with microwave measurements of water vapor and rain. *Weather and Forecasting*: 4:449–460.

Liu, W. T. (1986). Statistical relation between monthly mean precipitable water and surface-level humidity over global oceans. *Monthly Weather Review* 114:1591–1602.

Petty, G. W. and K. B. Katsaros (1990). Precipitation observed over the South China Sea by the Nimbus 7 Scanning Multichannel Microwave Radiometer during Winter MONEX. *J. Appl. Meteor.* 29:273–288.

Pierson, W. J. (1983) The measurement of the synoptic scale wind over the ocean. *J. Geophys. Res.* 88:1683–1708.

Spencer, R. W., H. M. Goodman, and R. E. Hood (1989). Precipitation retrieval over land and ocean with the SSM/I: Identification and characteristics of the scattering signal. *Journal of Atmospheric and Oceanic Technology* 6:254–273.

Ulaby, F. T., R. K. Moore, and A. K. Fung (1986). Microwave Remote Sensing Active and Passive, v. 3, Artech House, Norwood, MA, pp. 1440–1467.

Wentz, F. J. and L. A. Mattox (1986) New algorithms for microwave measurements of ocean winds: Applications to SEASAT and the Special Sensor Microwave Imager. *J. Geophys Res.* 91:2289–2307.

Figure 1.
(a) SSM/I windspeed analysis for 0540 UTC, 29 November1989. In the vicinity of the ice edge and near coastlines windspeeds are often anomalously high, e.g., the green ring off the southern coast of Iceland. Regions surrounded by dotted lines (between the British Isles and Iceland) indicate level 1 accuracy flags (Table 1); (b) marine level isotachs (m/s) and streamlines, interpolated to 0540 UTC, 29 November 1989.

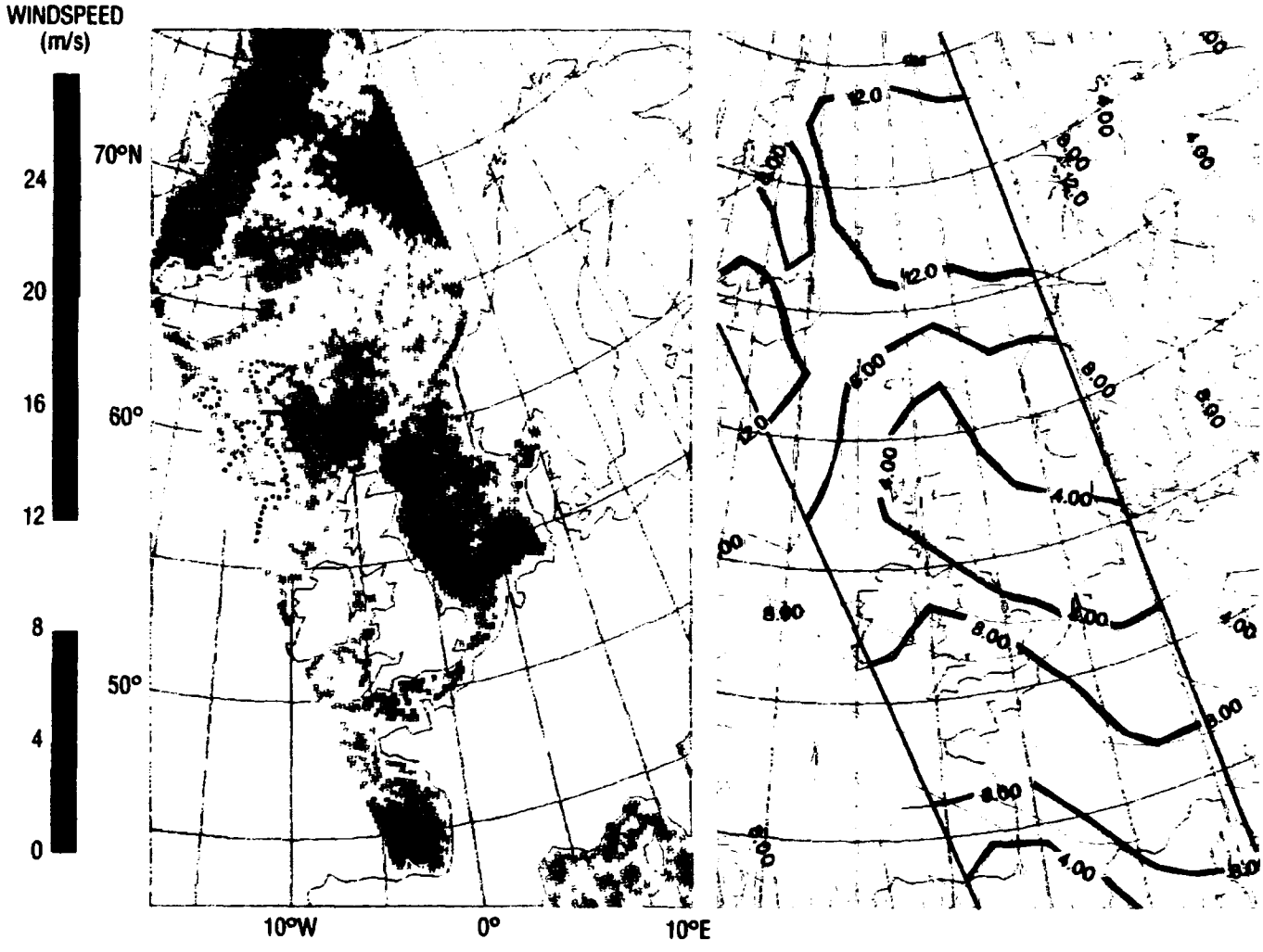
WINDSPEED
(m/s)
24
20
16
12
8
4
0
70°N
60°
50°
10°W
0°
10°E

Figure 2.
Surface chart for 0600 UTC, 29 November 1989. Winds are plotted as: full barb = 10 kt, half = 5 kt, isobars drawn every 4 mb.

Figure 3.
Surface chart for 1800 UTC, 1 December 1989. Winds are plotted as: full barb = 10 kt, half = 5 kt, pennant = 50 kt, isobars drawn every 4 mb.

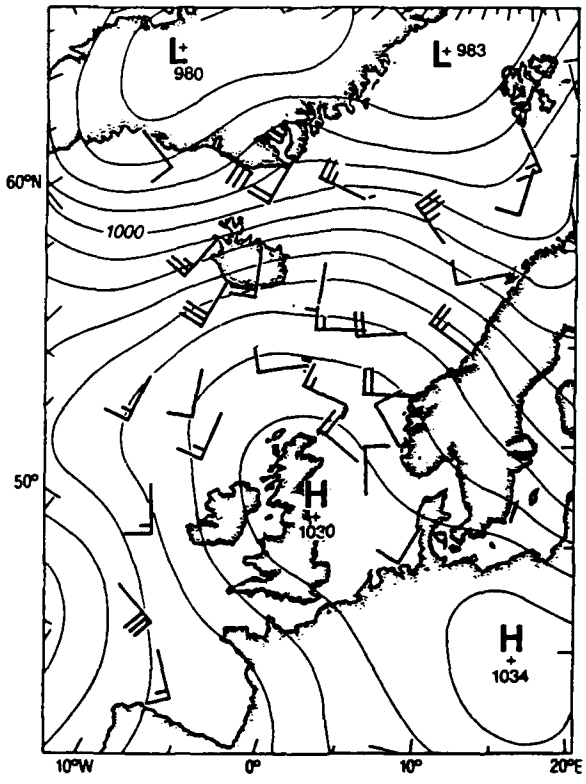
L
980
L
983
60°N
1000
50°
H
1030
H
1034
10°W
0°
10°
20°E

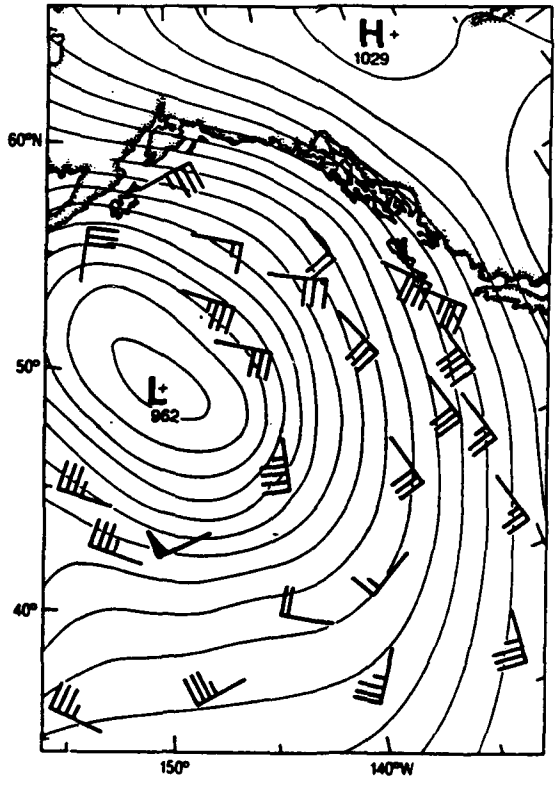
H
1029
60°N
50°
L
962
40°
150°
140°W

Figure 4.
Grayshade display: SSM/I precipitable water for 1510 UTC, 1 December 1989. Overlay: marine level streamlines interpolated to 1510 UTC (based on 1200 UTC analysis and following 0000 UTC forecast), 1 December 1989. Arrow indicates shift necessary to move the steamline field into better agreement with the SSM/I precipitable water product.

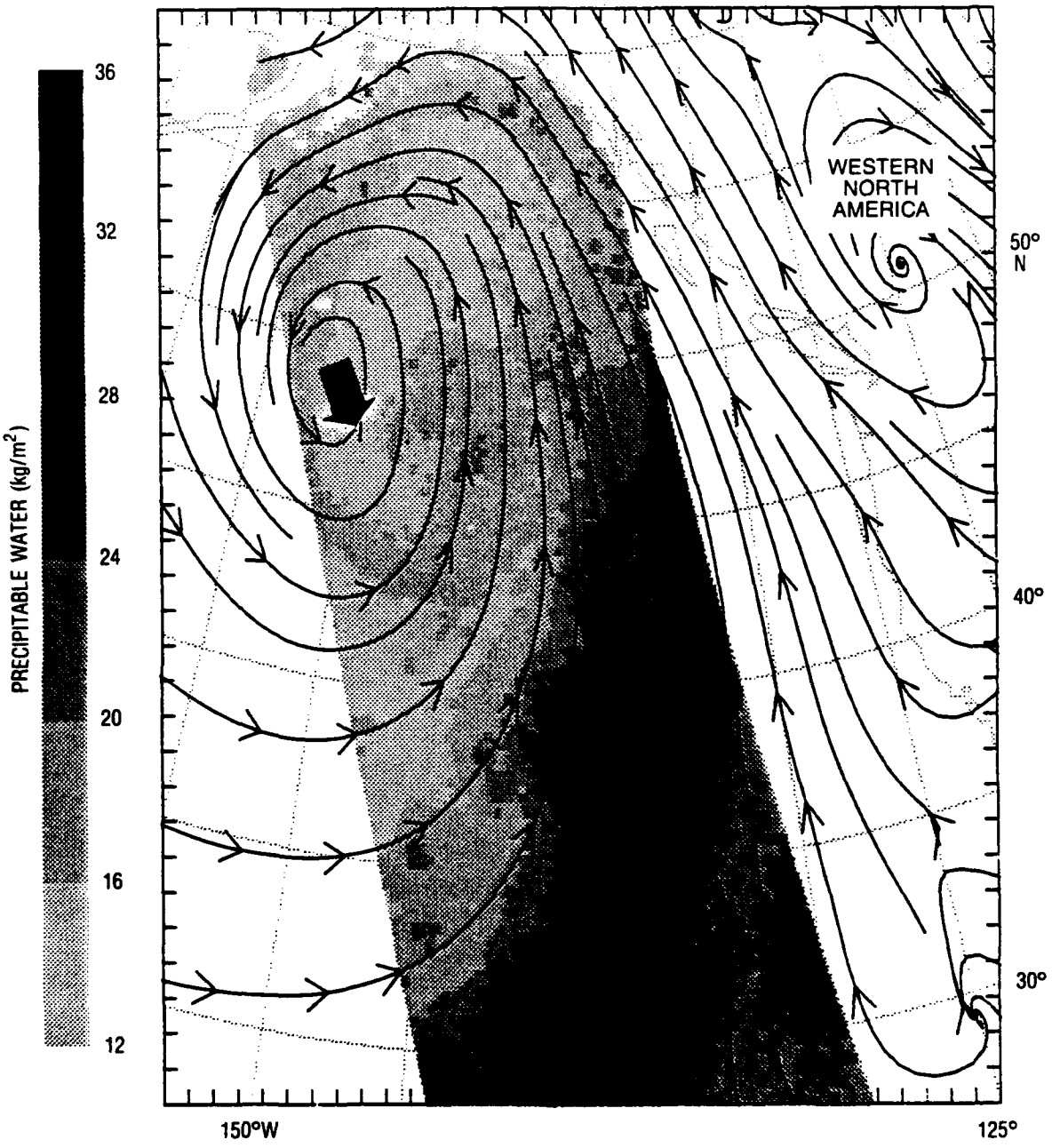
PRECIPITABLE WATER (kg/m²)
36
32
28
24
20
16
12
WESTERN
NORTH
AMERICA
50°
N
40°
30°
150°W
125°

Figure 5.
Grayshade display: SSM/I windspeed analysis for 1510 UTC, 1 December 1989. Overlays: marine level isotachs in m/s (black lines) and streamlines (light gray arrows) interpolated to 1510 UTC (based on 1200 UTC analysis and following 0000 UTC forecast), 1 December 1989. Blank (white) regions correspond to accuracy-flagged regions.

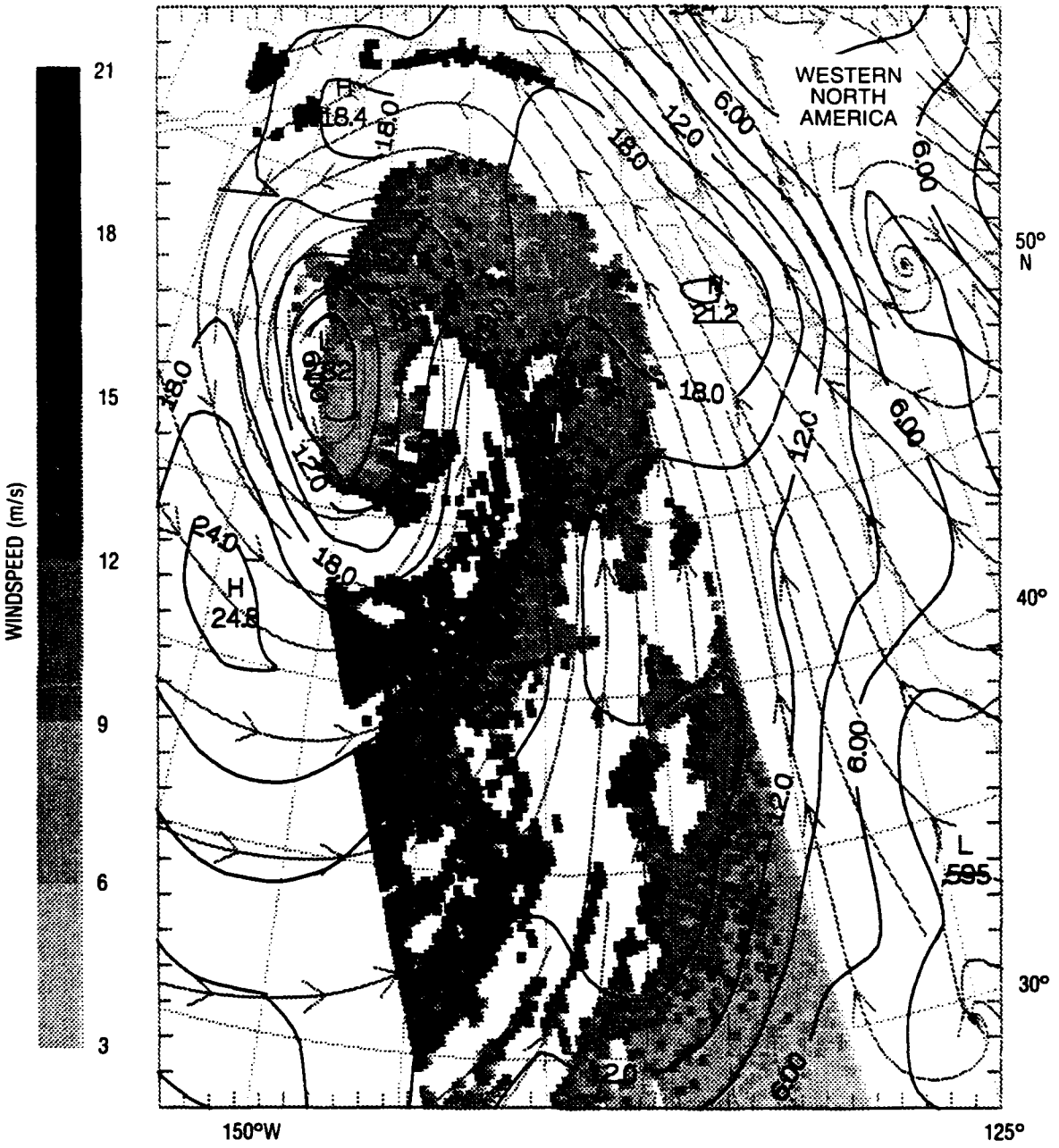
WINDSPEED (m/s)
21
18
15
12
9
6
3
WESTERN
NORTH
AMERICA
H
18.4
18.0
12.0
6.00
H
21.2
18.0
12.0
6.00
24.0
H
24.8
18.0
12.0
6.00
L
595
50°
N
40°
30°
150°W
125°

Figure 6.
SSM/I accuracy flags for 1510 UTC, 1 December 1989. Black = flag value of 3, dark gray = 2, light gray = 1, white (blank) = 0 (see Table 1).

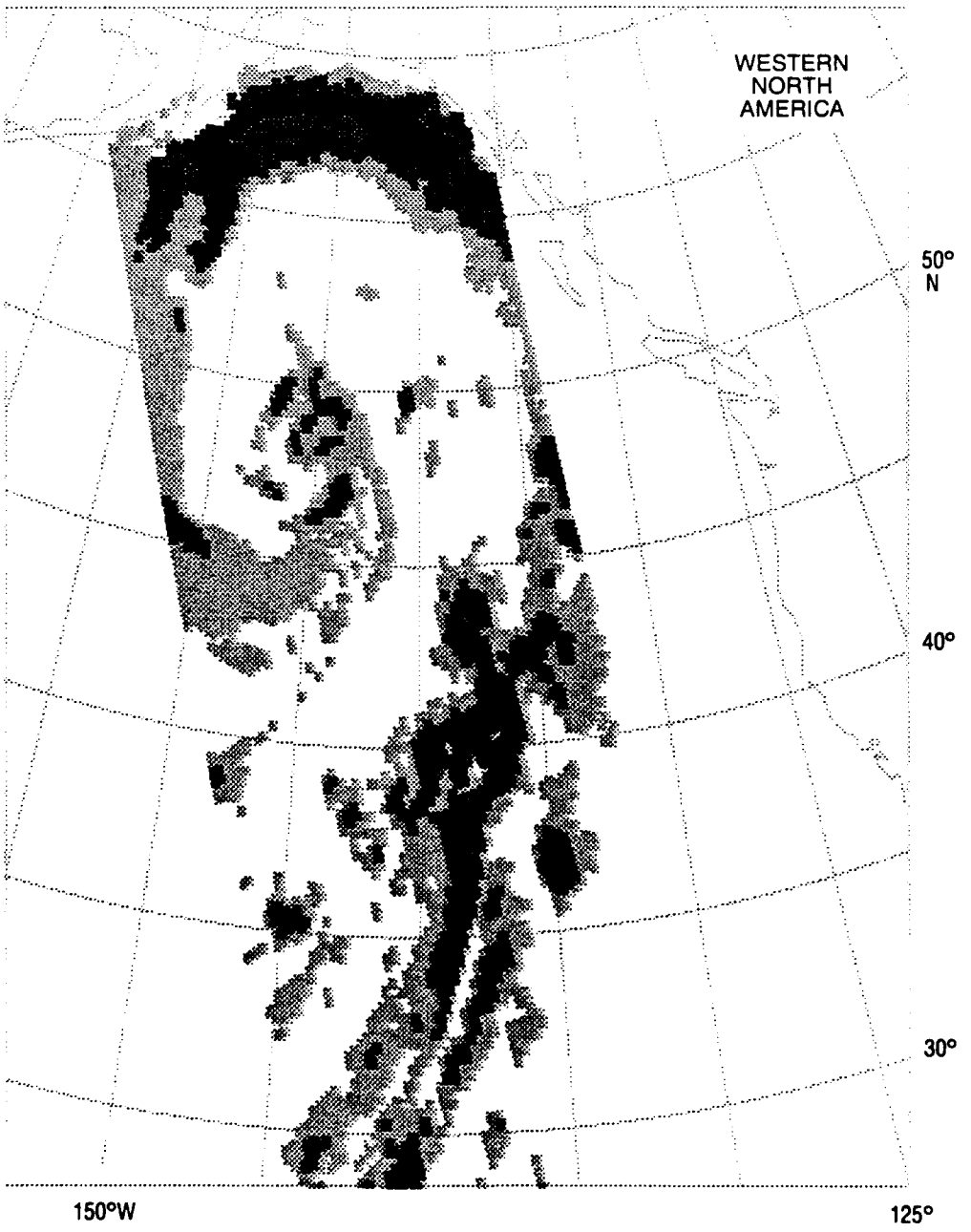
WESTERN
NORTH
AMERICA
50°
N
40°
30°
150°W
125°

Figure 7.
Grayshade display: SSM/I precipitable water for 1435 UTC, 3 September 1990. Overlay: marine level streamlines interpolated to 1400 UTC (based on 1200 UTC analysis and following 0000 UTC forecast), 3 September 1990.

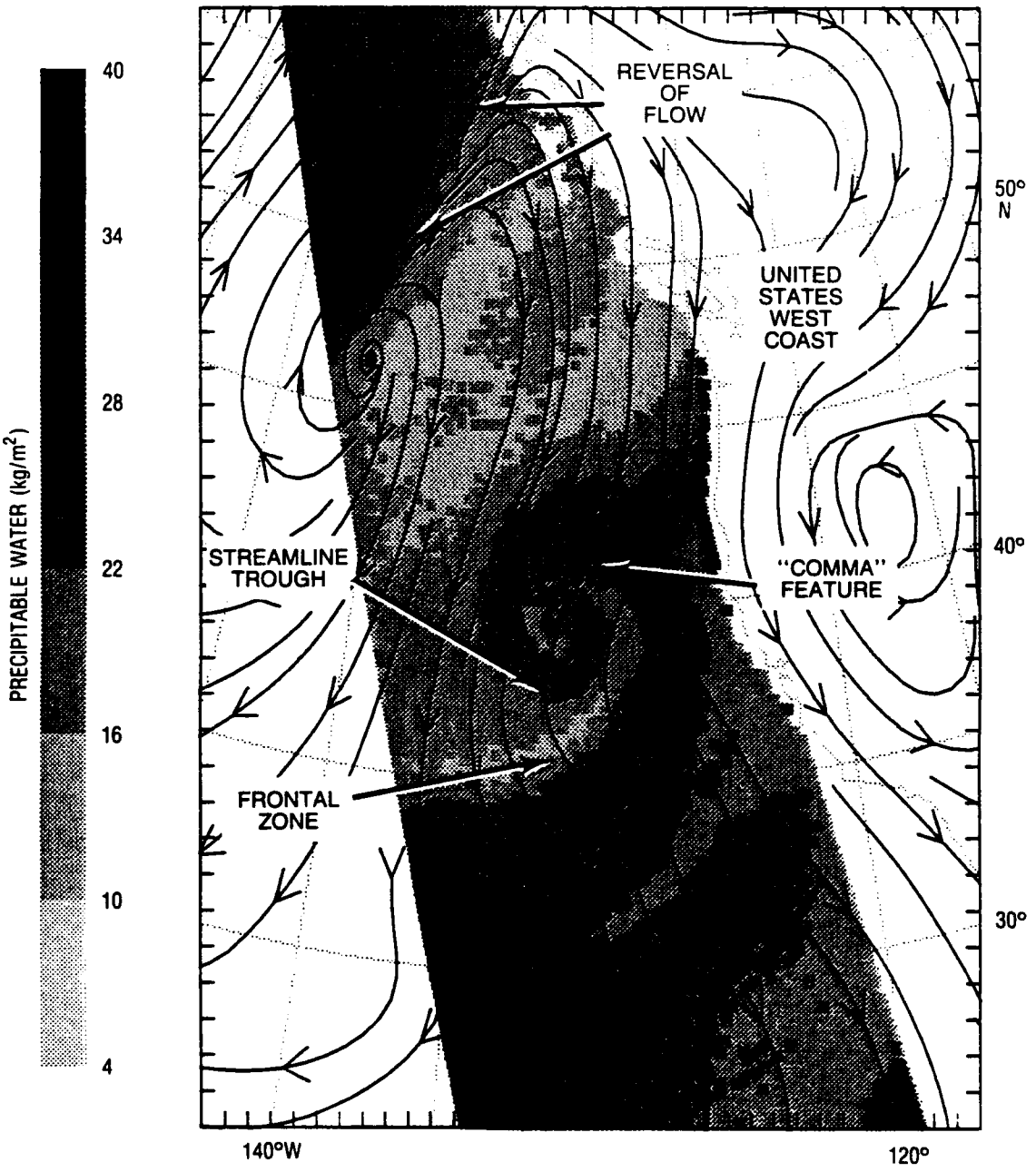
PRECIPITABLE WATER (kg/m²)
40
34
28
22
16
10
4
REVERSAL OF FLOW
UNITED STATES WEST COAST
STREAMLINE TROUGH
"COMMA" FEATURE
FRONTAL ZONE
50° N
40°
30°
140°W
120°

Figure 8.
Grayshade display: SSM/I windspeed analysis for 1435 UTC, 3 September 1990. Overlays: marine level isotachs in m/s (black lines) and streamlines (light gray arrows) interpolated to 1400 UTC (based on 1200 UTC analysis and following 0000 UTC forecast), 3 September 1990. Blank (white) regions correspond to accuracy-flagged regions.

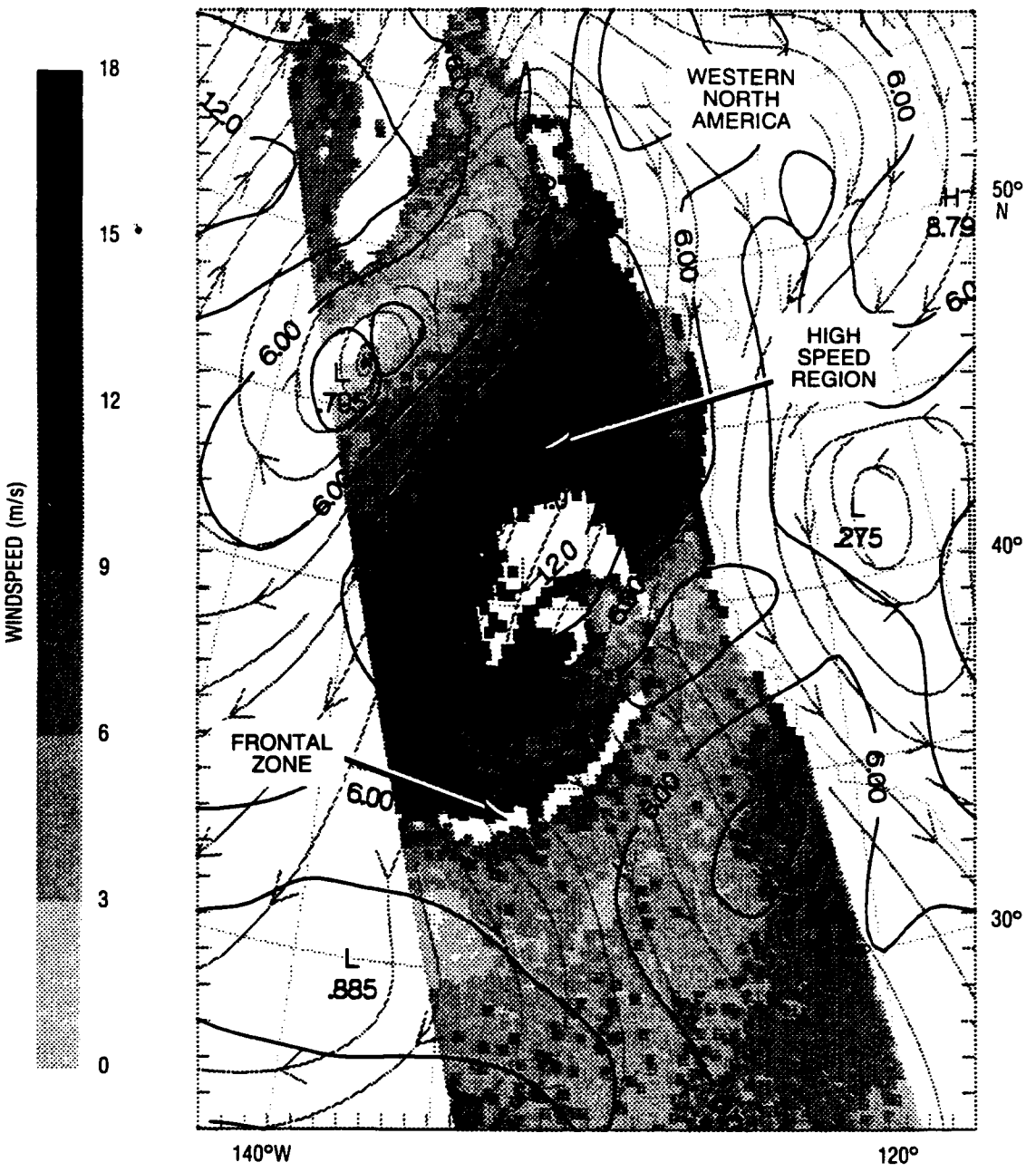
WINDSPEED (m/s)
18
15
12
9
6
3
0
WESTERN
NORTH
AMERICA
HIGH
SPEED
REGION
FRONTAL
ZONE
L
.885
L
.785
L
.975
H
8.79
6.00
120
50°
N
40°
30°
140°W
120°

Figure 9.
Surface Chart for 0200, 27 April 1990. Isobars drawn for every 4 mb.

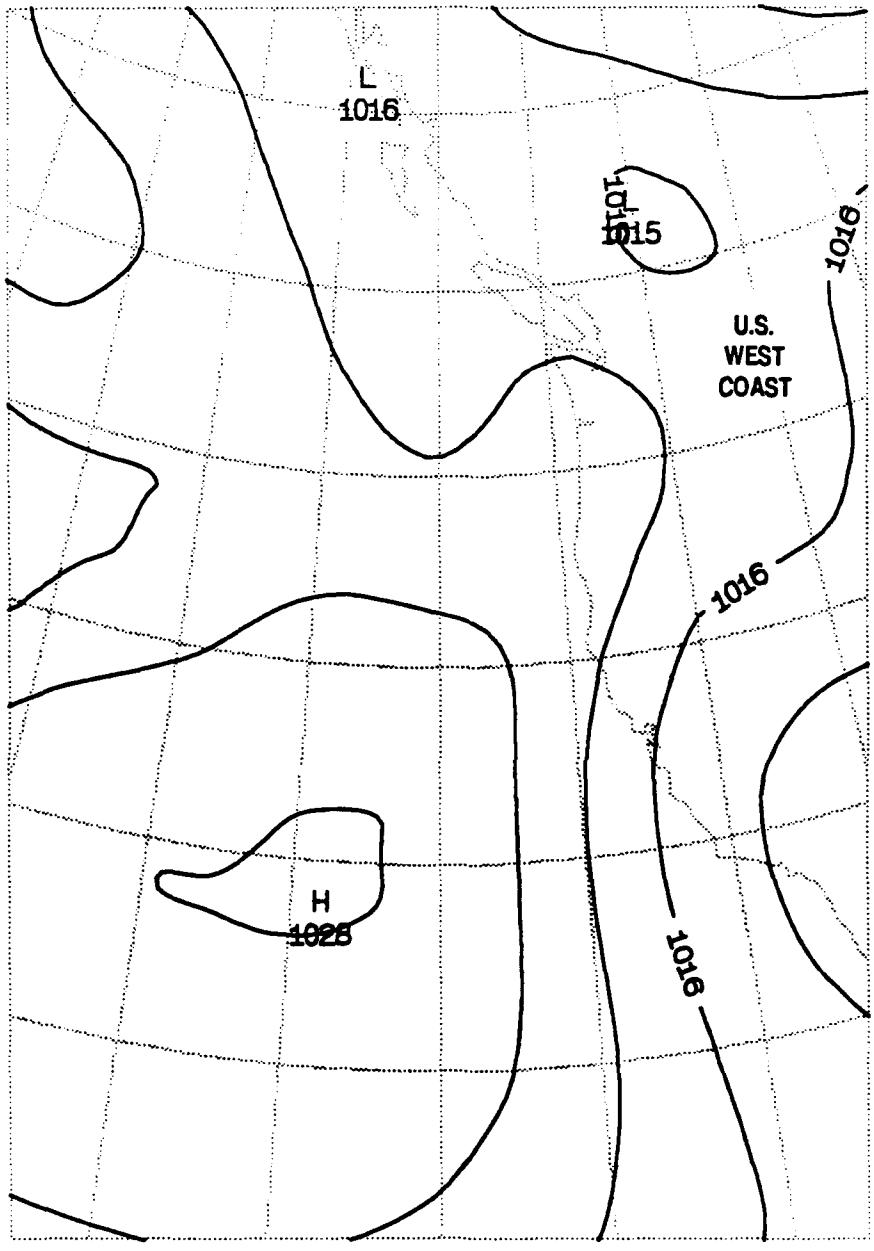
L
1016
1015
1016
U.S.
WEST
COAST
1016
H
1028
1016

Figure 10.
Grayshade display: SSM/I windspeed analysis for 0355 UTC, 26 April 1990. Overlays: marine level isotachs in m/s (black lines) and streamlines (light gray arrows) interpolated to 0200 UTC, 26 April 1990. Blank (white) regions correspond to accuracy-flagged regions.

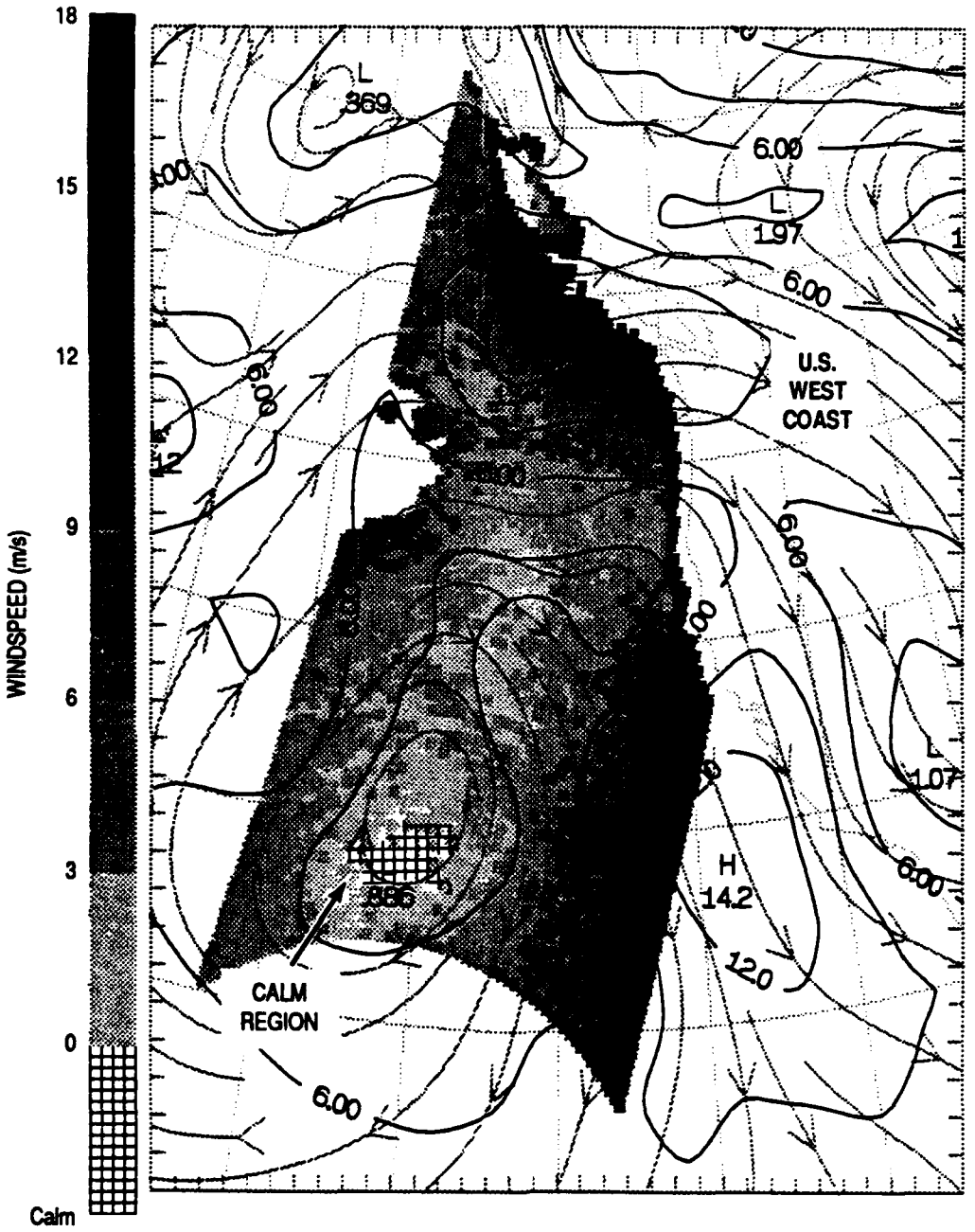
WINDSPEED (m/s)
18
15
12
9
6
3
0
Calm
L
369
6.00
L
1.97
6.00
U.S.
WEST
COAST
6.00
6.00
6.00
L
1.07
H
14.2
12.0
6.00
CALM
REGION
6.00

Figure 11.
Grayshade display: SSM/I windspeed analysis for 1500 UTC, 26 April 1990. Overlays: marine level isotachs in m/s (black lines) and streamlines (light gray arrows) interpolated to 1400 UTC, 26 April 1990. Blank (white) regions correspond to accuracy-flagged regions.

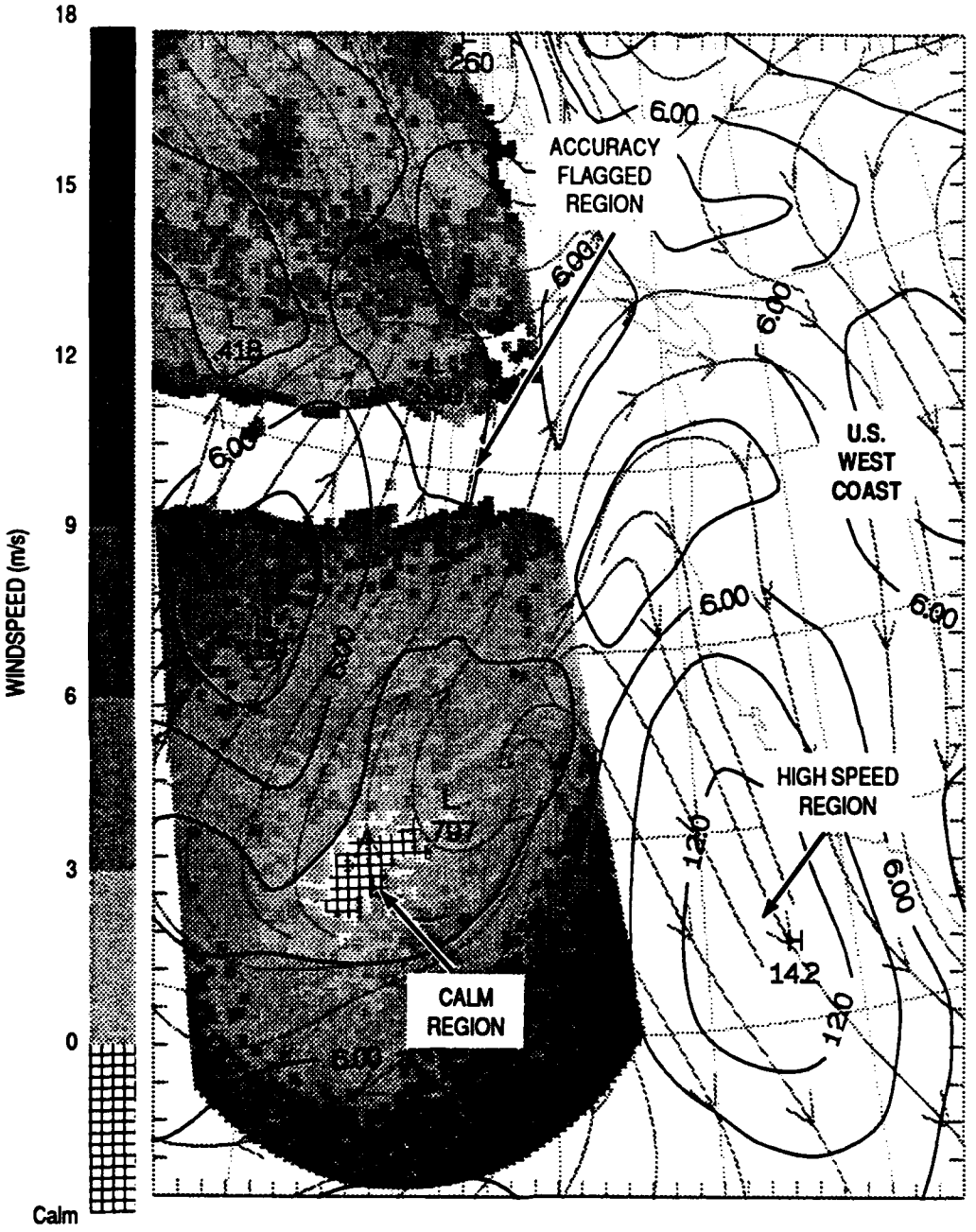
18
15
12
9
6
3
0
Calm
WINDSPEED (m/s)
ACCURACY
FLAGGED
REGION
U.S.
WEST
COAST
HIGH SPEED
REGION
CALM
REGION
6.00
L
H
1420
1320

Figure 12.
Grayshade display: SSM/I windspeed analysis for 0310 UTC, 27 April 1990. Overlays: marine level isotachs in m/s (black lines) and streamlines (light gray arrows) interpolated to 0200 UTC, 27 April 1990. Blank (white) regions correspond to accuracy-flagged regions.

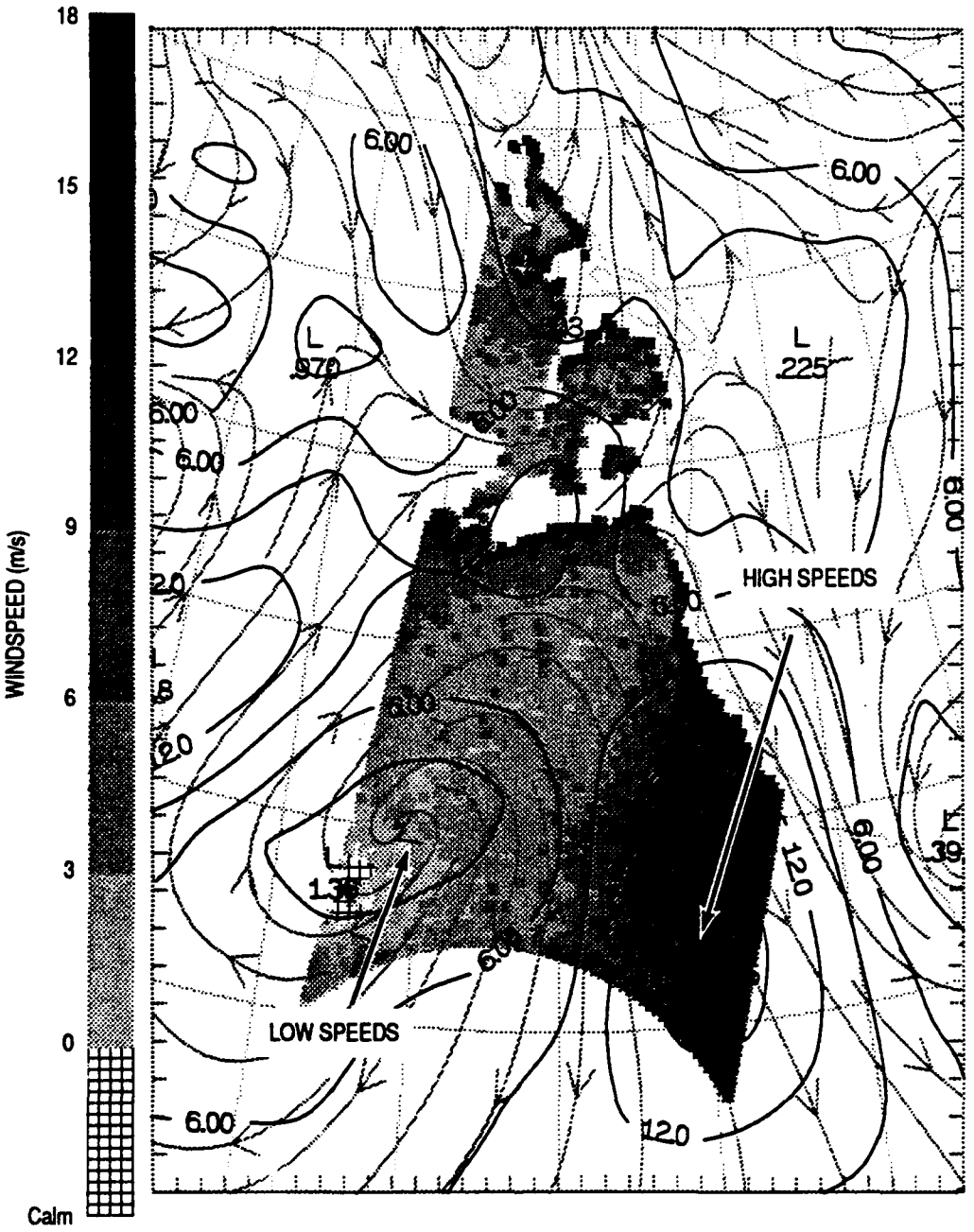
18
15
12
9
6
3
0
Calm
WINDSPEED (m/s)
6.00
6.00
6.00
6.00
6.00
6.00
6.00
6.00
L
970
L
225
L
HIGH SPEEDS
LOW SPEEDS
12.0
12.0

Figure 13.
Surface chart for 1400 UTC, 7 April 1990. Isobars drawn for every 4 mb.

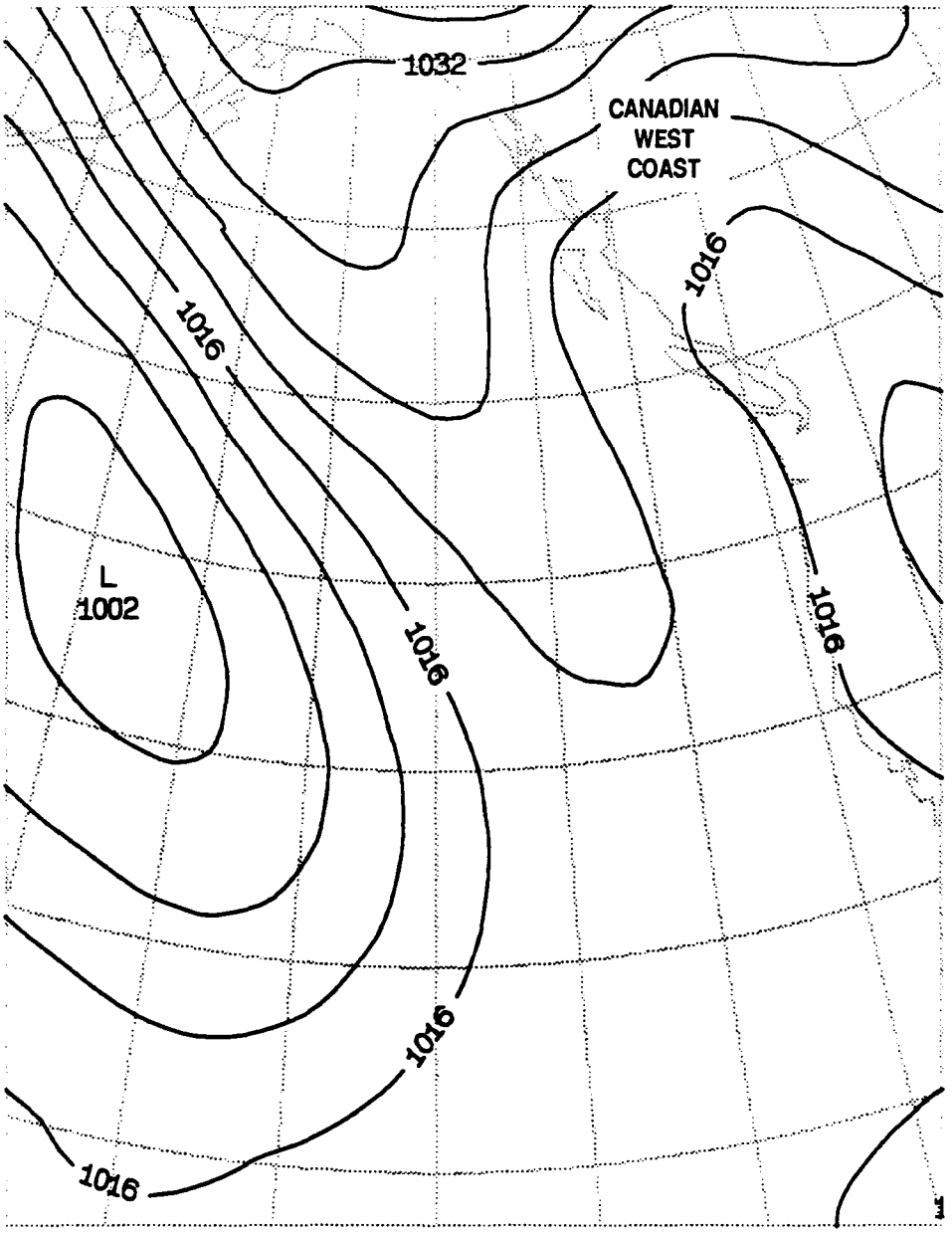
1032
CANADIAN
WEST
COAST
1016
1016
1016
1016
1016
L
1002

Figure 14.
Surface chart for 1400 UTC, 9 April 1990. Isobars drawn for every 4 mb.

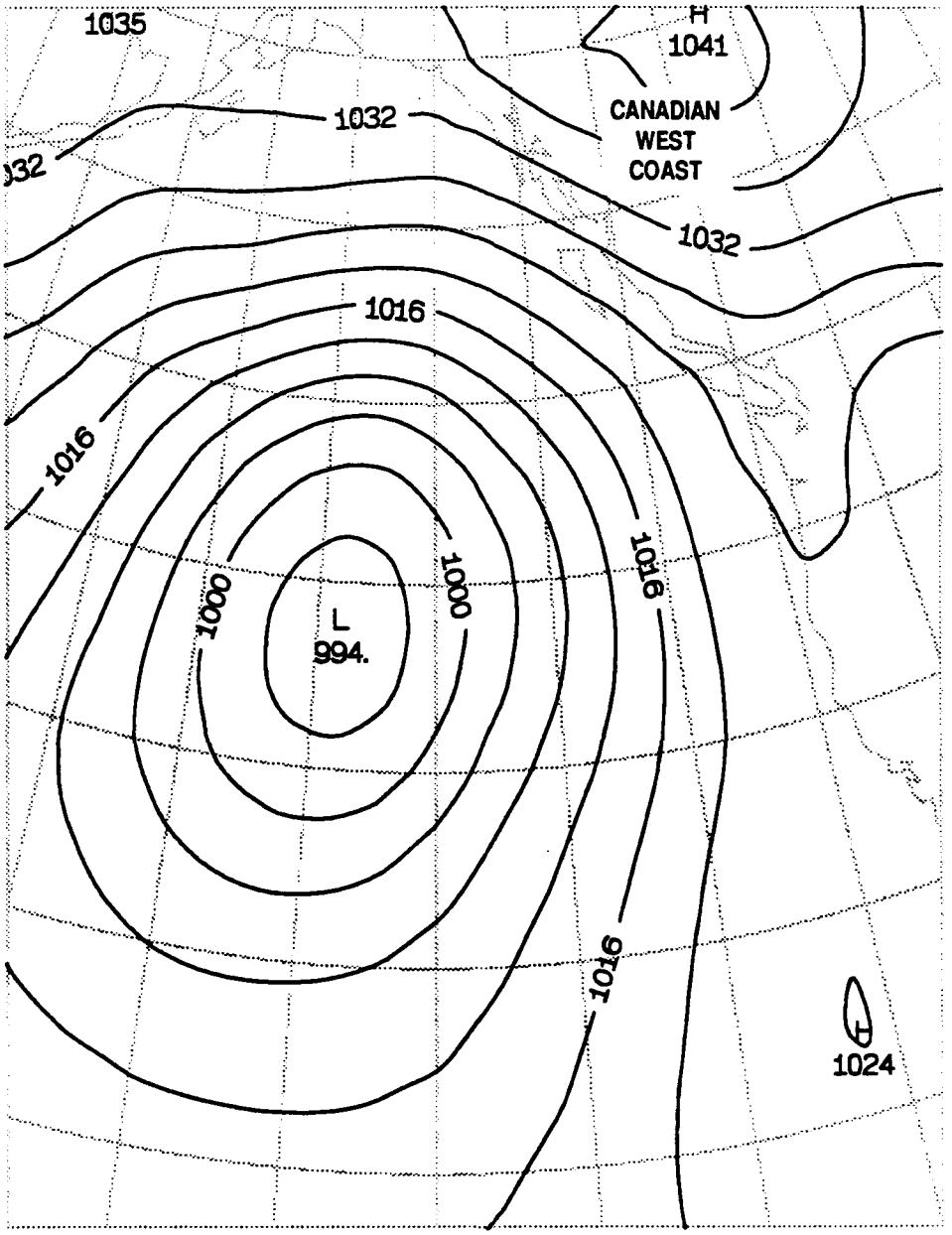
1035
H
1041
CANADIAN
WEST
COAST
1032
1032
1032
1016
1016
1016
1000
1000
L
994.
1016
1024

Figure 15.
Grayshade display: SSM/I precipitable water analysis for 1500 UTC, 7 April 1990. Overlay: streamlines (black arrows) interpolated to 1400 UTC, 7 April 1990.

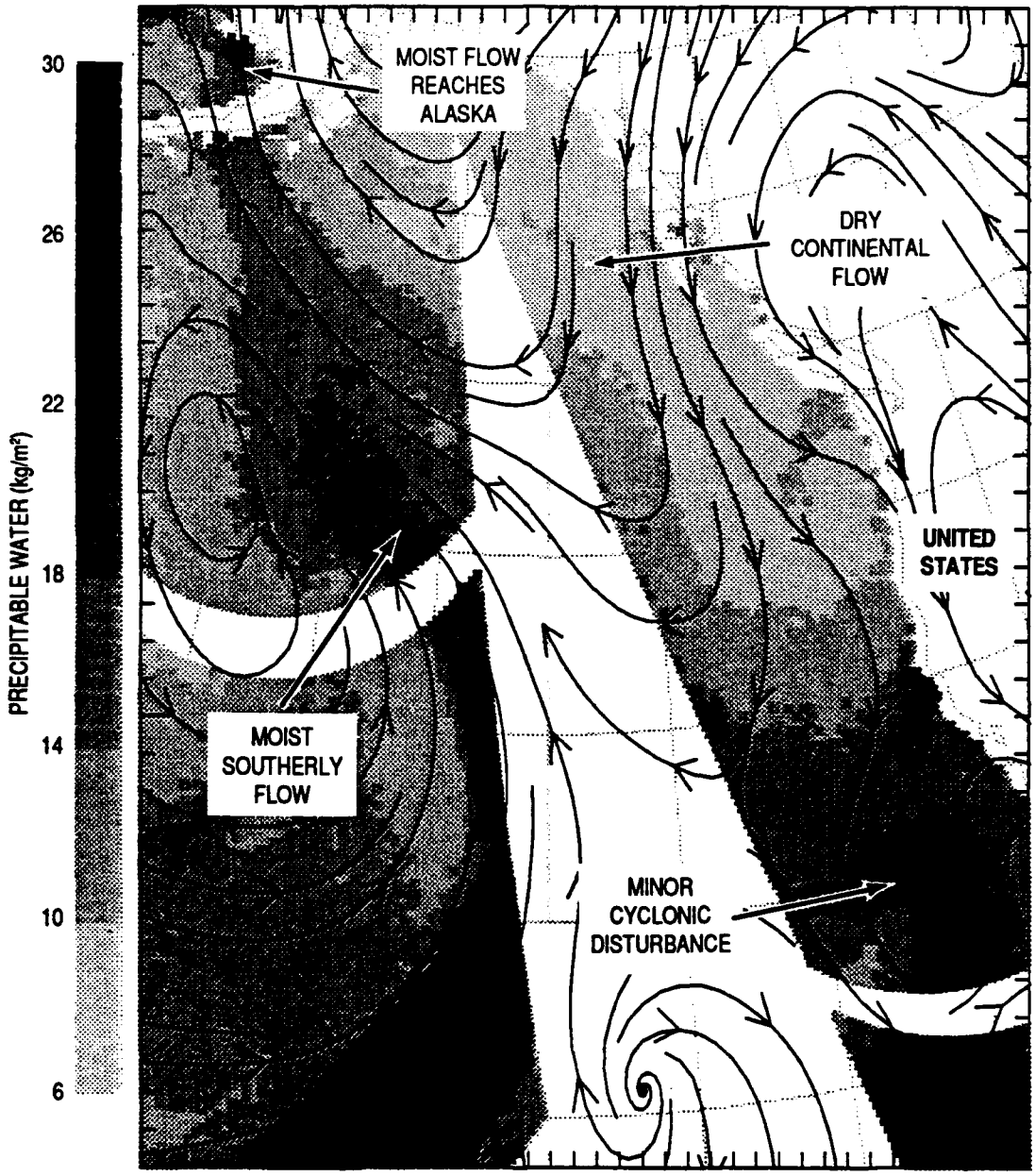
30
26
22
18
14
10
6
PRECIPITABLE WATER (kg/m²)
MOIST FLOW REACHES ALASKA
DRY CONTINENTAL FLOW
UNITED STATES
MOIST SOUTHERLY FLOW
MINOR CYCLONIC DISTURBANCE

Figure 16.
Grayshade display: SSM/I precipitable water analysis for 1430 UTC, 8 April 1990. Overlays: streamlines (black arrows) interpolated to 1400 UTC, 8 April 1990.

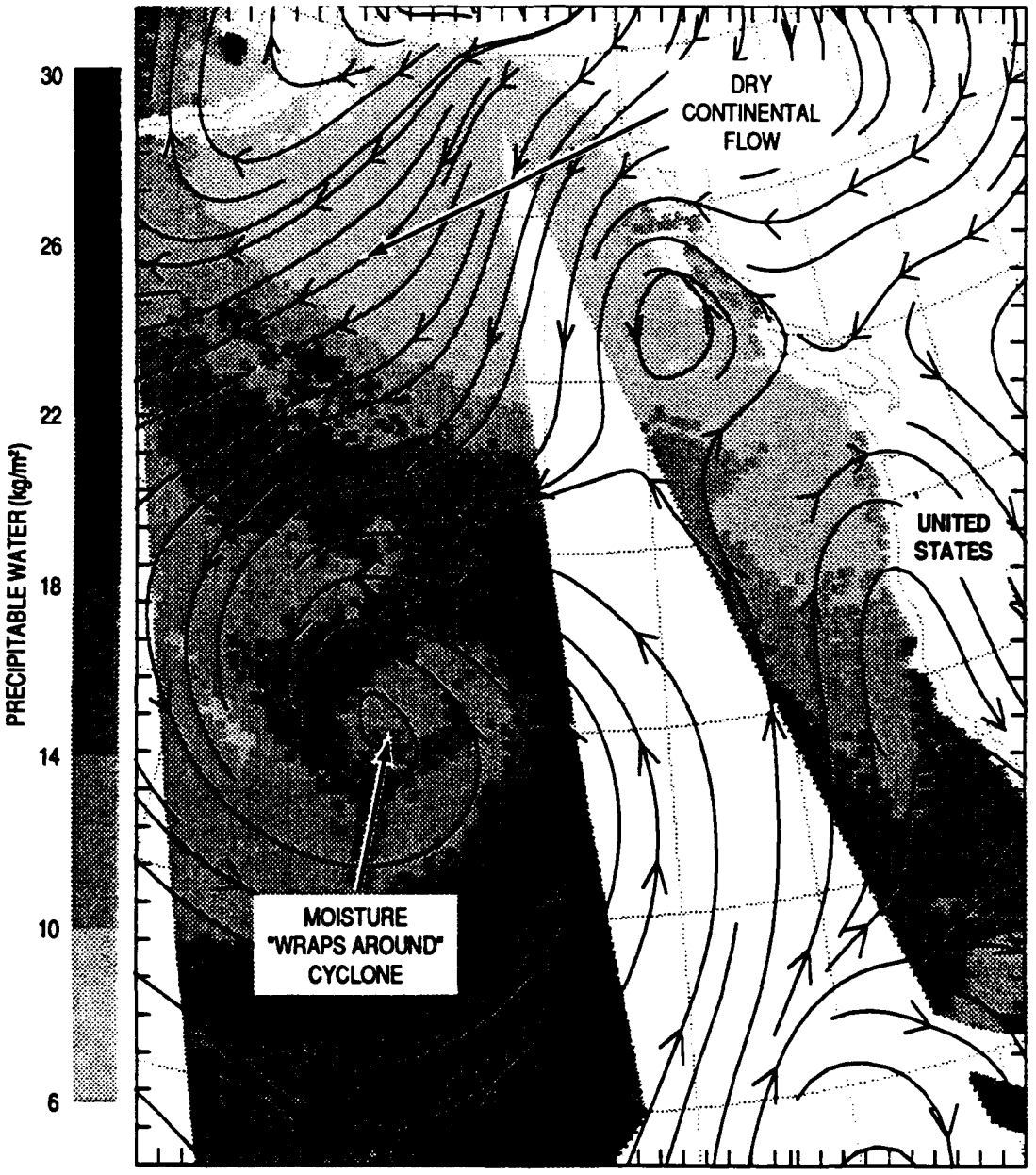
30
26
22
18
14
10
6
PRECIPITABLE WATER (kg/m²)
DRY
CONTINENTAL
FLOW
UNITED
STATES
MOISTURE
"WRAPS AROUND"
CYCLONE

Figure 17.
Grayshade display: SSM/I precipitable water analysis for 1430 UTC, 9 April 1990. Overlays: streamlines (black arrows) interpolated to 1400 UTC, 9 April 1990.

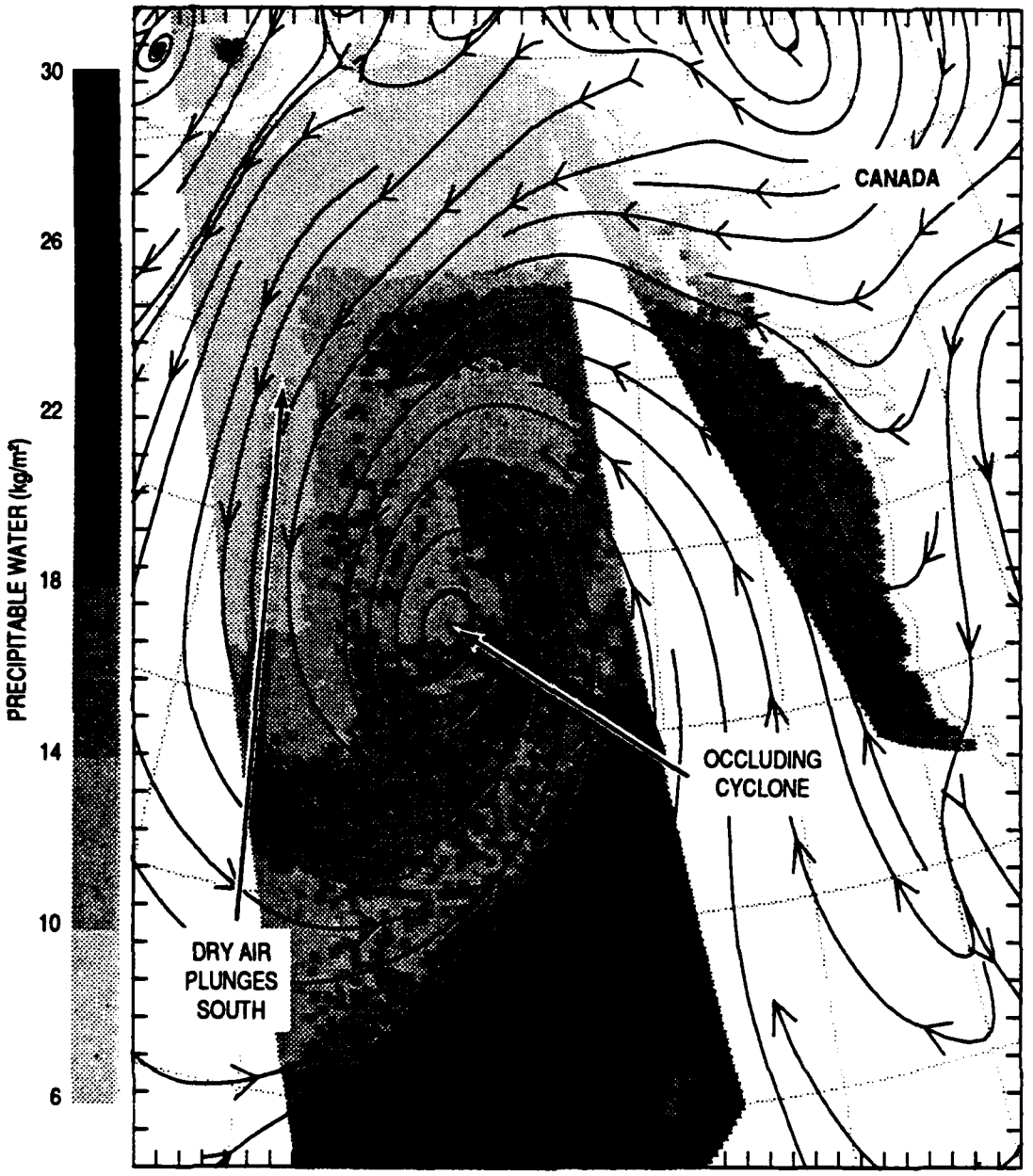
30
26
22
18
14
10
6
PRECIPITABLE WATER (kg/m²)
CANADA
OCCLUDING
CYCLONE
DRY AIR
PLUNGES
SOUTH

Figure 18.
Grayshade display: Blowup of SSM/I windspeed analysis for 1553 UTC, 29 November 1989. Overlays: marine level isotachs in m/s (black lines) and streamlines (light gray arrows) interpolated to 1600 UTC, 29 November 1989. Blank (white) regions correspond to accuracy-flagged regions or ice-covered regions.

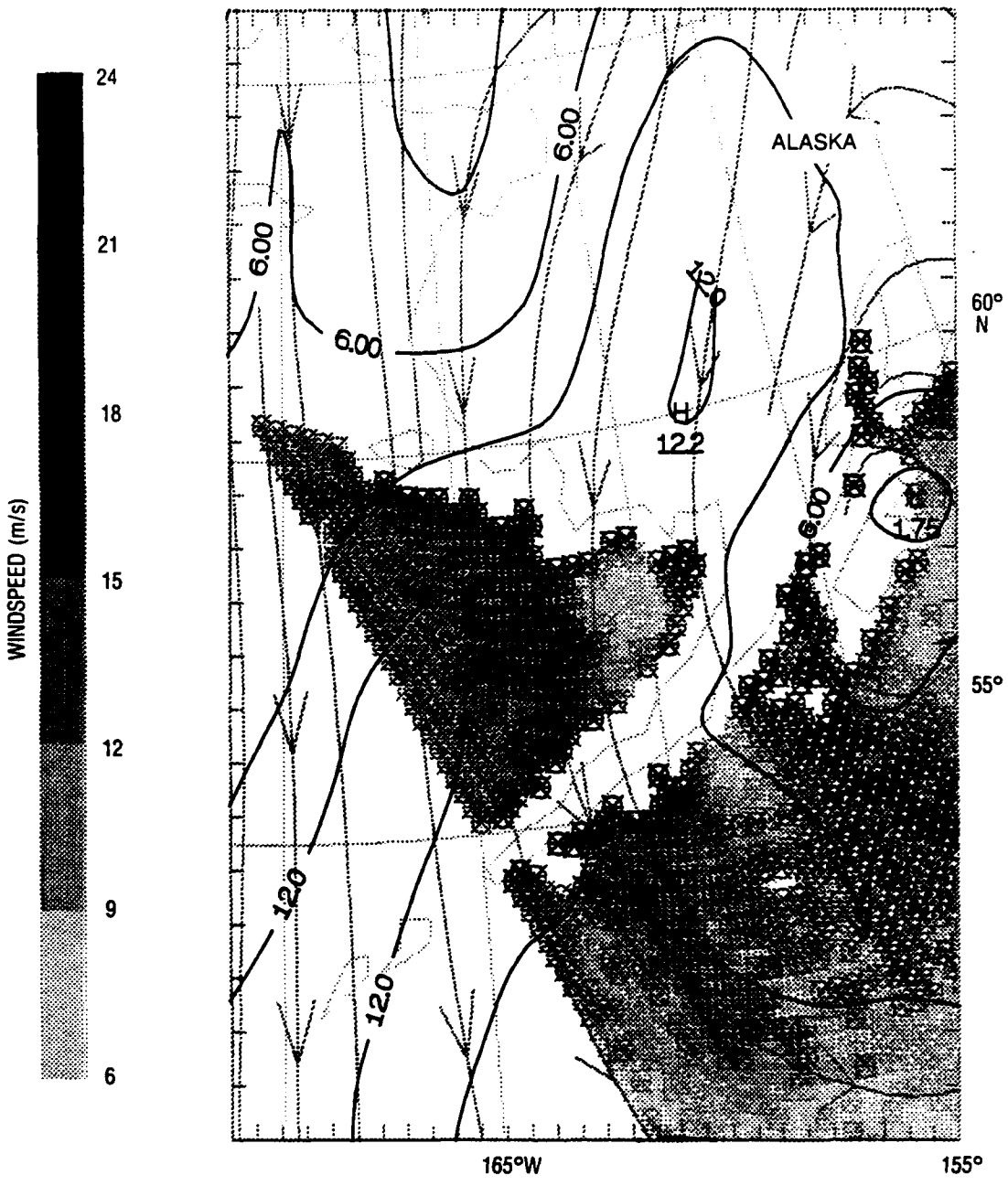
WINDSPEED (m/s)
24
21
18
15
12
9
6
ALASKA
6.00
6.00
6.00
6.00
6.00
12.0
12.0
12.2
1.75
60° N
55°
165°W
155°

Figure 19.
Topographic map of region depicted in Figure 18. Contour interval is 200 m.

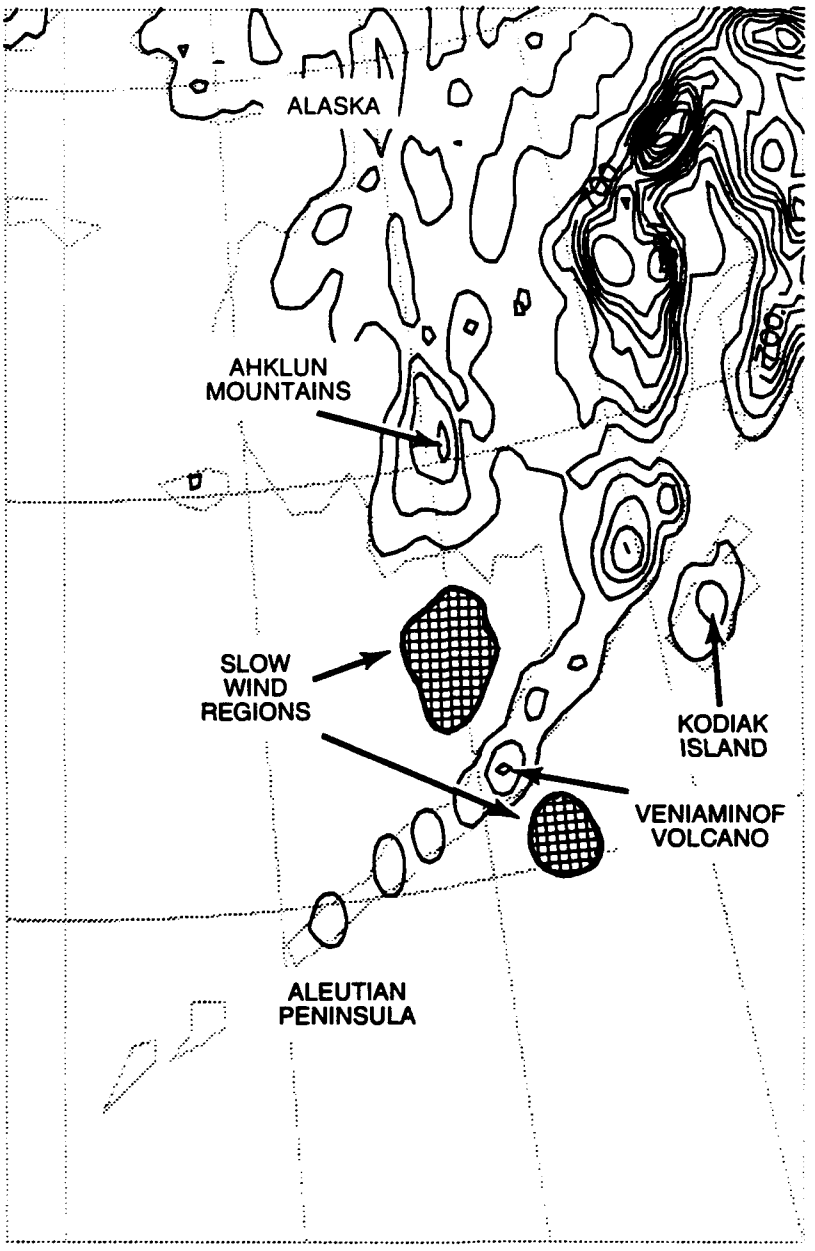
ALASKA
AHKLUN
MOUNTAINS
SLOW
WIND
REGIONS
KODIAK
ISLAND
VENIAMINOF
VOLCANO
ALEUTIAN
PENINSULA

Figure 20.
Surface chart for 1600 UTC, 3 April 1990. Isobars drawn for every 4 mb.

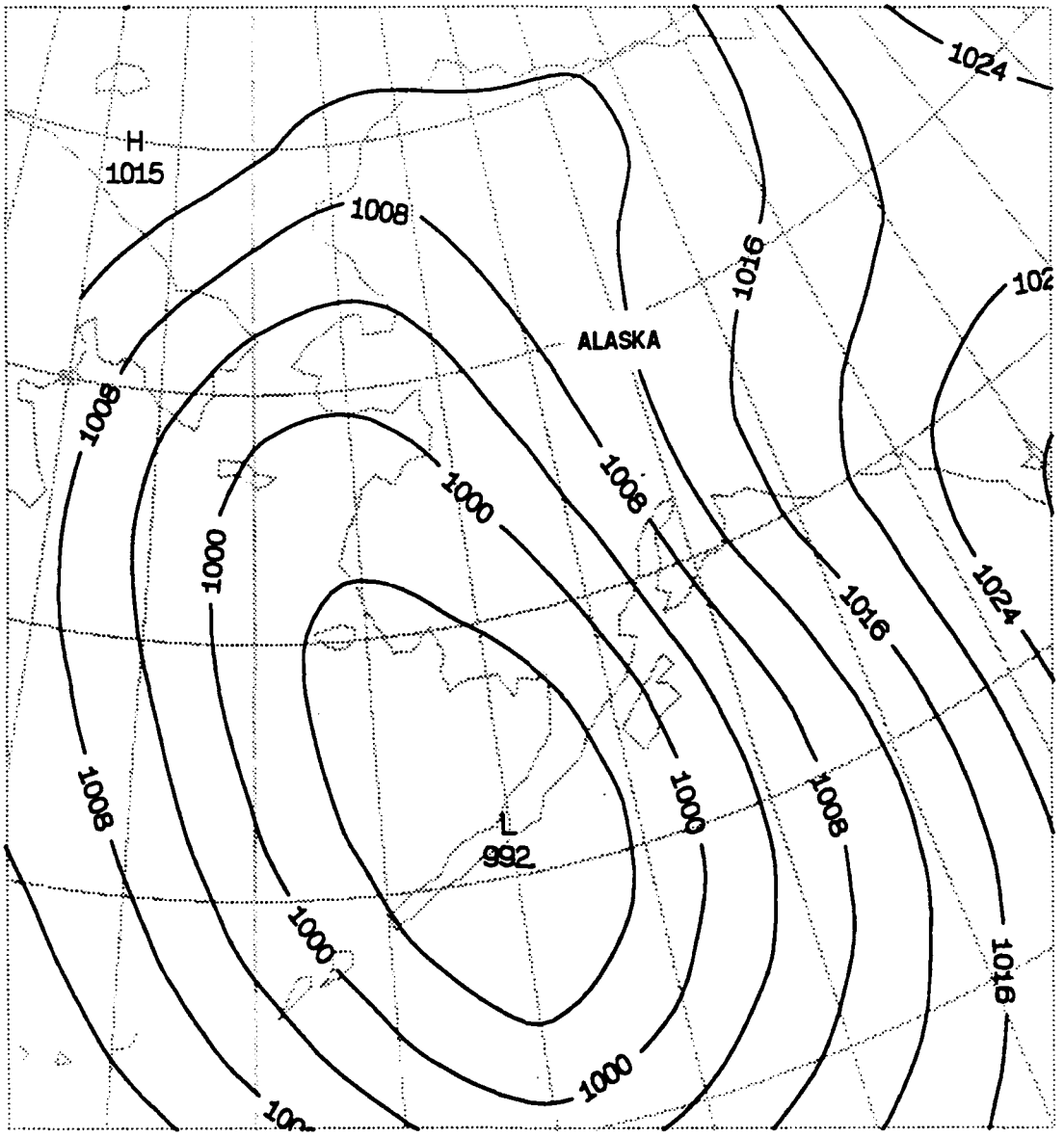
H
1015
1008
1016
1024
ALASKA
1000
1008
1016
1024
L
992
1000
1008
1016

Figure 21.
Grayshade display: SSM/I precipitable water analysis for 1600 UTC, 3 April 1990. Overlays: streamlines (black arrows) interpolated to 1600 UTC, 3 April 1990.

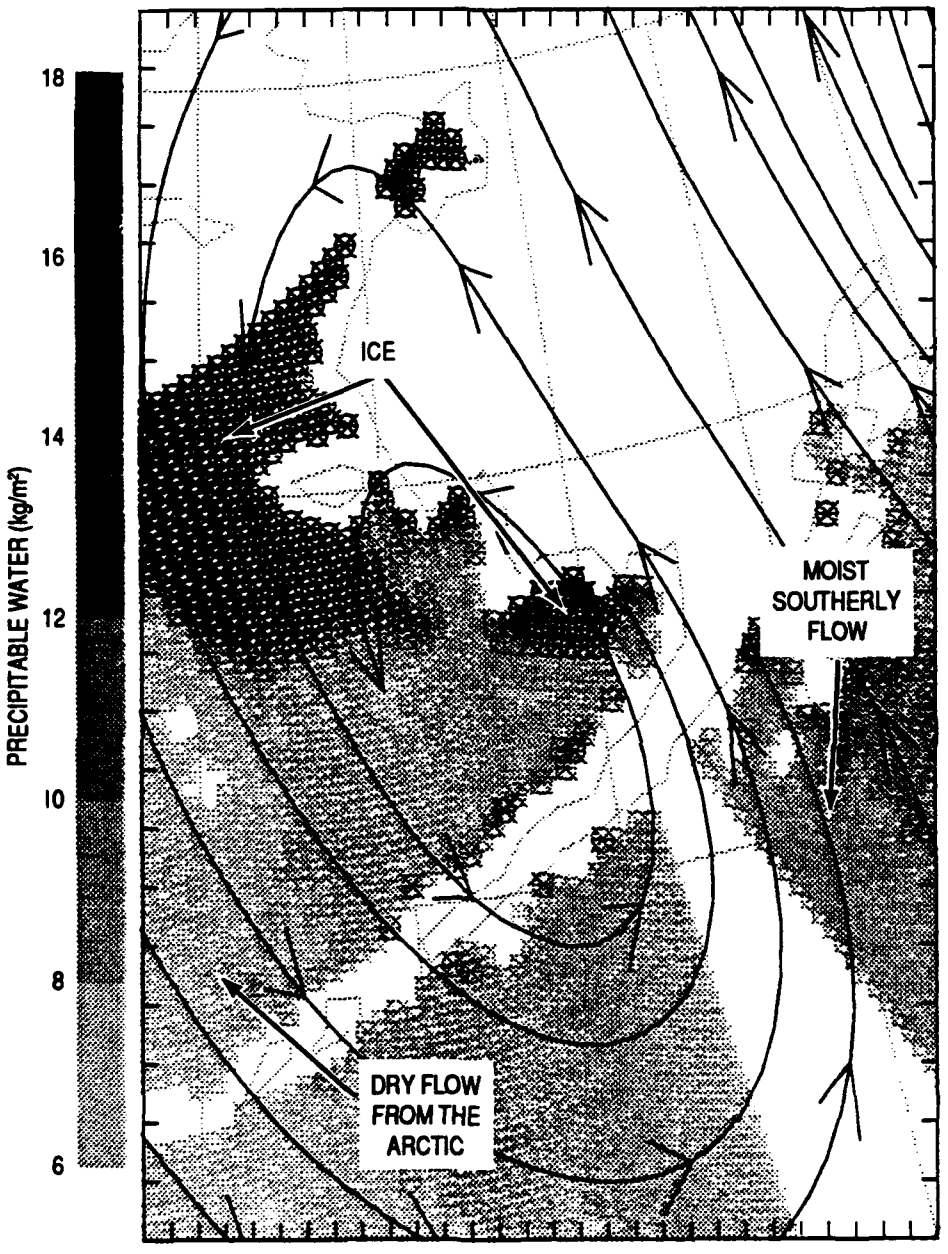
PRECIPITABLE WATER (kg/m²)
18
16
14
12
10
8
6
ICE
MOIST SOUTHERLY FLOW
DRY FLOW FROM THE ARCTIC

Figure 22.
Grayshade display: SSM/I windspeed analysis for 1600 UTC, 3 April 1990. Overlays: streamlines (light gray arrows) and isotachs in m/s (black lines) interpolated to 1600 UTC, 3 April 1990.

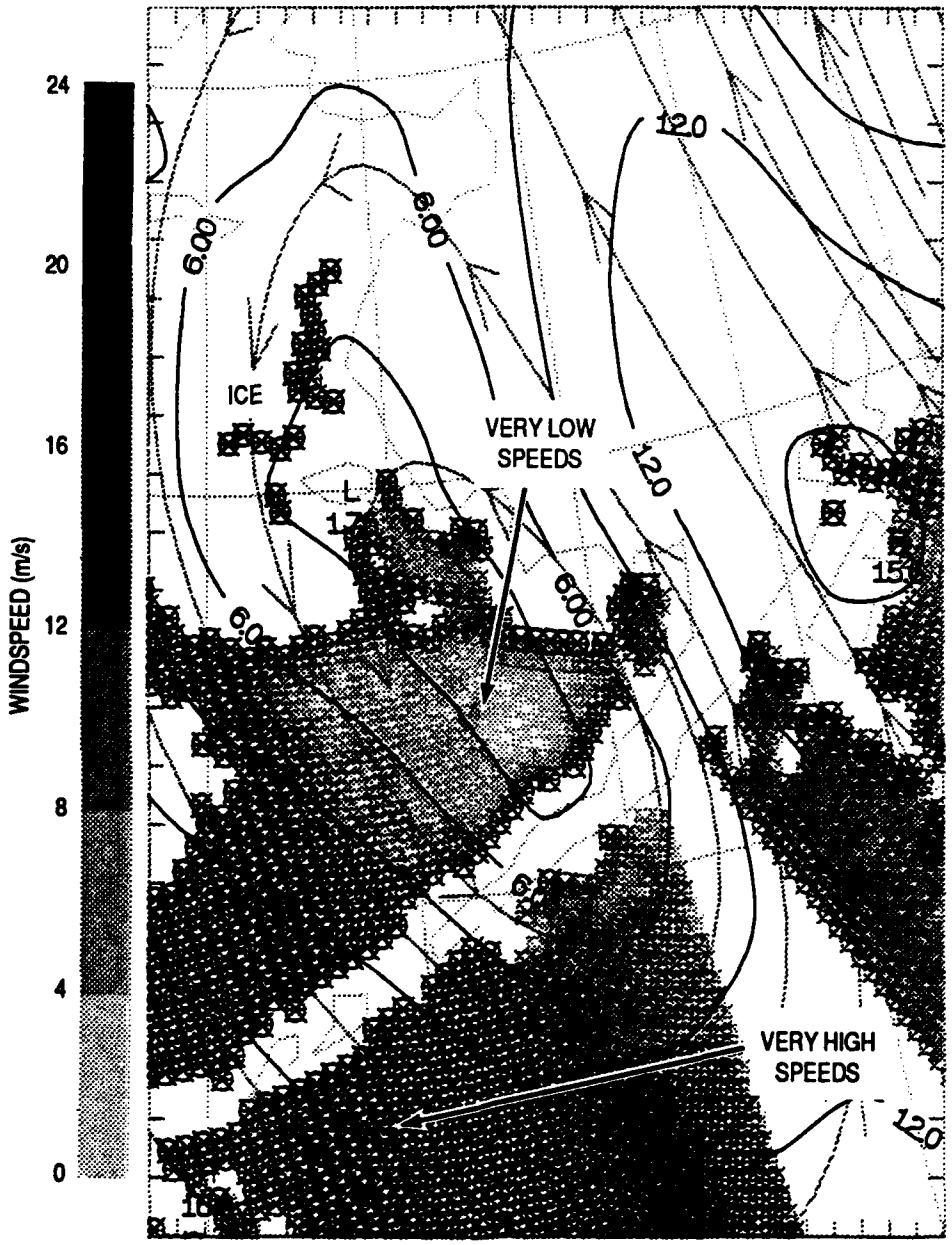
WINDSPEED (m/s)
24
20
16
12
8
4
0
ICE
VERY LOW
SPEEDS
VERY HIGH
SPEEDS
L
6.00
12.0

Figure 23.
Surface chart for 0340 UTC, 28 November 1989. Isobars drawn for every 4 mb.

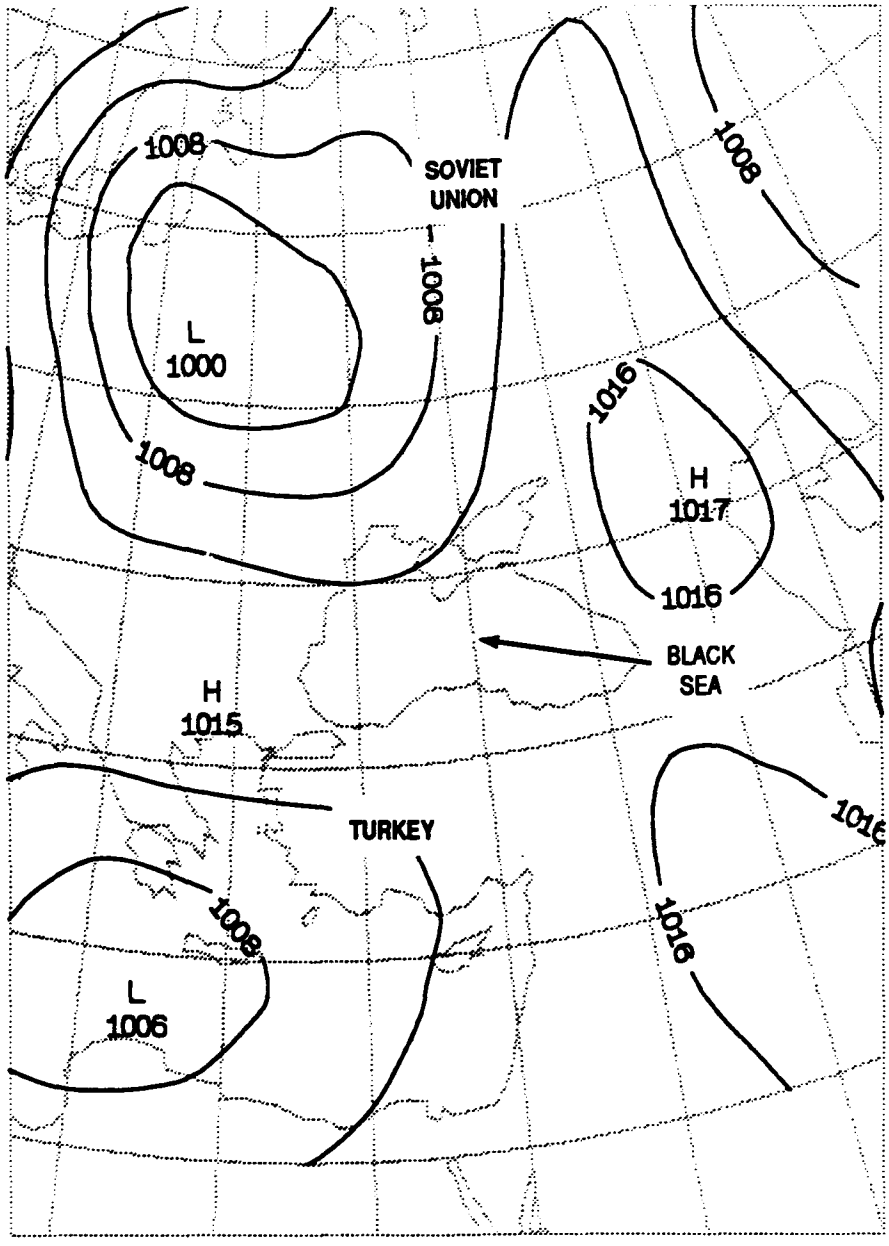
1008
SOVIET
UNION
1008
1008
L
1000
1008
1016
H
1017
1016
BLACK
SEA
H
1015
TURKEY
1016
1008
1016
L
1006

Figure 24.
Grayshade display: SSM/I windspeed analysis for 0340 UTC, 28 November 1989. Overlays: streamlines (light gray arrows) and isotachs in m/s (black lines) interpolated to 0341 UTC, 28 November 1989.

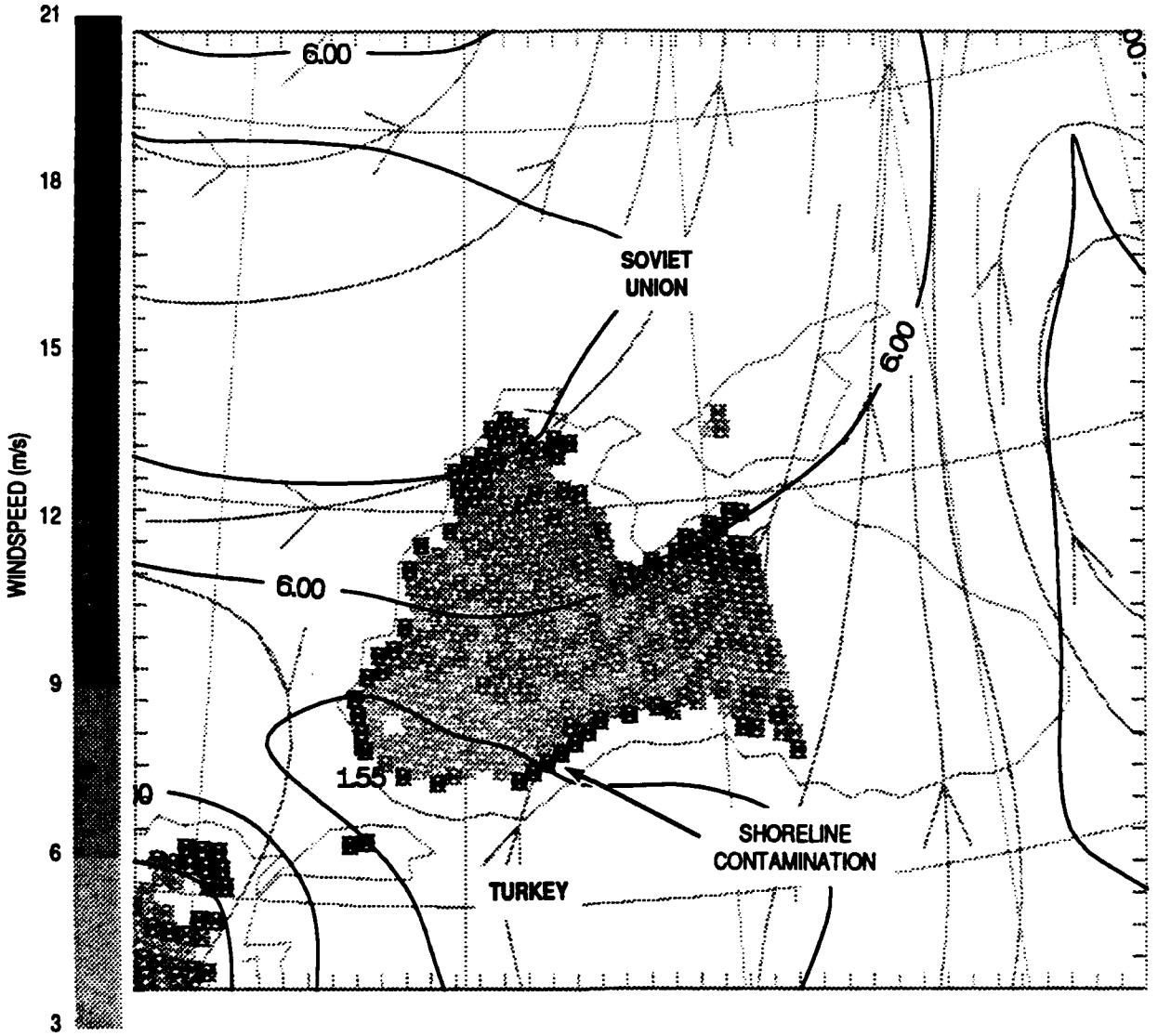
21
18
15
12
9
6
3
WINDSPEED (m/s)
6.00
SOVIET
UNION
6.00
6.00
1.55
SHORELINE
CONTAMINATION
TURKEY

Figure 25.
Surface chart for 0340 UTC, 29 November 1989. Contours drawn for every 4 mb.

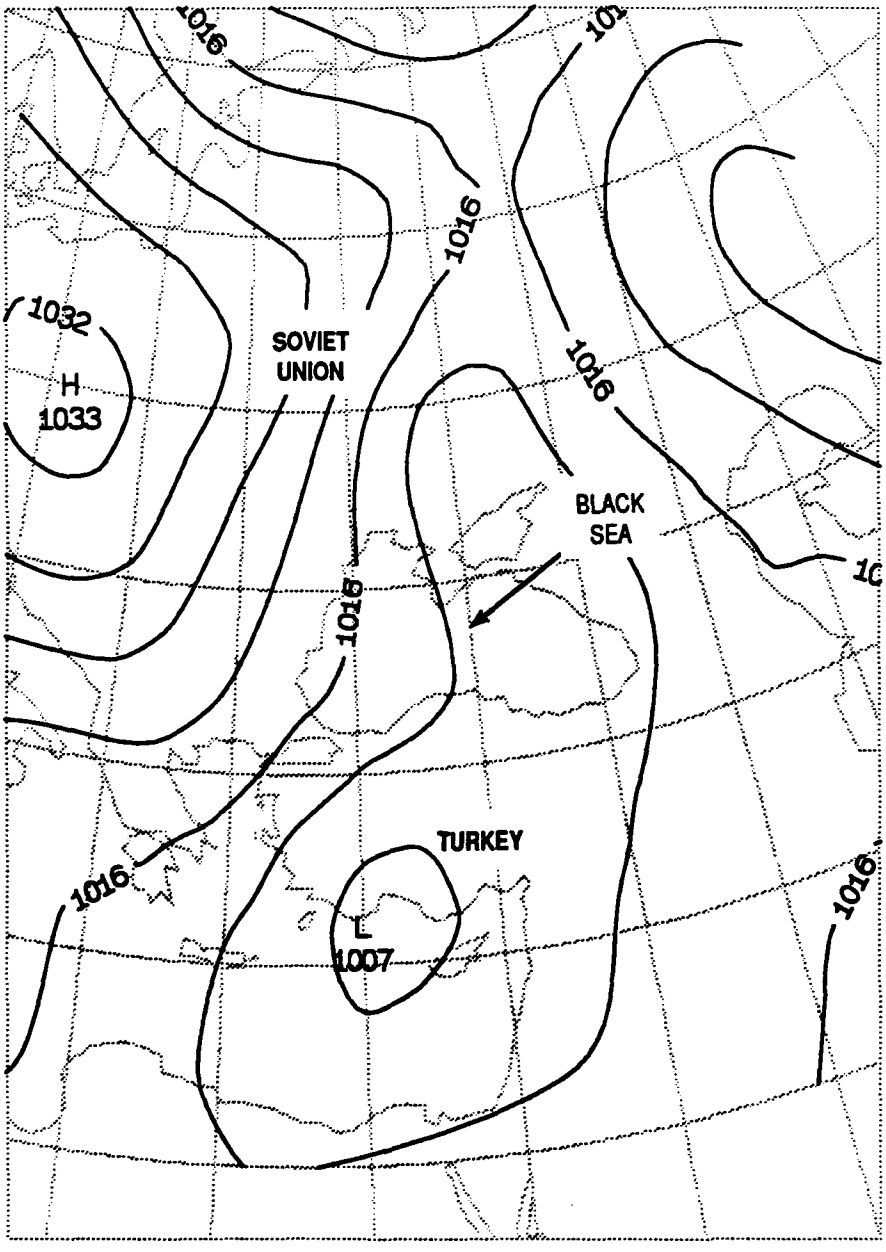
1016
1016
1016
1016
1016
1016
1016
1032
H
1033
SOVIET
UNION
BLACK
SEA
TURKEY
L
1007

Figure 26.
Grayshade display: SSM/I windspeed analysis for 0340 UTC, 29 November 1989. Overlays: streamlines (light gray arrows) and isotachs in m/s (black lines) interpolated to 0340, 29 November 1989.

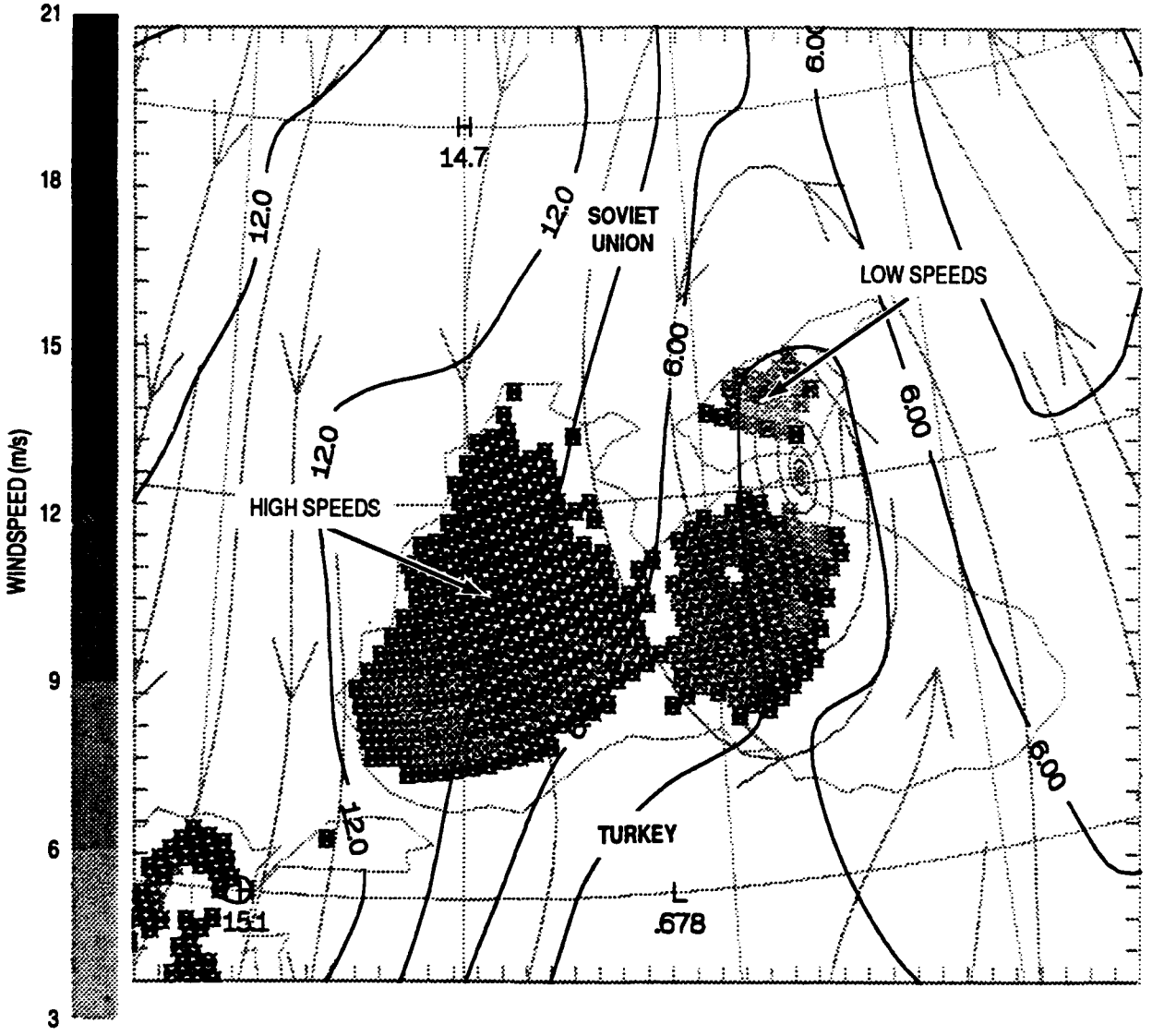
WINDSPEED (m/s)
21
18
15
12
9
6
3
H
14.7
12.0
12.0
SOVIET
UNION
6.00
LOW SPEEDS
6.00
12.0
HIGH SPEEDS
6.00
12.0
TURKEY
L
.678
15.1

Figure 27.
Grayshade display: SSM/I precipitable water analysis for 0341 UTC, 29 November 1989. Overlay: streamlines (black arrows) interpolated to 0340 UTC, 29 November 1989.

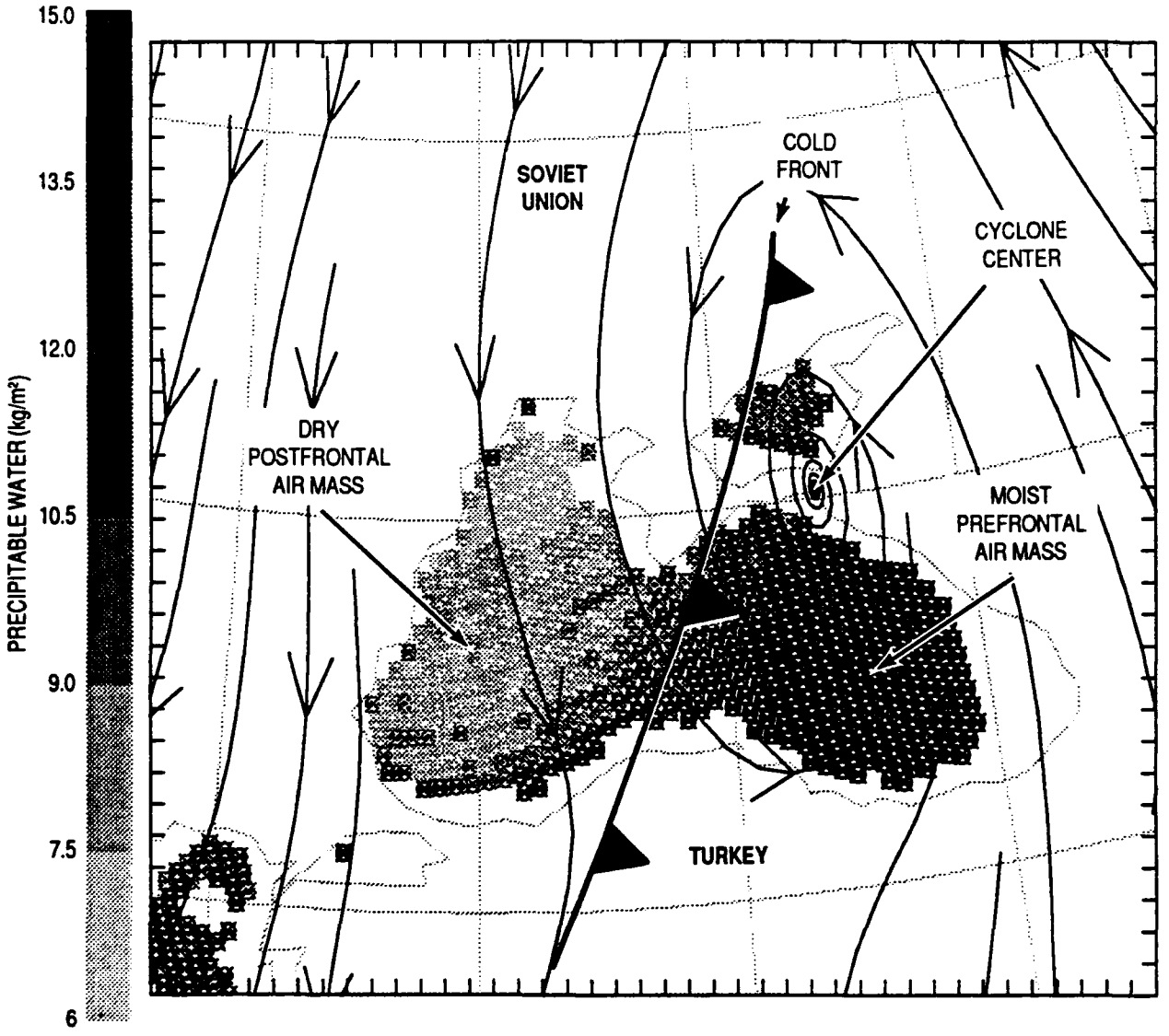
15.0
13.5
12.0
10.5
9.0
7.5
6
PRECIPITABLE WATER (kg/m²)
SOVIET UNION
COLD FRONT
CYCLONE CENTER
DRY POSTFRONTAL AIR MASS
MOIST PREFRONTAL AIR MASS
TURKEY

Figure 28.
SSM/I precipitation rate for 0341 UTC, 29 November 1989.

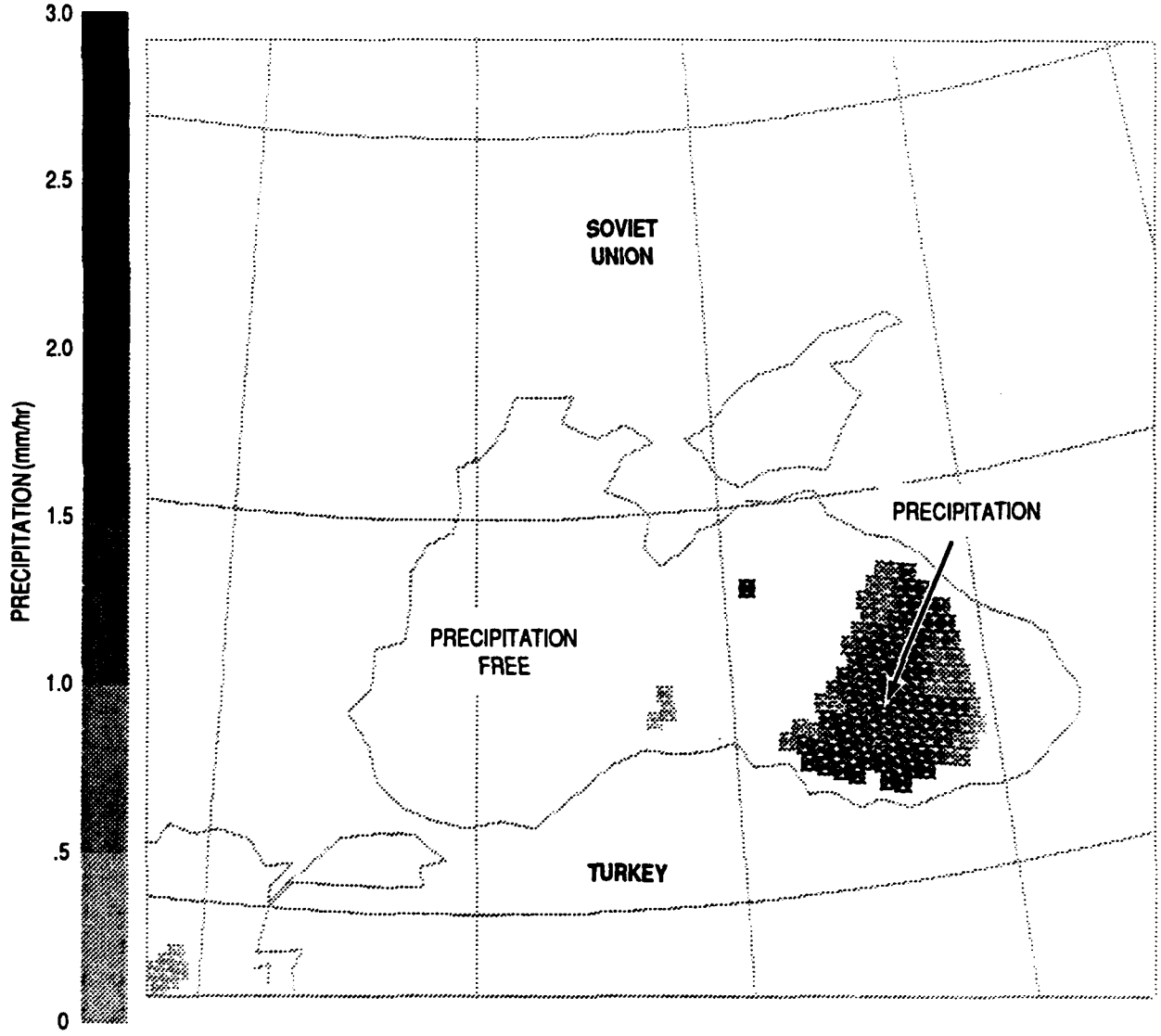
3.0
2.5
2.0
1.5
1.0
.5
0
PRECIPITATION (mm/hr)
SOVIET
UNION
PRECIPITATION
PRECIPITATION
FREE
TURKEY

Figure 29.
Surface chart for 1200 UTC, 10 April 1990. Isobars drawn for every 4 mb.

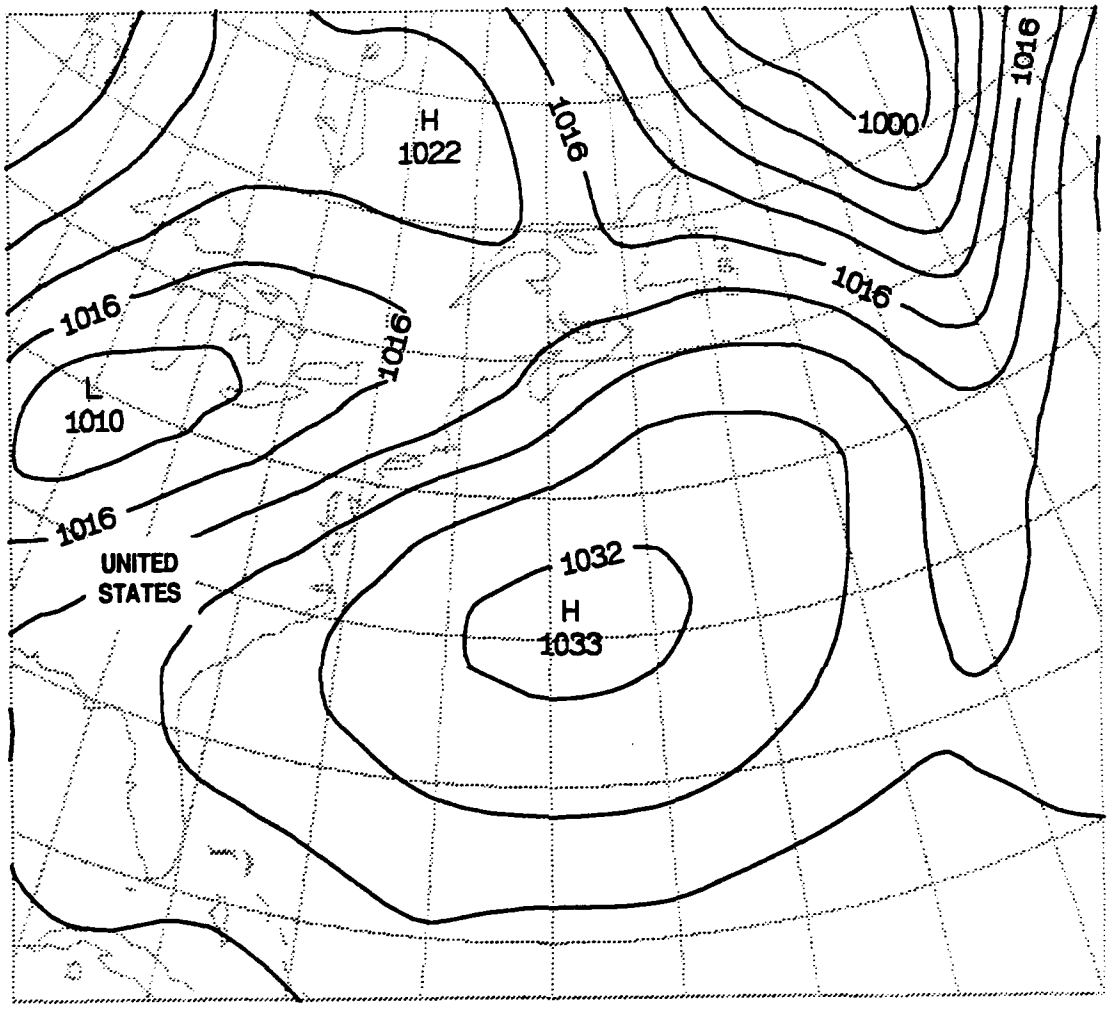
H
1022
1016
1000
1016
1016
1016
L
1010
1016
1016
UNITED
STATES
1032
H
1033

Figure 30.
Grayshade display: SSM/I precipitable water analysis for 1100 UTC, 10 April 1990. Overlay: streamlines (black arrows) interpolated to 1200 UTC, 10 April 1990.

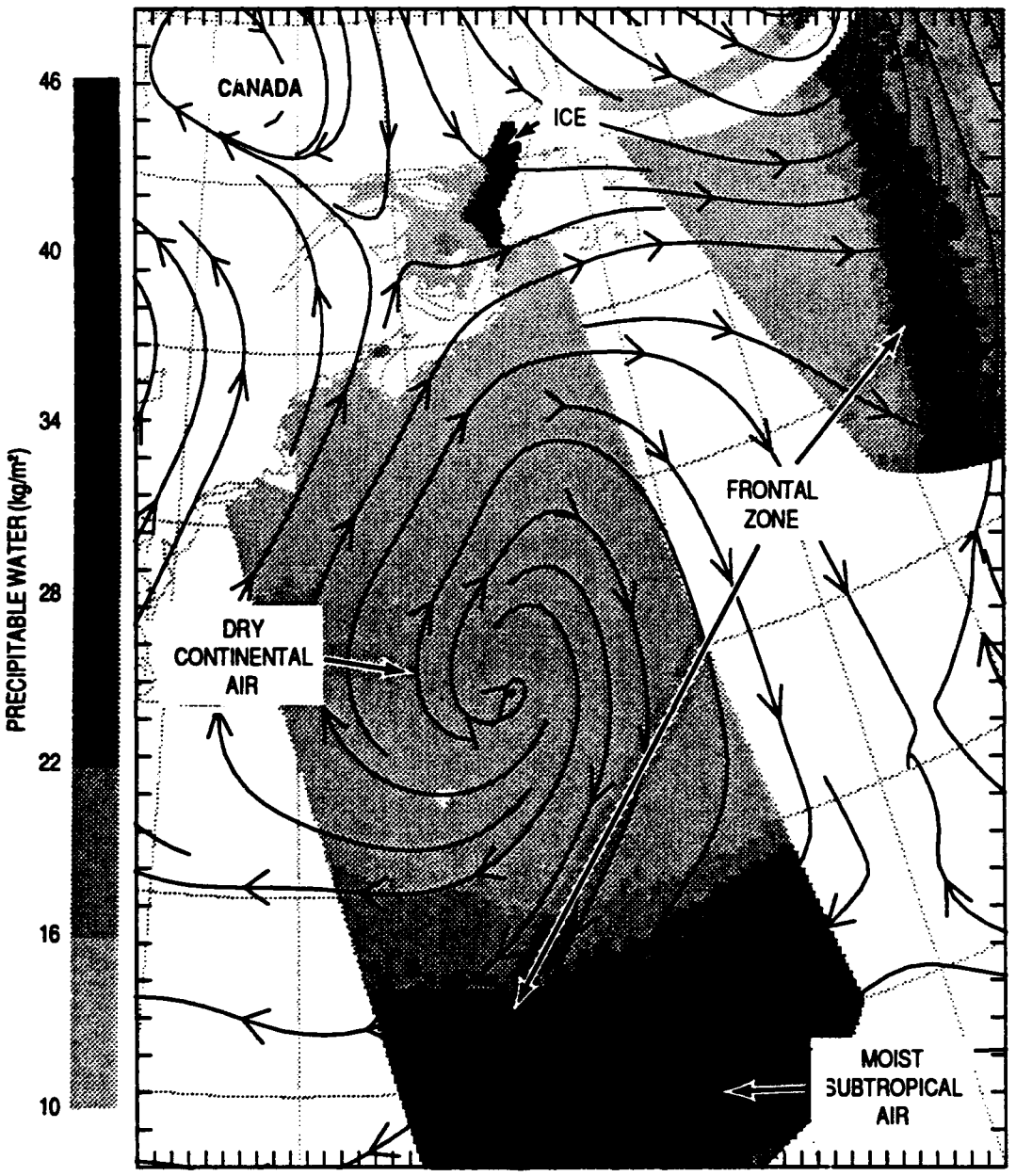
PRECIPITABLE WATER (kg/m²)
46
40
34
28
22
16
10
CANADA
ICE
FRONTAL ZONE
DRY CONTINENTAL AIR
MOIST SUBTROPICAL AIR

Figure 31.
Grayshade display: SSM/I windspeed analysis for 1100 UTC, 10 April 1990. Overlay: streamlines (black arrows) interpolated to 1200 UTC, 10 April 1990.

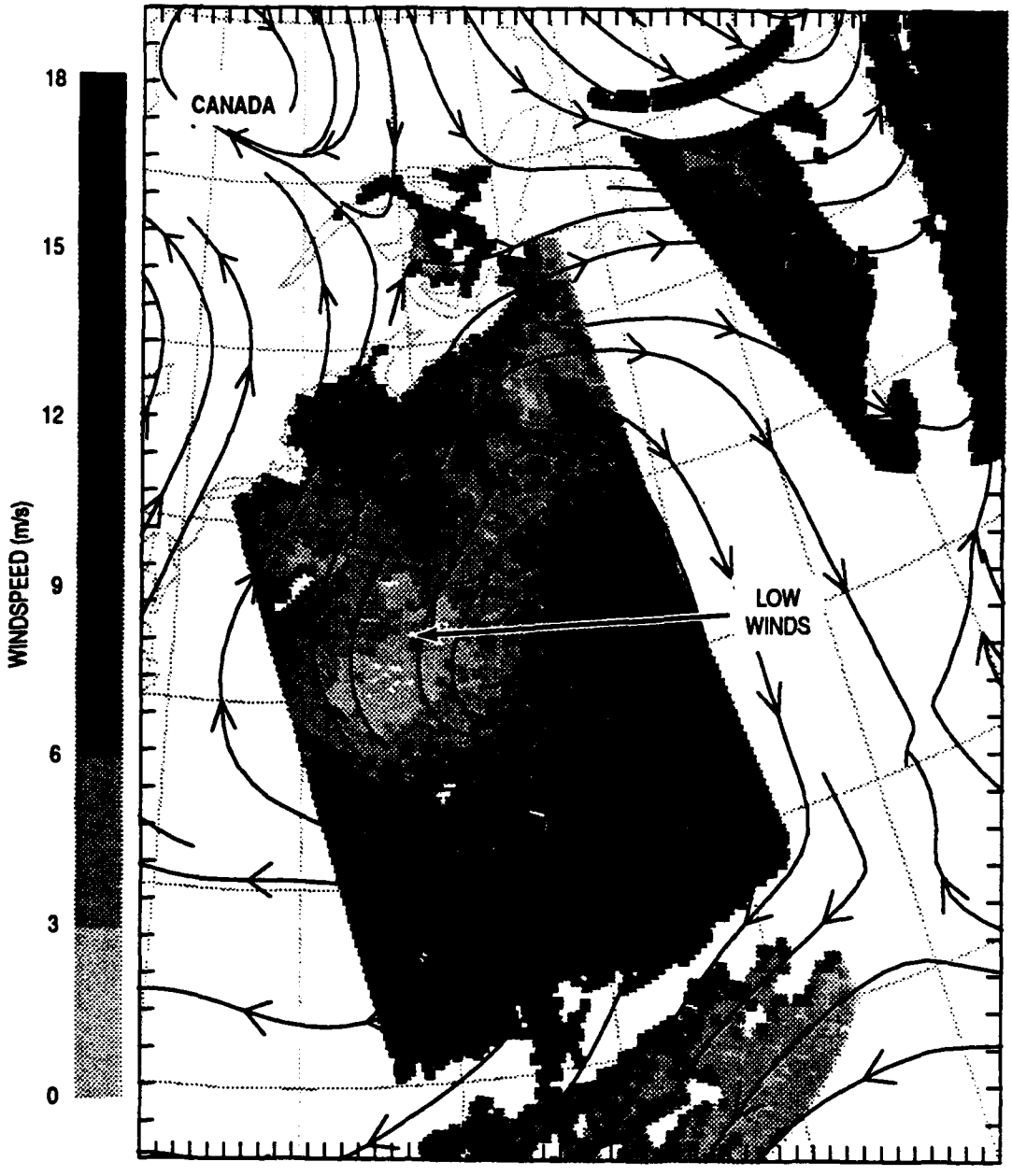
18
15
12
9
6
3
0
WINDSPEED (m/s)
CANADA
LOW
WINDS

Figure 32.
Grayshade display: SSM/I precipitation rate for 1100 UTC, 10 April 1990.

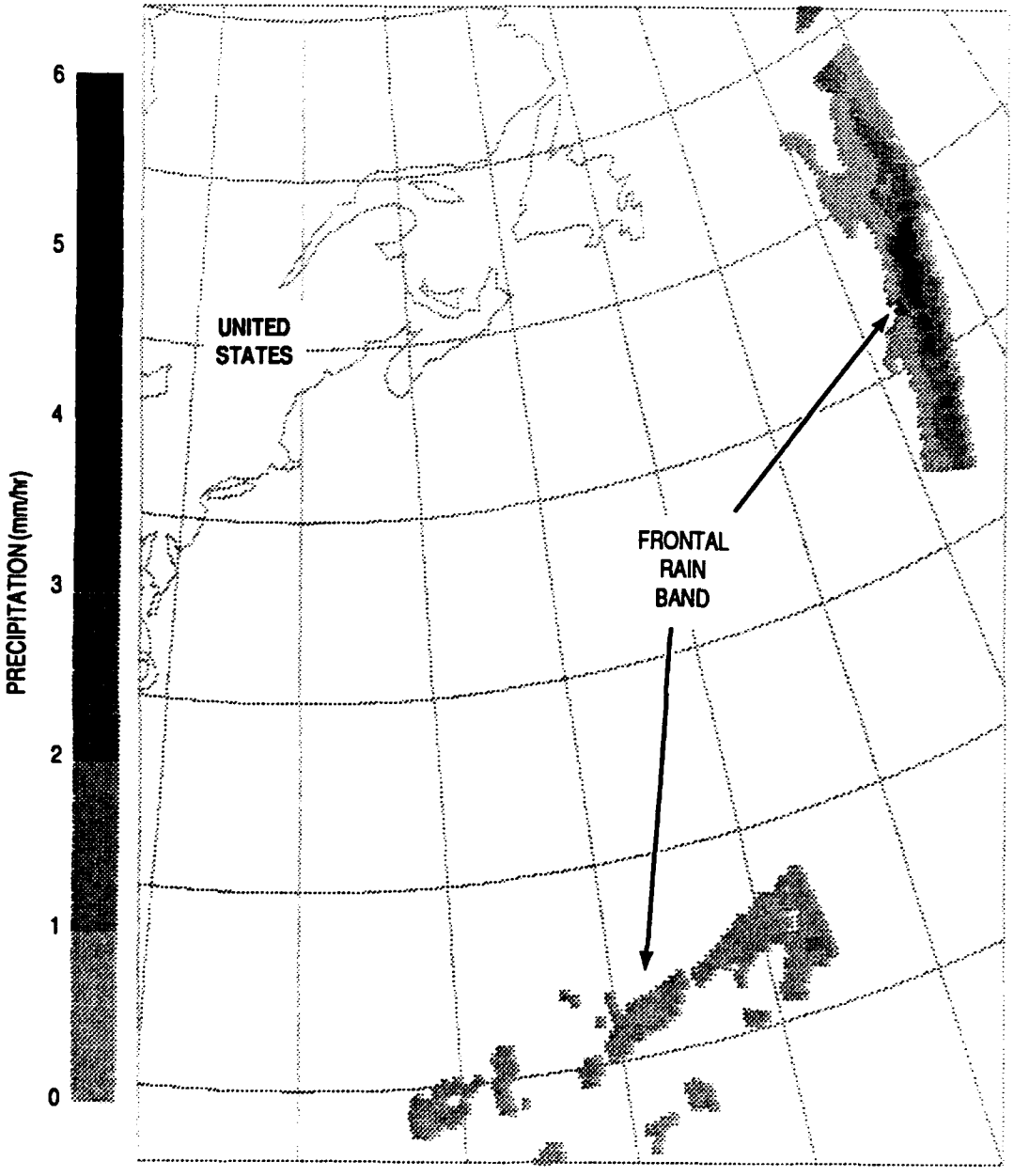
PRECIPITATION (mm/hr)
6
5
4
3
2
1
0
UNITED STATES
FRONTAL RAIN BAND

Figure 33.
Vertical motion for 1200 UTC, 10 April 1990. Contours drawn in units of microbars/second. Negative values indicate rising air at 700 mb; positive values indicate descending air at 700 mb.

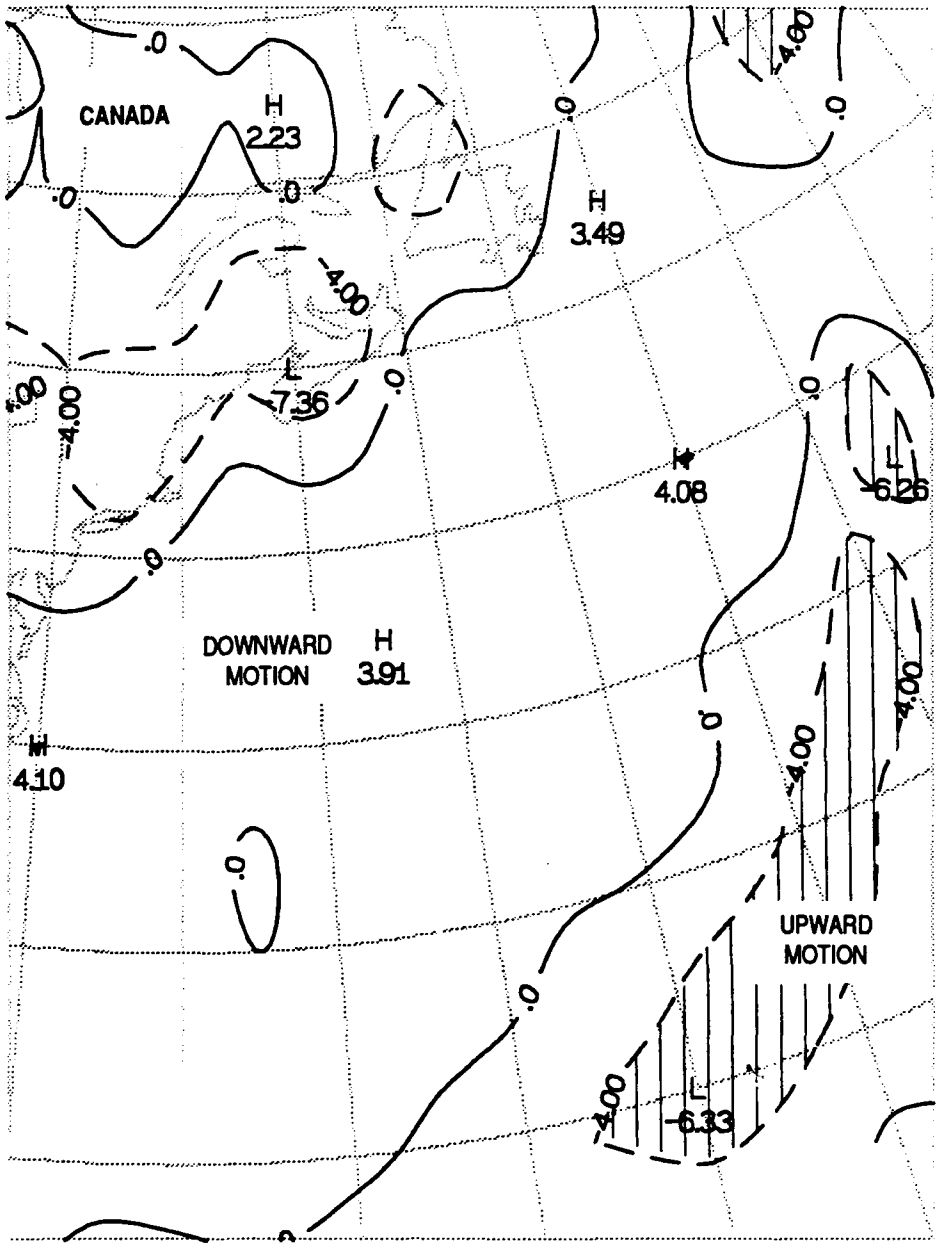
CANADA
H
2.23
H
3.49
L
-7.36
H
4.08
L
-6.26
DOWNWARD
MOTION
H
3.91
H
4.10
UPWARD
MOTION
L
-6.33
.0
-4.00

Figure 34.
Surface chart for 2200 UTC, 10 April 1990. Isobars drawn for every 4 mb.

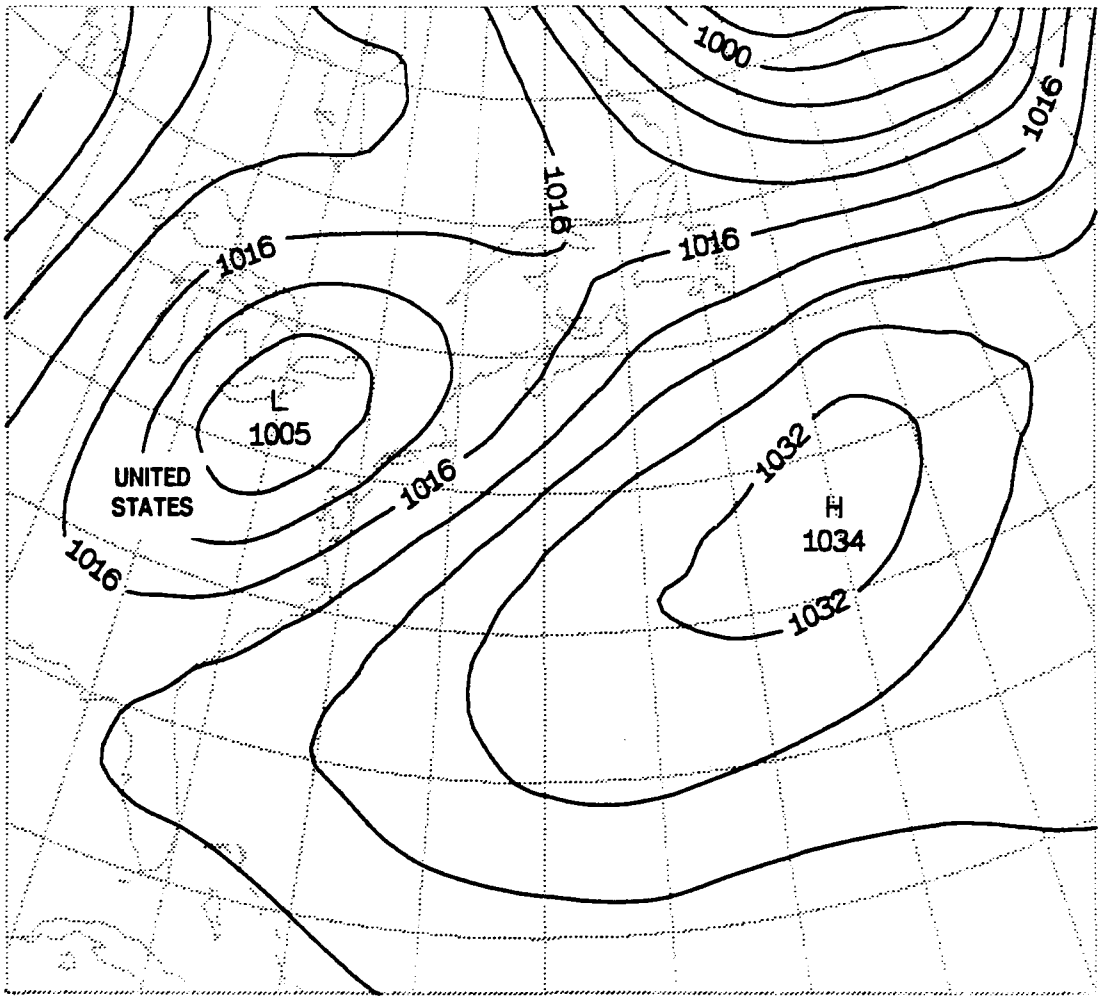
1000
1016
1016
1016
1016
1016
1016
L
1005
UNITED
STATES
1032
H
1034
1032

Figure 35.
Grayshade display: SSM/I precipitable water analysis for 2300 UTC, 10 April 1990. Overlay: streamlines (black arrows) interpolated to 2200 UTC, 10 April 1990.

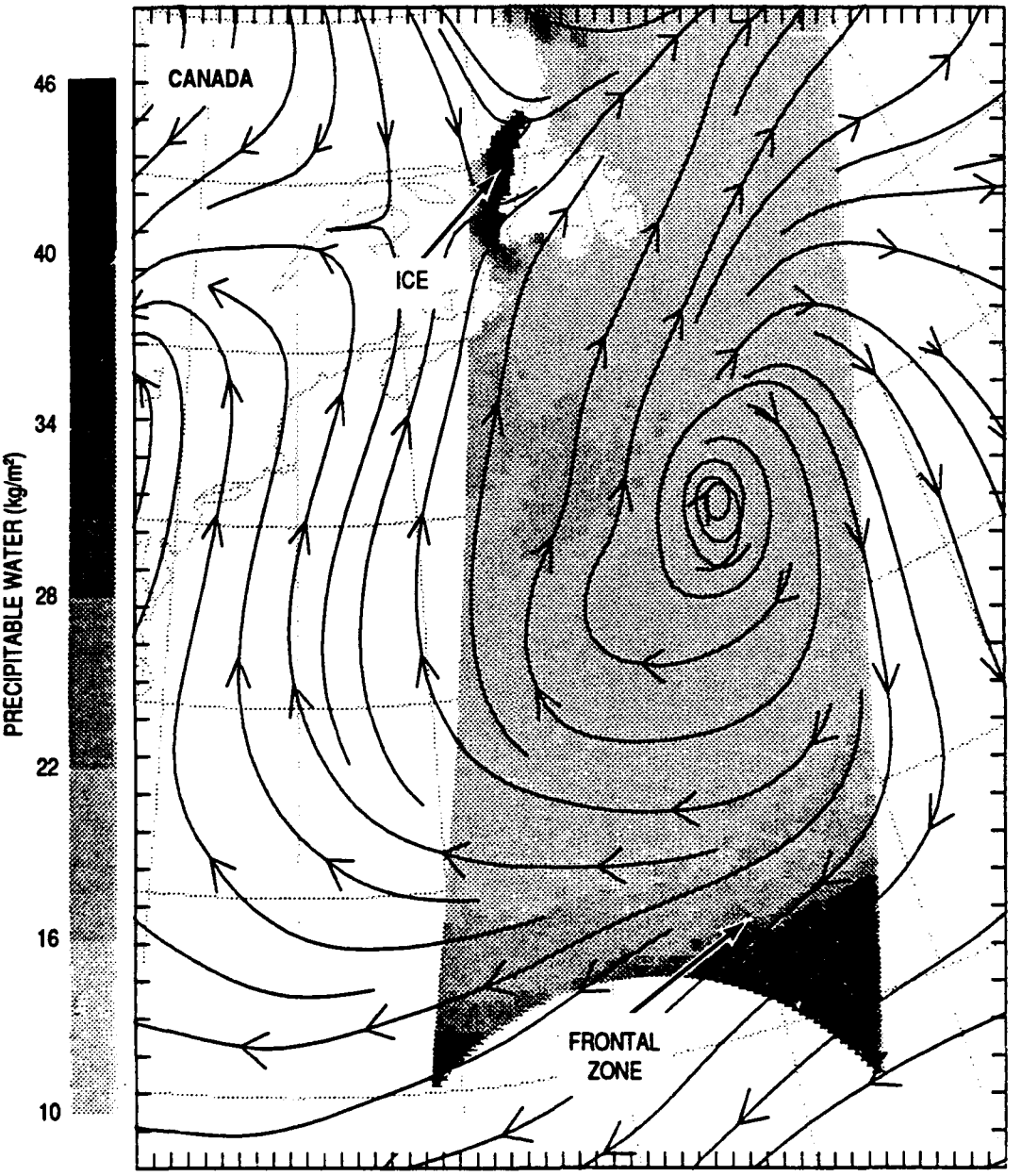
CANADA
ICE
FRONTAL
ZONE
PRECIPITABLE WATER (kg/m²)
46
40
34
28
22
16
10

Figure 36.
Grayshade display: SSM/I precipitable water analysis for 2300 UTC, 10 April 1990. Overlay: NOGAPS isopleths of precipitable water (kg/m^2) for 2200 UTC, 10 April 1990.

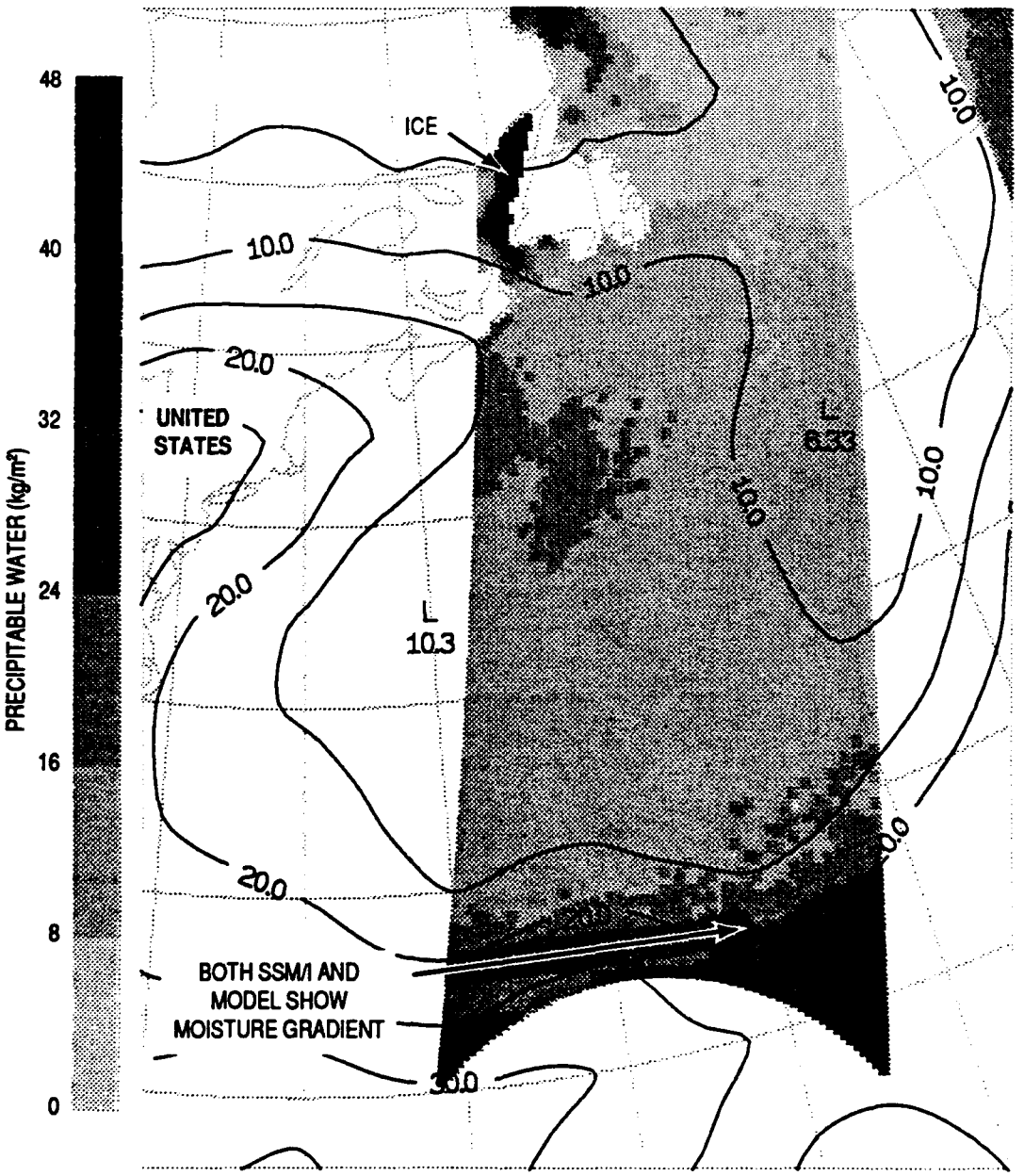
PRECIPITABLE WATER (kg/m²)
48
40
32
24
16
8
0
ICE
10.0
10.0
20.0
UNITED STATES
L
8.33
10.0
10.0
20.0
L
10.3
20.0
BOTH SSM/I AND MODEL SHOW MOISTURE GRADIENT
30.0

Figure 37.
Grayshade display: SSM/I windspeed analysis for 2300 UTC, 10 April 1990. Overlay: streamlines (black arrows) interpolated to 2200 UTC, 10 April 1990.

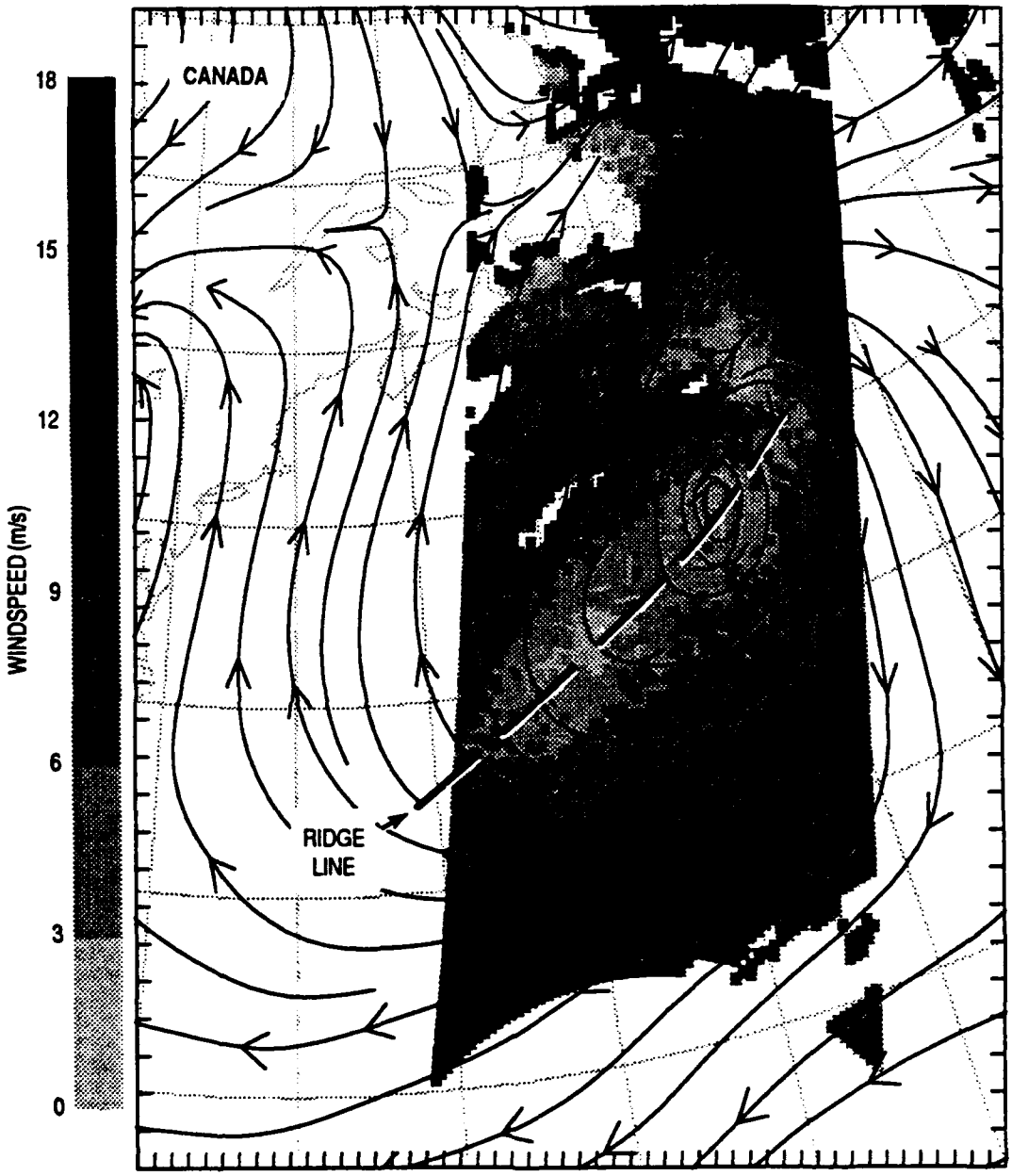
CANADA
RIDGE
LINE
WINDSPEED (m/s)
18
15
12
9
6
3
0

Figure 38.
Surface chart for 1200 UTC, 11 April 1990. Isobars drawn for every 4 mb.

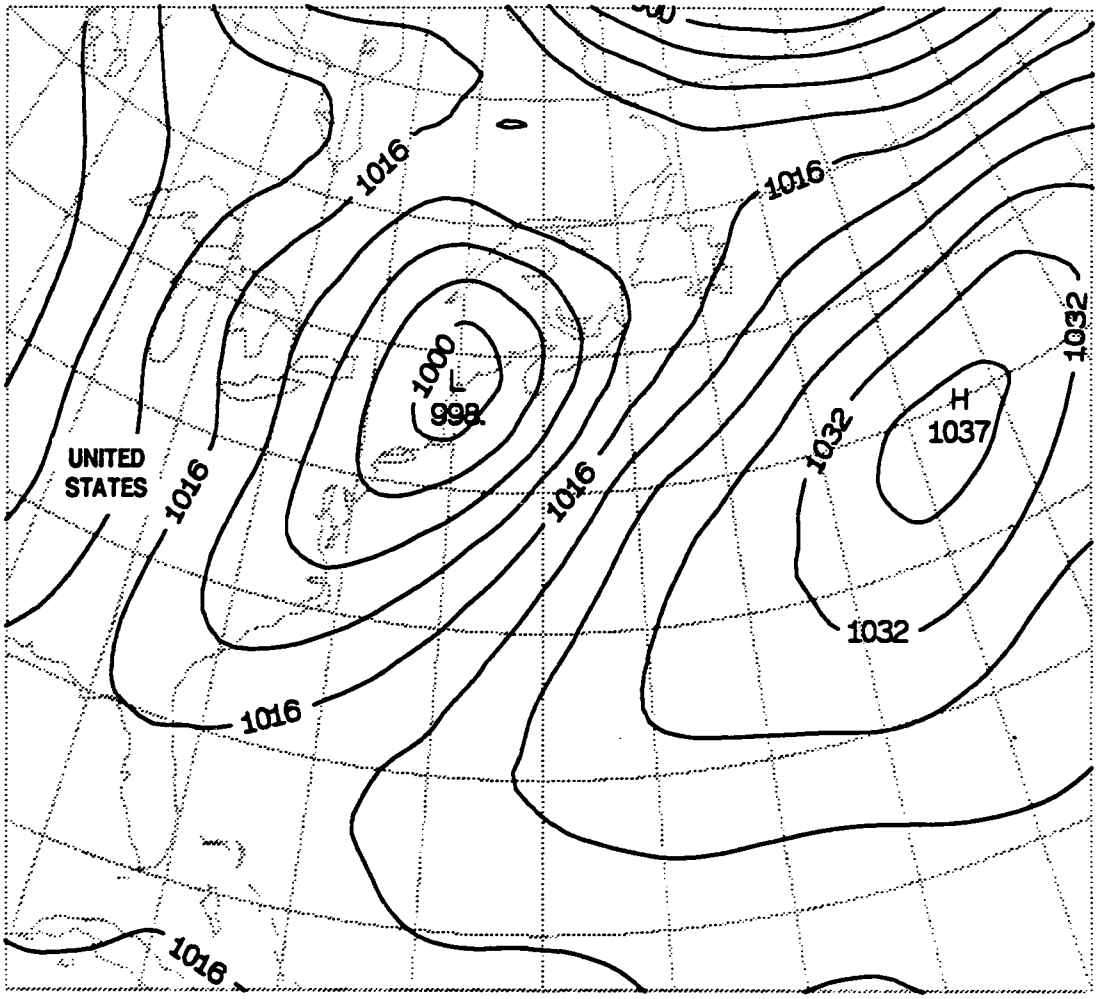
1016
1016
1000
L
998
H
1037
1032
1032
1032
UNITED
STATES
1016
1016
1016
1016

Figure 39.
Grayshade display: SSM/I precipitable water analysis for 1100 UTC, 11 April 1990. Overlay: streamlines (black arrows) valid at 1200 UTC, 11 April 1990.

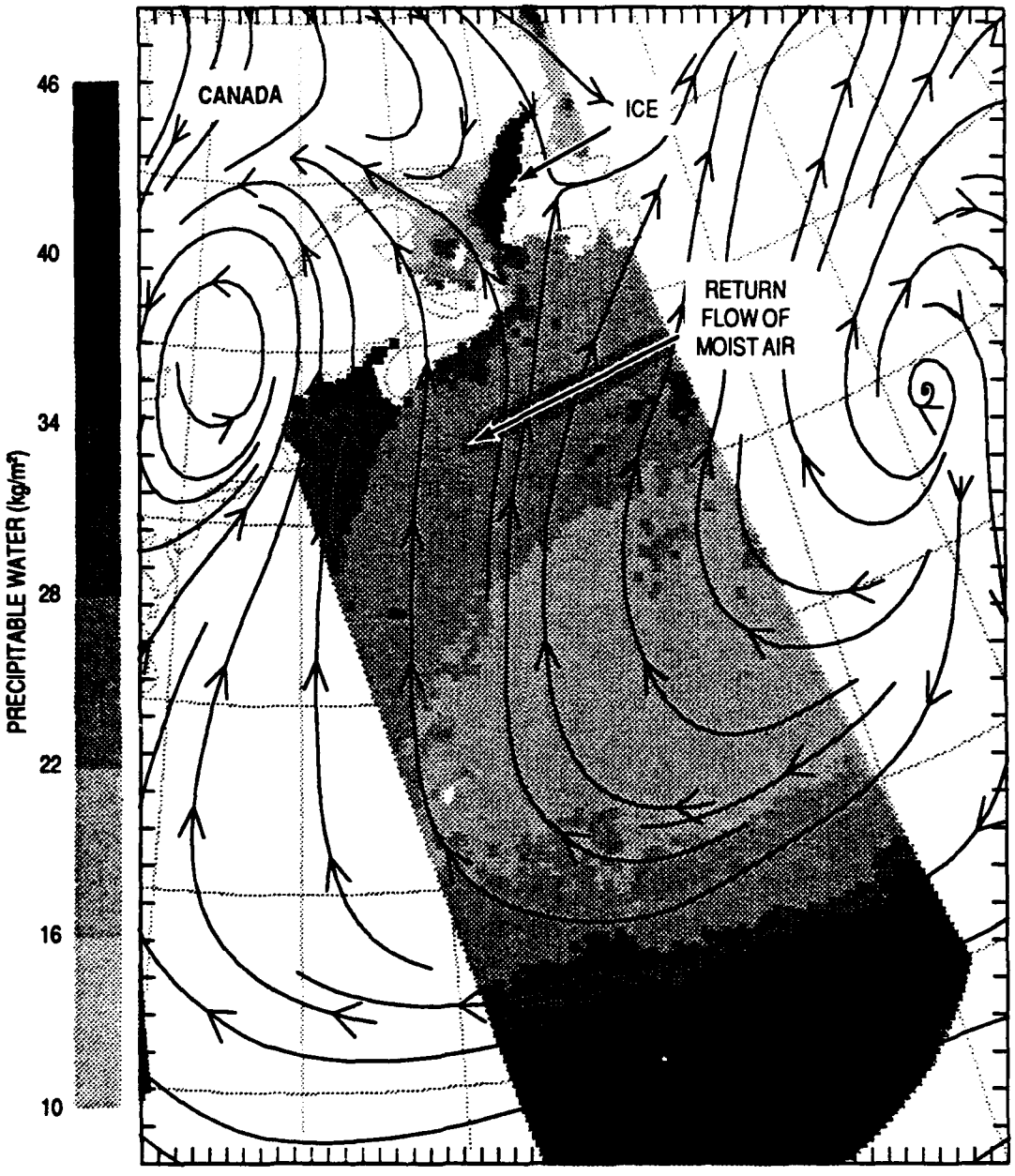
CANADA
ICE
RETURN
FLOW OF
MOIST AIR
PRECIPITABLE WATER (kg/m²)
46
40
34
28
22
16
10

Figure 40.
Grayshade display: SSM/I precipitable water analysis for 1100 UTC, 11 April 1990. Overlay: NOGAPS isopleths of precipitable water (kg/m^2) valid at 1200 UTC, 11 April 1990.

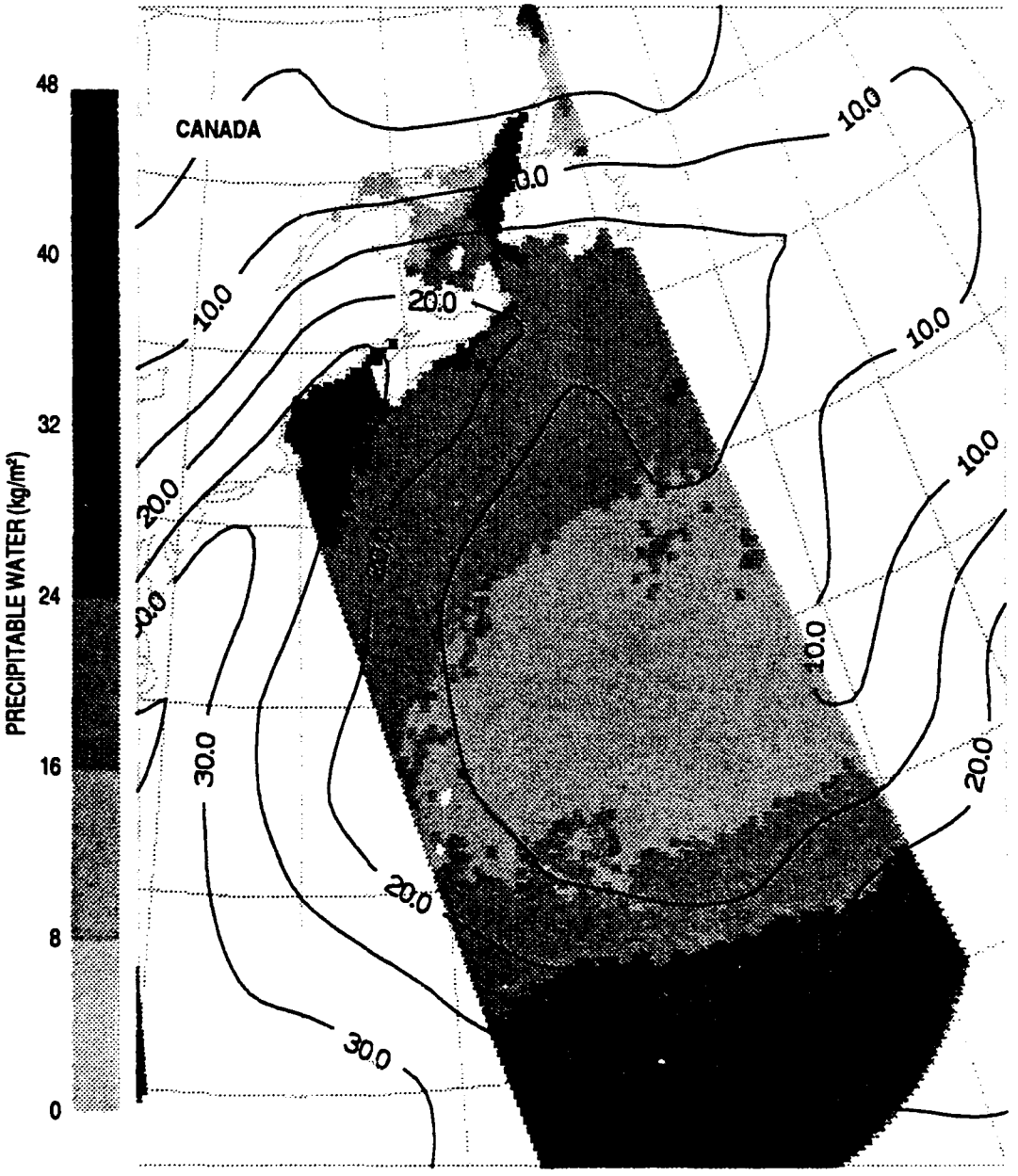
PRECIPITABLE WATER (kg/m²)
48
40
32
24
16
8
0
CANADA
10.0
20.0
30.0

Figure 41.
Grayshade display: SSM/I windspeed analysis for 1100 UTC, 11 April 1990. Overlay: streamlines (black arrows) valid at 1200 UTC, 11 April 1990.

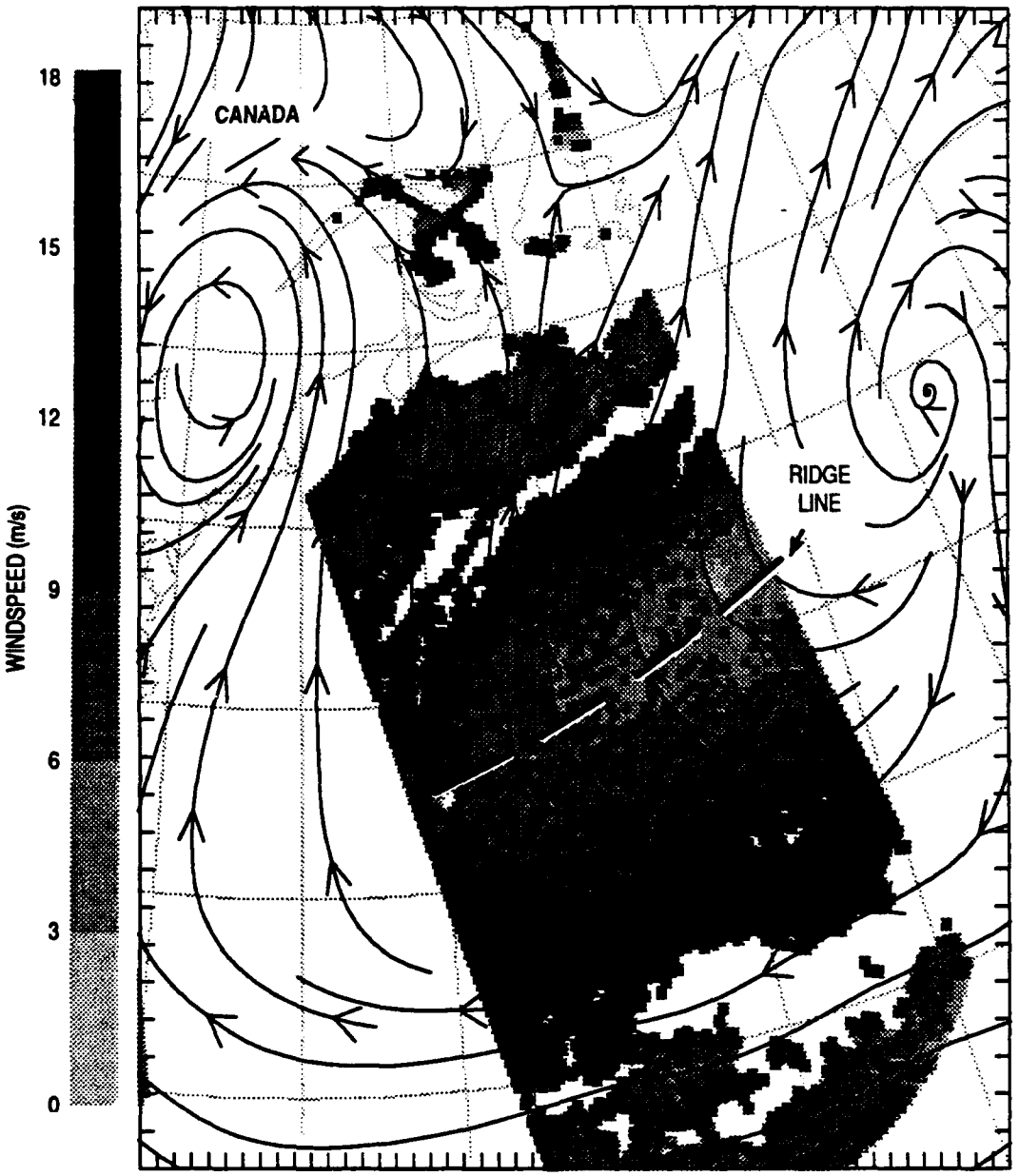
18
15
12
9
6
3
0
WINDSPEED (m/s)
CANADA
RIDGE
LINE

Figure 42.
Surface chart for 2200 UTC, 11 April 1990. Isobars drawn for every 4 mb.

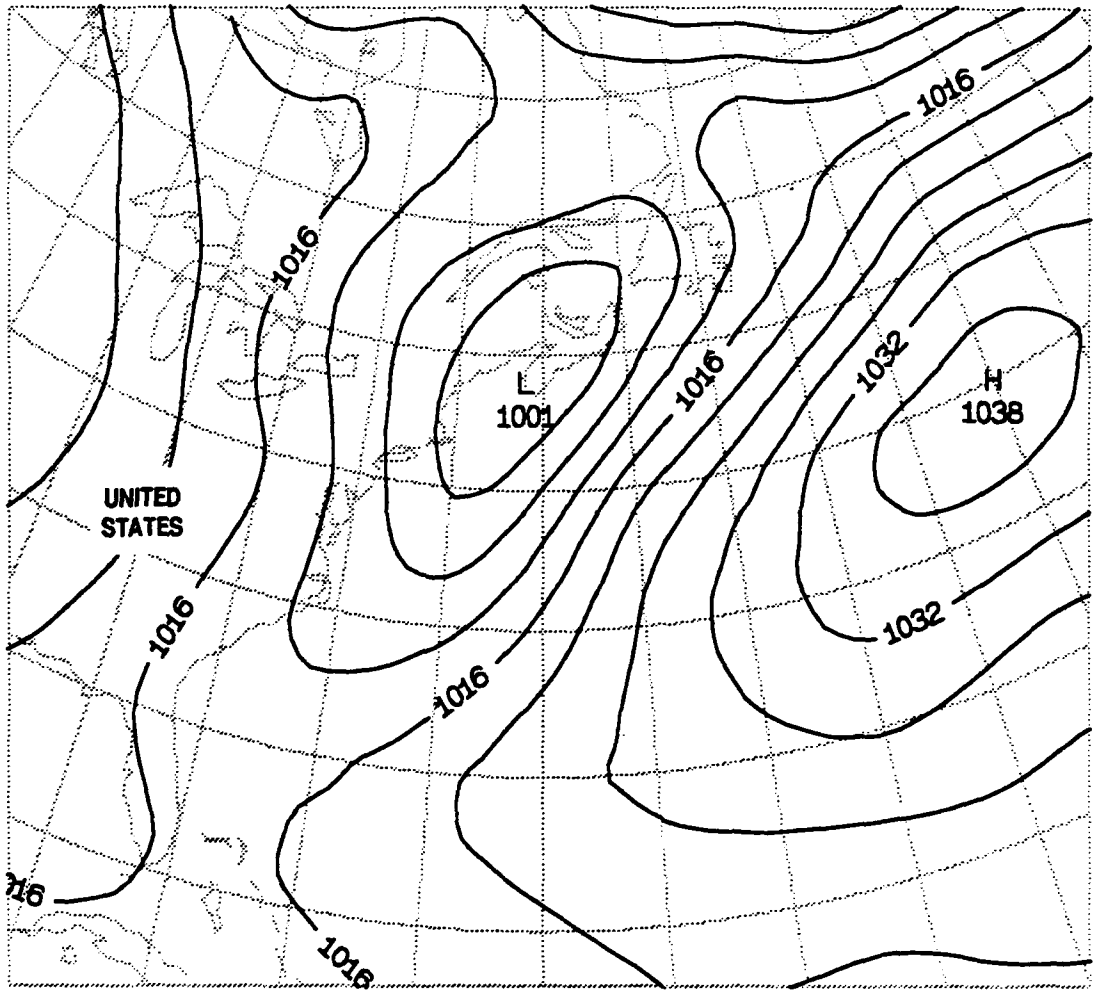
1016
1016
L
1001
1016
1032
H
1038
UNITED
STATES
1016
1032
1016
1016

Figure 43.
Grayshade display: SSM/I precipitable water analysis for 2300 UTC, 11 April 1990. Overlay: streamlines (black arrows) valid at 2200 UTC, 11 April 1990.

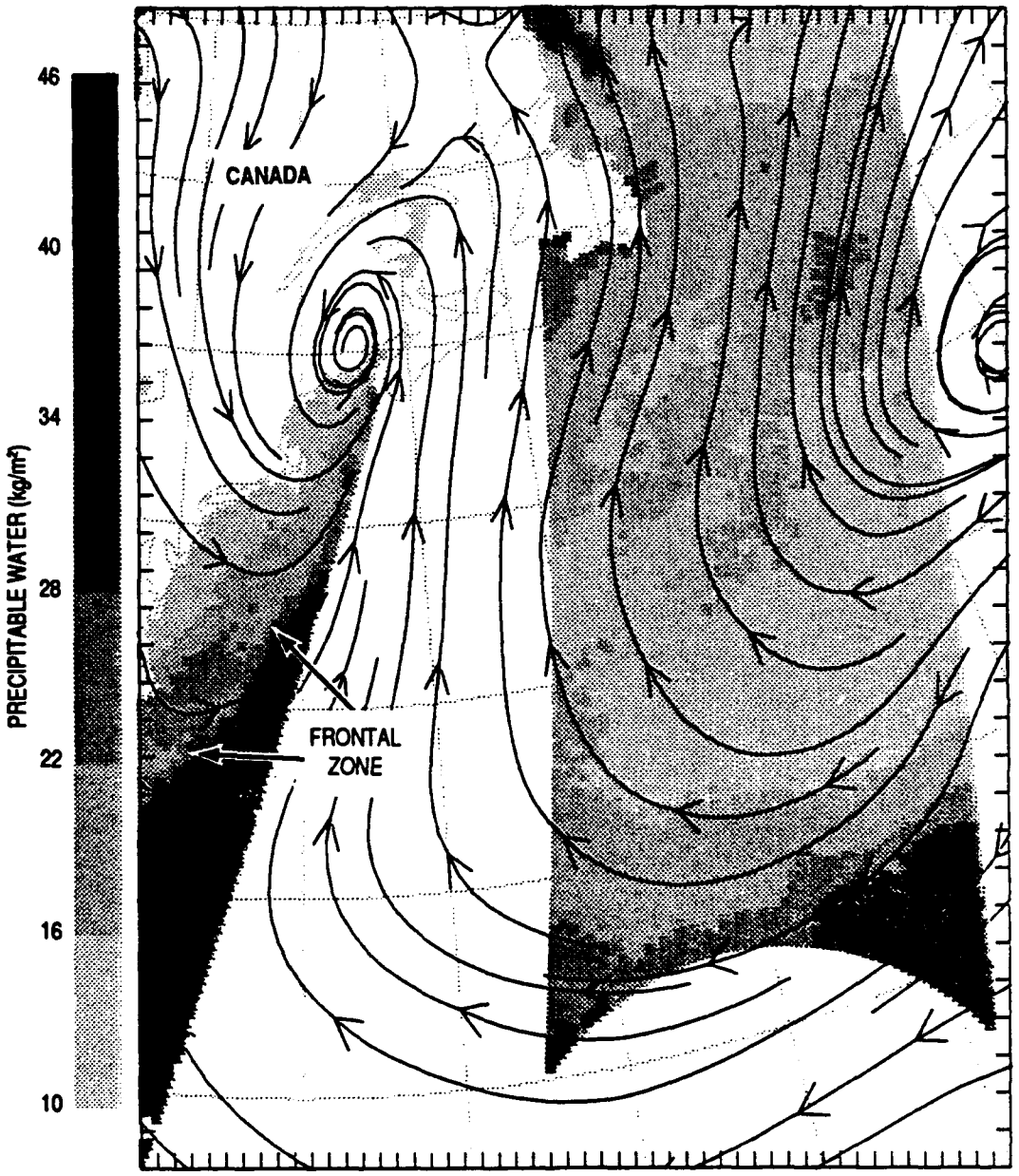
46
40
34
28
22
16
10
PRECIPITABLE WATER (kg/m²)
CANADA
FRONTAL
ZONE

Figure 44.
Grayshade display: SSM/I windspeed analysis for 2300 UTC, 11 April 1990. Overlay: streamlines (black arrows) valid at 2200 UTC, 11 April 1990.

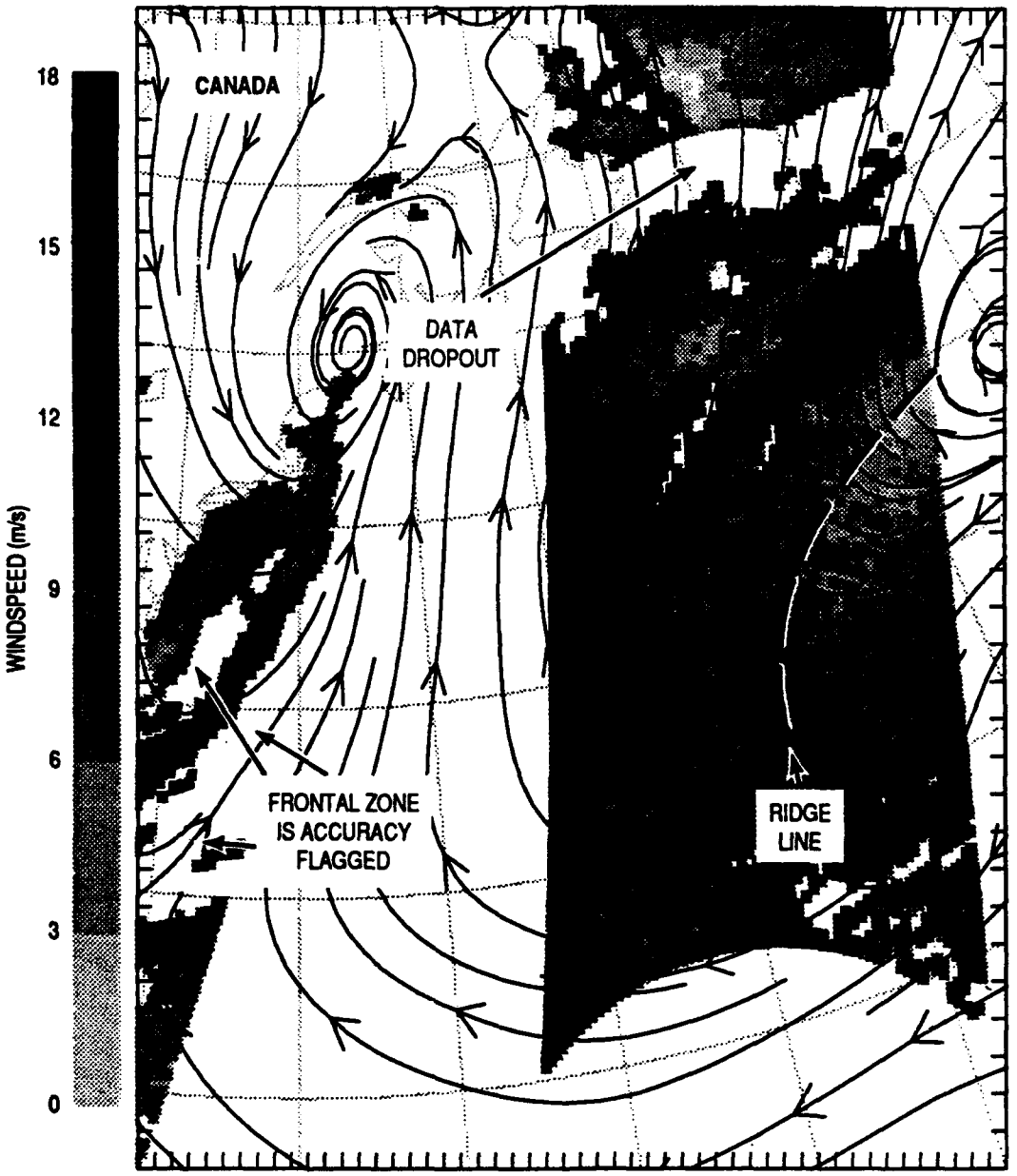
WINDSPEED (m/s)
18
15
12
9
6
3
0
CANADA
DATA
DROPOUT
FRONTAL ZONE
IS ACCURACY
FLAGGED
RIDGE
LINE

Figure 45.
Surface chart for 1200 UTC, 12 April 1990. Isobars drawn for every 4 mb.

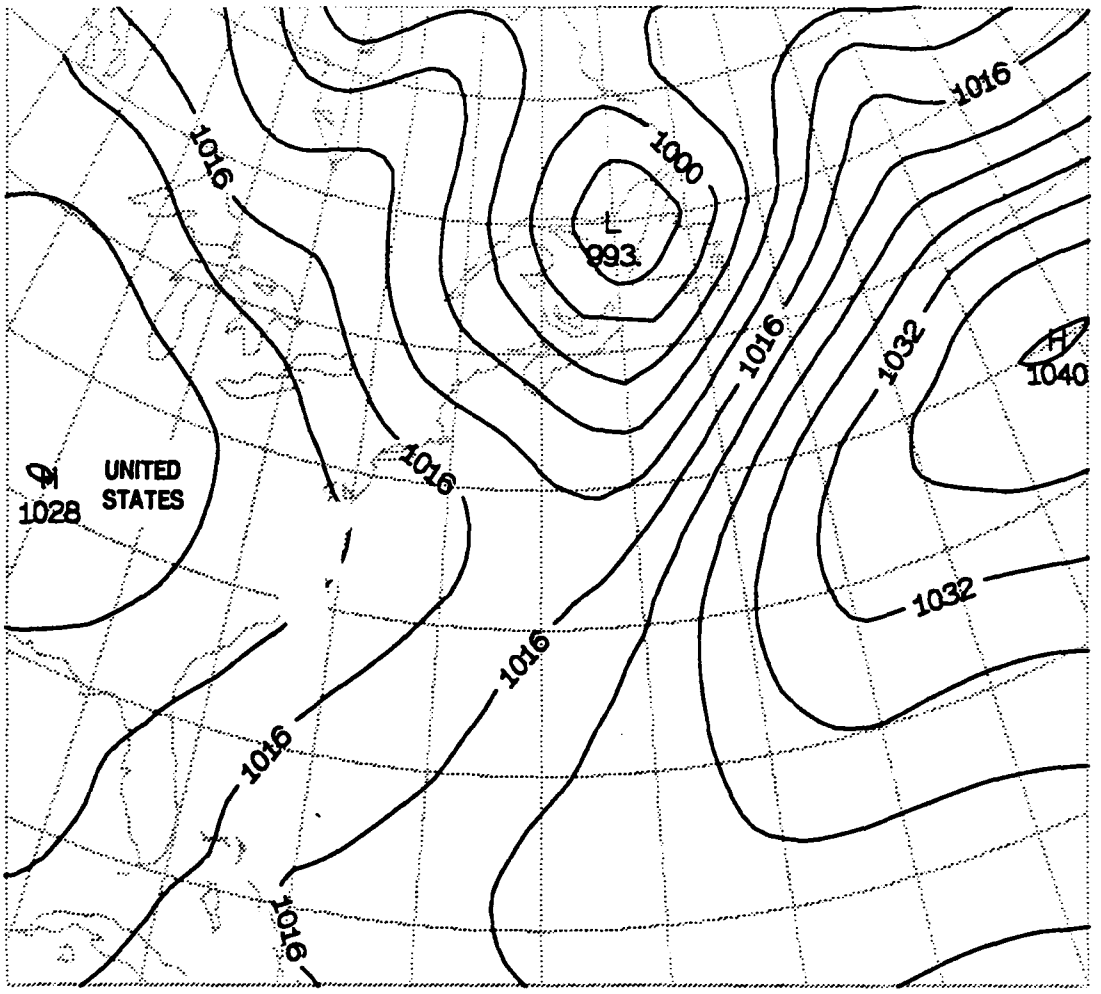
1016
1000
L
993
1016
1032
H
1040
1016
H
1028
UNITED
STATES
1016
1032
1016
1016
1016

Figure 46.
Grayshade display: SSM/I precipitable water analysis for 1100 UTC, 12 April 1990. Overlay: streamlines (black arrows) valid at 1200 UTC, 12 April 1990.

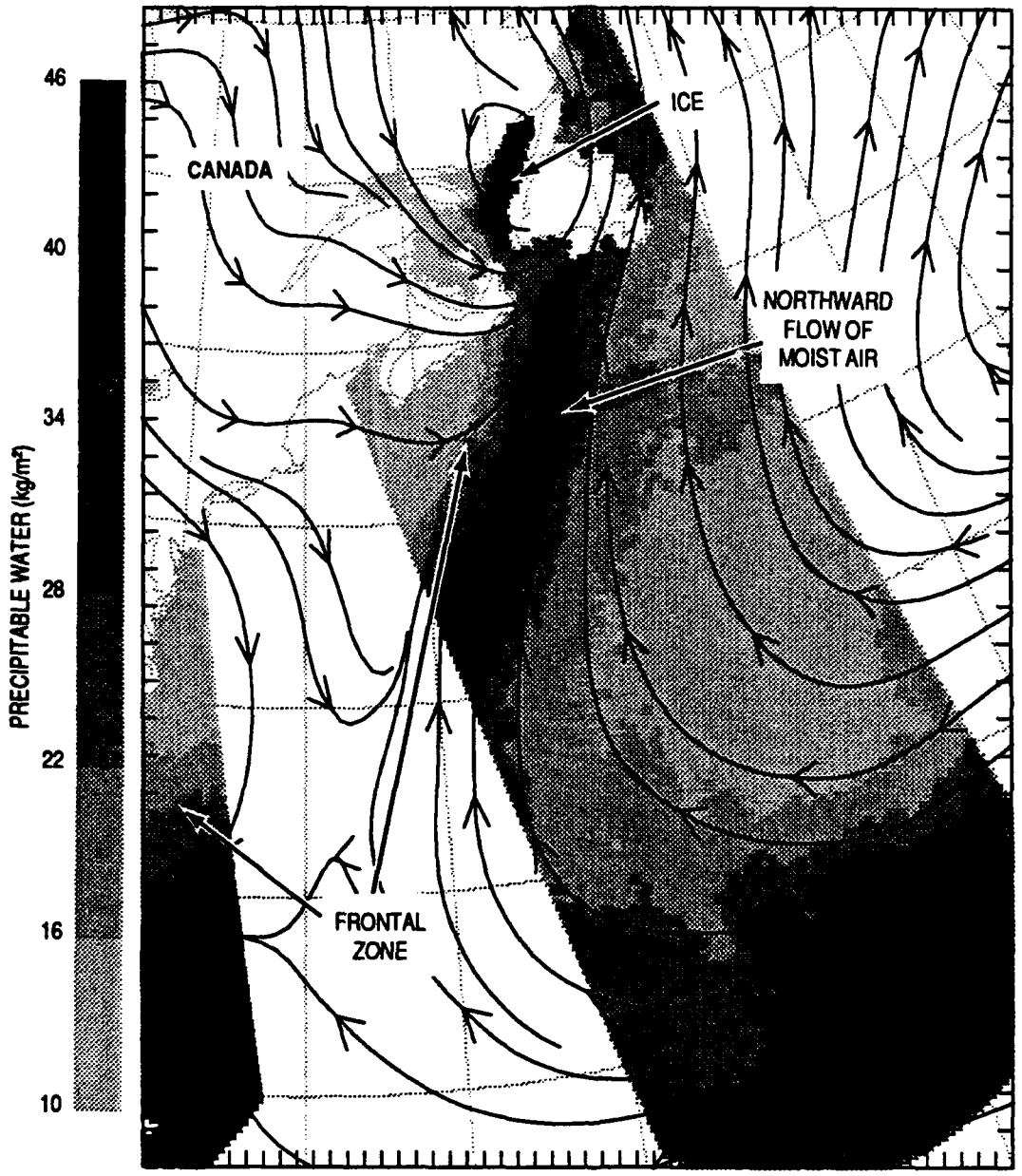
46
40
34
28
22
16
10
PRECIPITABLE WATER (kg/m²)
CANADA
ICE
NORTHWARD
FLOW OF
MOIST AIR
FRONTAL
ZONE

Figure 47.
SSM/I precipitation rate for 1100 UTC, 12 April 1990.

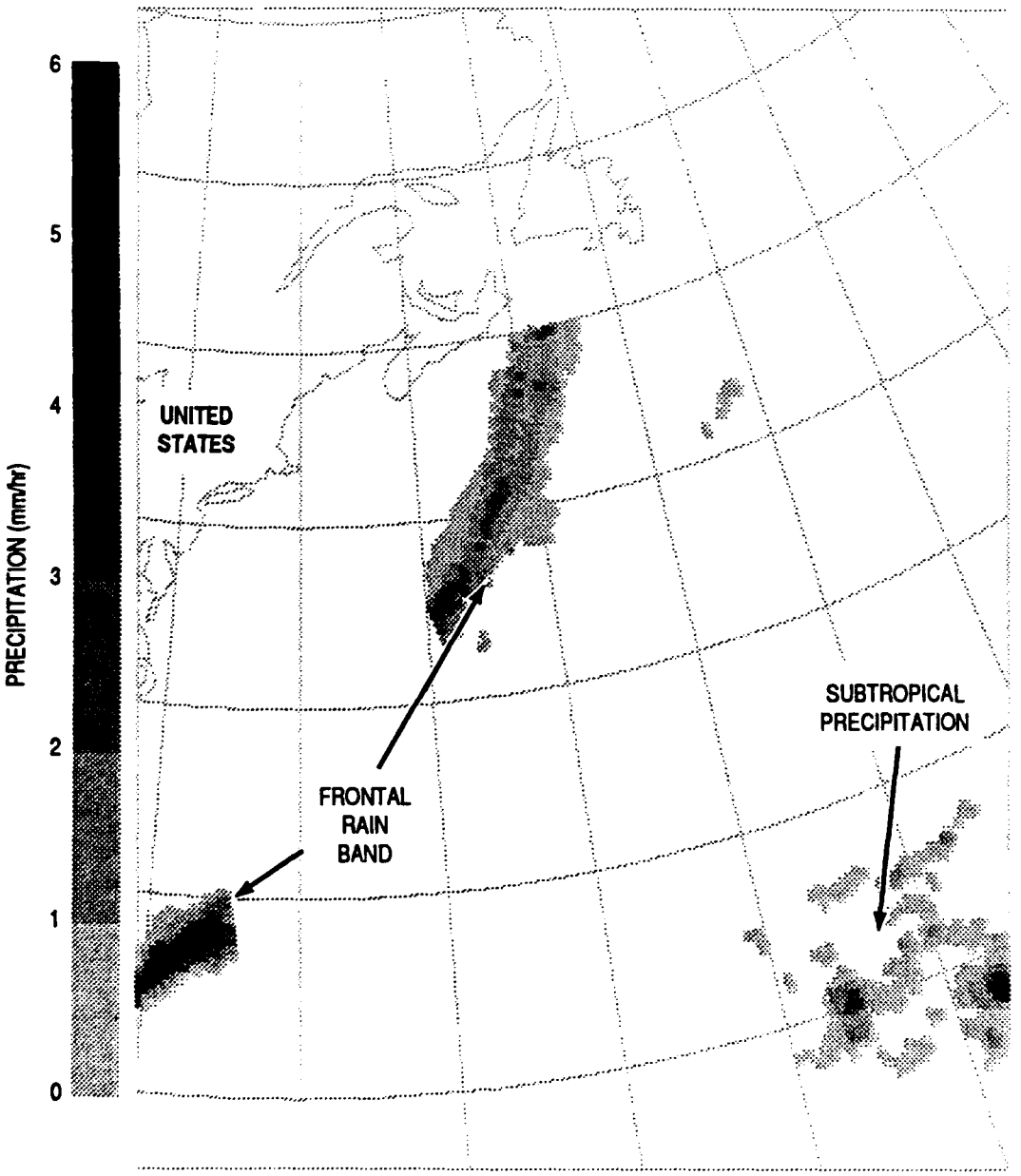
PRECIPITATION (mm/hr)
6
5
4
3
2
1
0
UNITED STATES
FRONTAL RAIN BAND
SUBTROPICAL PRECIPITATION

Figure 48.
Vertical motion for 1200 UTC, 12 April 1990. Contours drawn in units of microbars/second. Negative values indicate rising air at 700 mb; positive values indicate descending air at 700 mb.

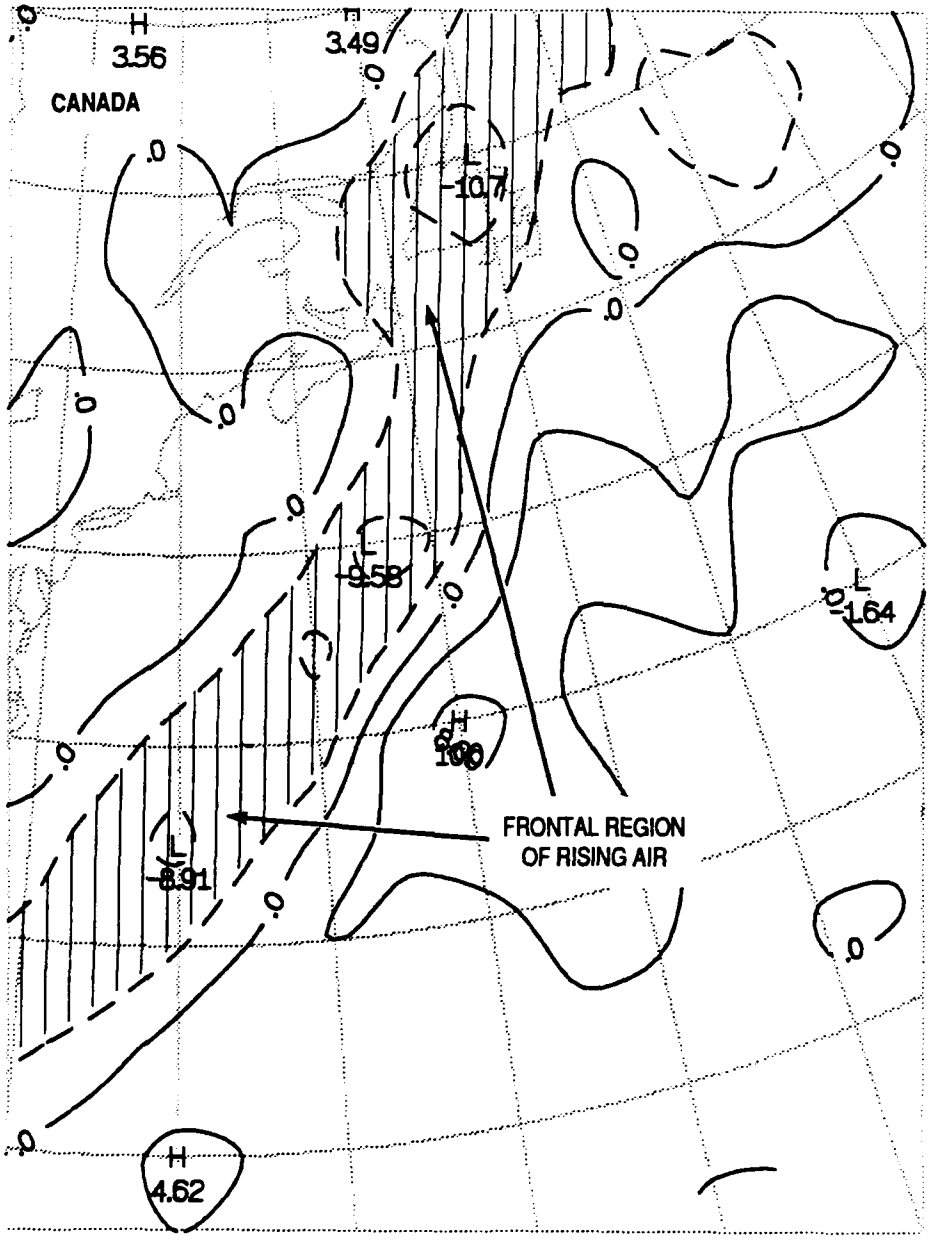
H
3.56
CANADA
H
3.49
L
-10.7
L
-9.58
L
-1.64
H
1.00
L
-8.91
H
4.62
FRONTAL REGION
OF RISING AIR

Figure 49.
Grayshade display: SSM/I precipitable water analysis for 1100 UTC, 12 April 1990. Overlay: NOGAPS isopleths of precipitable water (kg/m^2) valid at 1200 UTC, 12 April 1990.

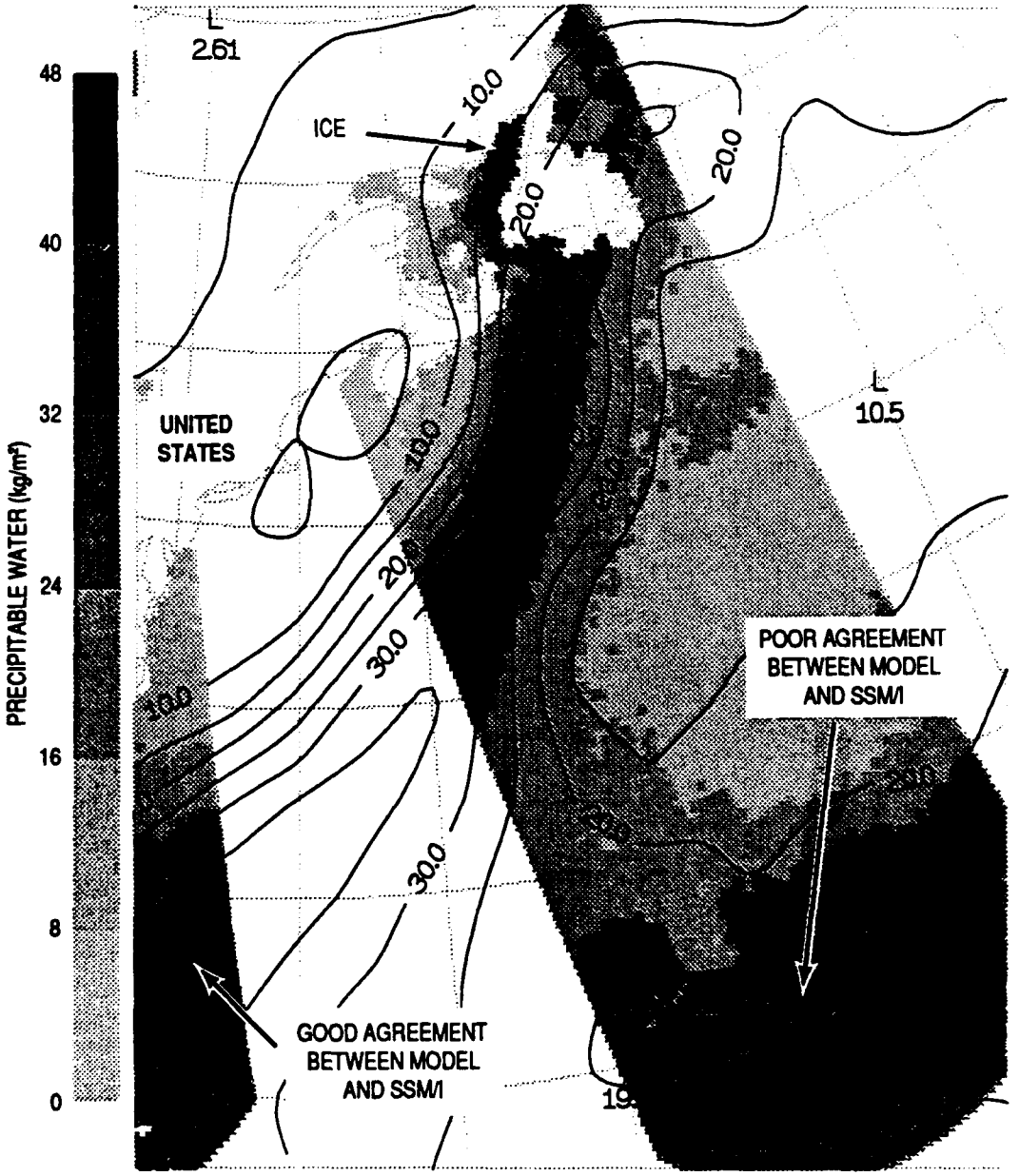
PRECIPITABLE WATER (kg/m²)
48
40
32
24
16
8
0
L
2.61
ICE
10.0
20.0
20.0
UNITED
STATES
L
10.5
10.0
20.0
30.0
10.0
POOR AGREEMENT
BETWEEN MODEL
AND SSM/I
30.0
GOOD AGREEMENT
BETWEEN MODEL
AND SSM/I

Figure 50.
Grayshade display: SSM/I windspeed water analysis for 1100 UTC, 12 April 1990. Overlay: streamlines (black arrows) valid at 1200 UTC, 12 April 1990.

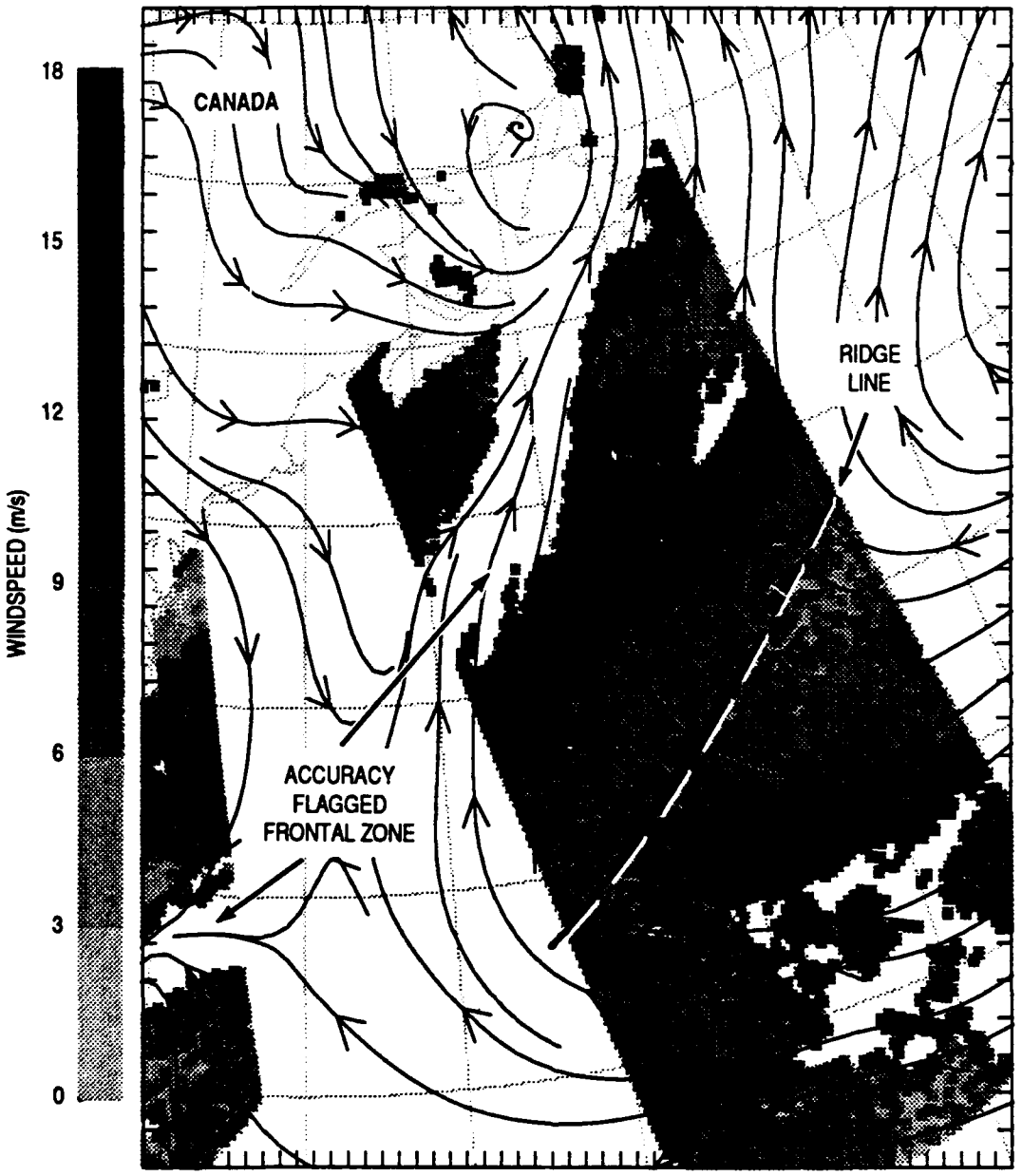
WINDSPEED (m/s)
18
15
12
9
6
3
0
CANADA
RIDGE
LINE
ACCURACY
FLAGGED
FRONTAL ZONE

Figure 51.
Topographic map of study area shown in Figs. 52–55.

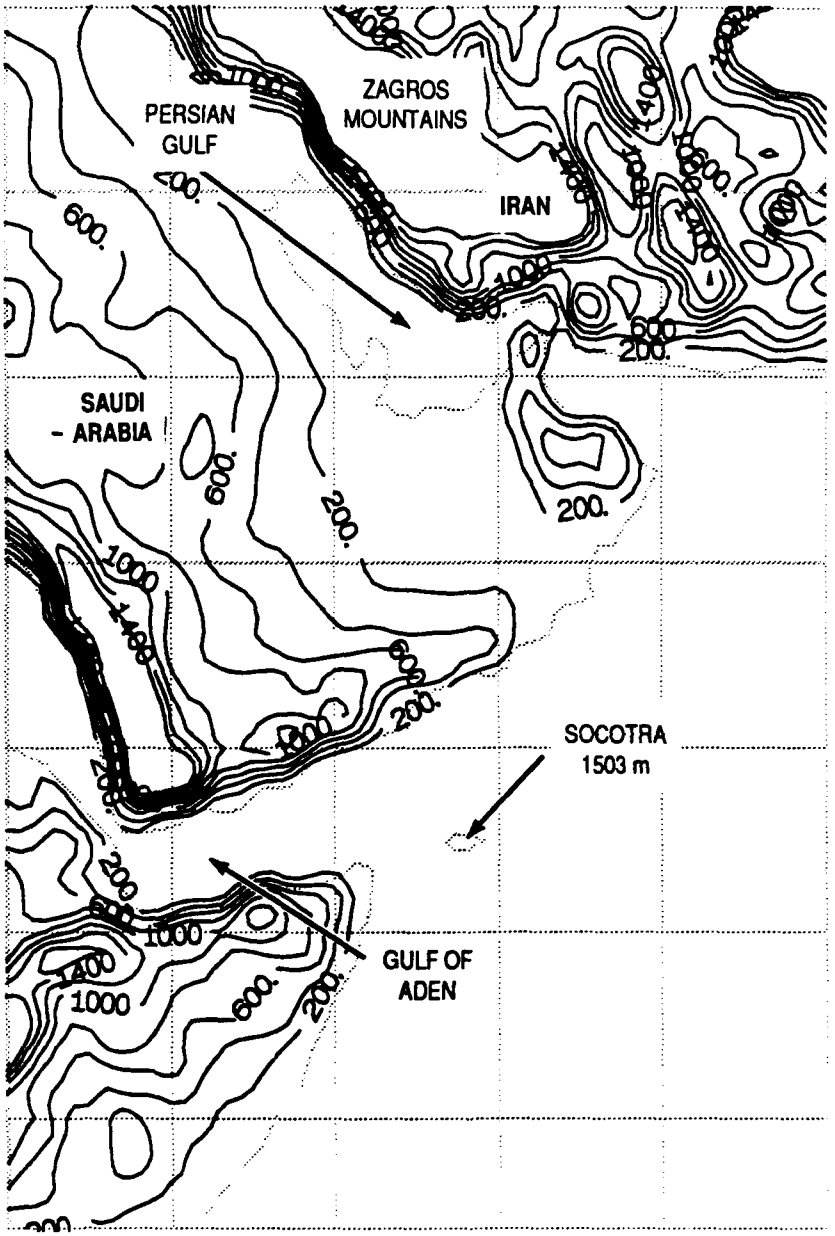
PERSIAN
GULF
ZAGROS
MOUNTAINS
IRAN
SAUDI
- ARABIA
SOCOTRA
1503 m
GULF OF
ADEN

Figure 52.
Grayshade display: SSM/I windspeed analysis for 0240 UTC, 2 October 1990. Overlay: streamlines (black arrows) valid at 0300 UTC, 2 October 1990.

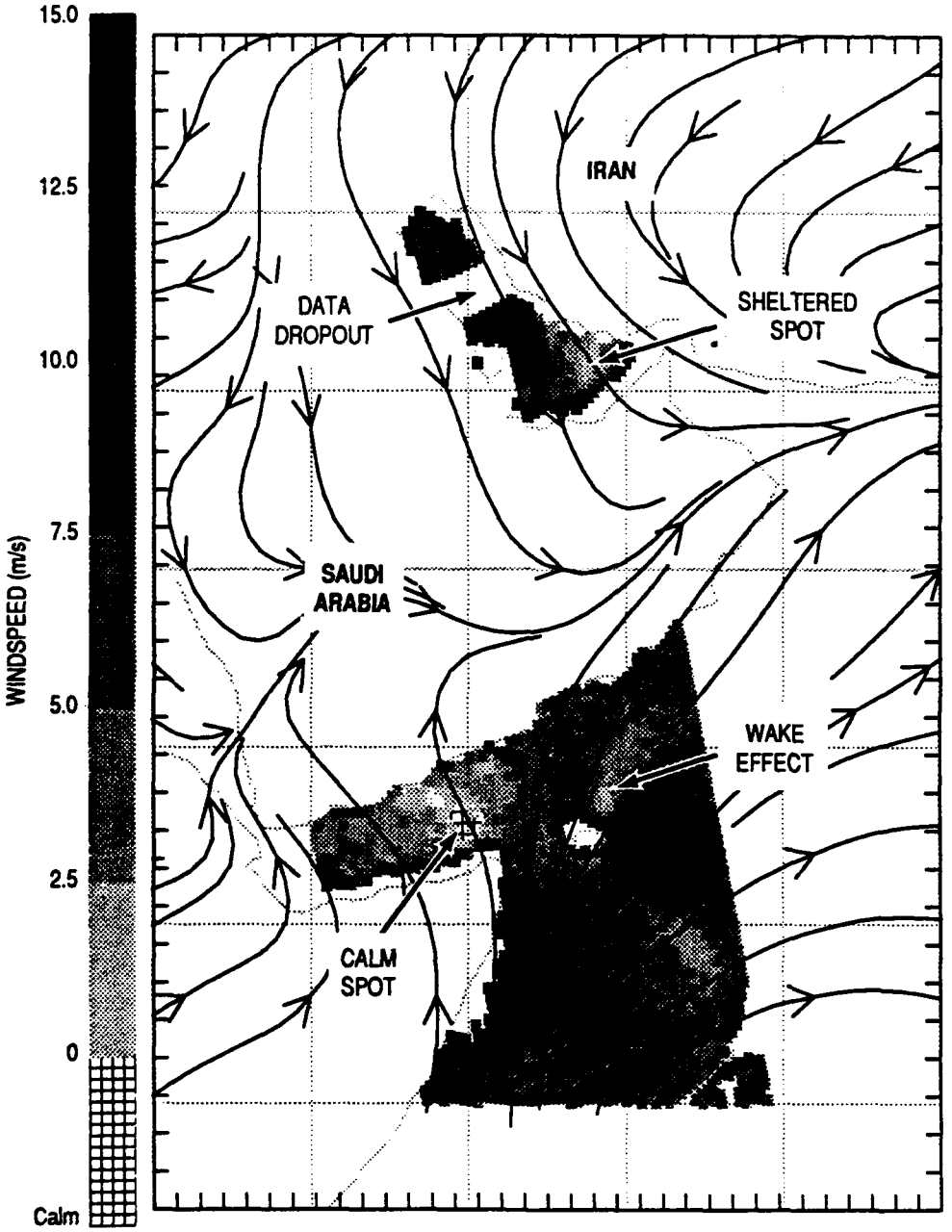
15.0
12.5
10.0
7.5
5.0
2.5
0
Calm
WINDSPEED (m/s)
IRAN
DATA
DROPOUT
SHELTERED
SPOT
SAUDI
ARABIA
WAKE
EFFECT
CALM
SPOT

Figure 53.
Grayshade display: SSM/I windspeed analysis for 1520 UTC, 2 October 1990. Overlay: streamlines (black arrows) valid at 1500 UTC, 2 October 1990.

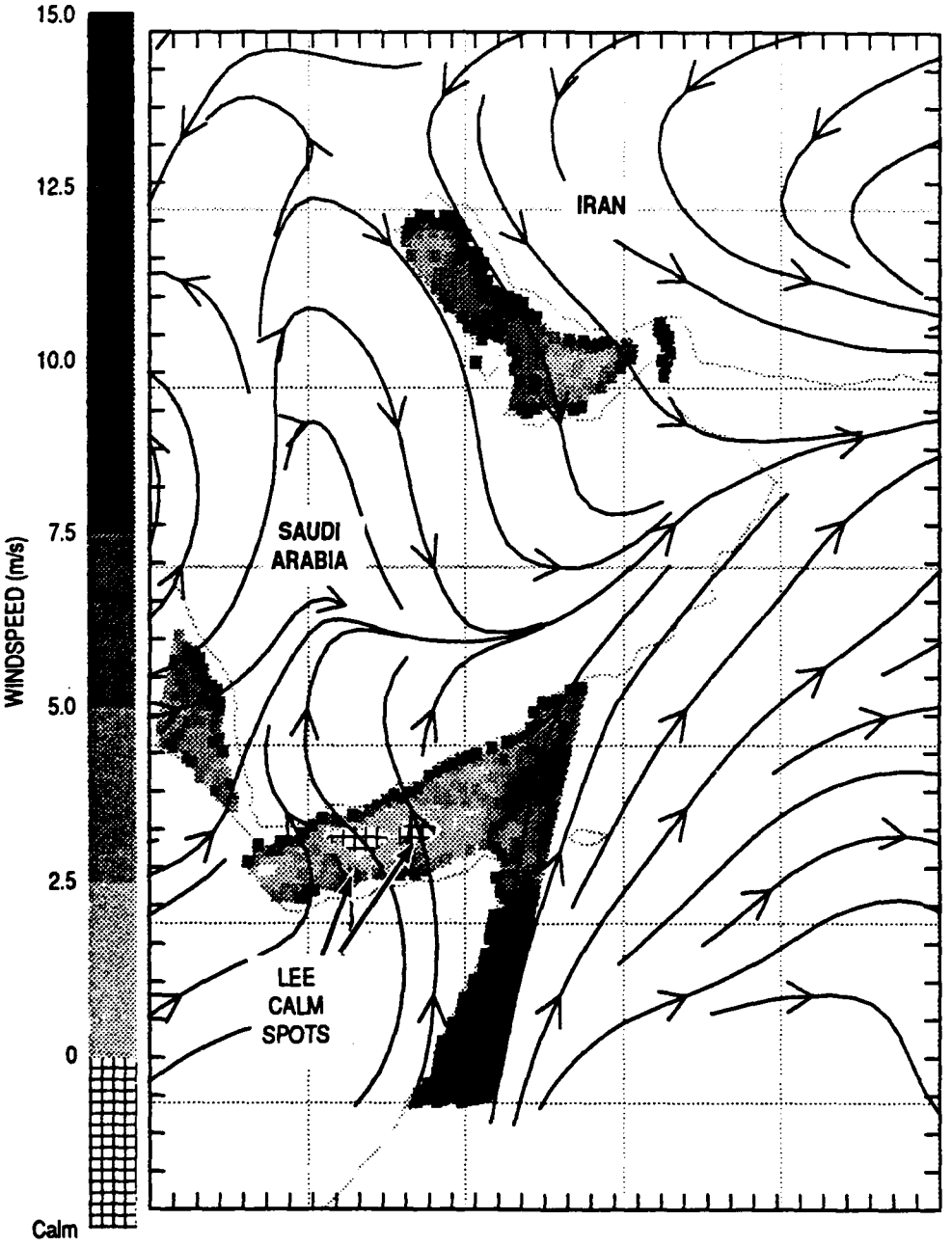
15.0
12.5
10.0
7.5
5.0
2.5
0
Calm
WINDSPEED (m/s)
IRAN
SAUDI
ARABIA
LEE
CALM
SPOTS

Figure 54.
Grayshade display: SSM/I windspeed analysis for 0225 UTC, 3 October 1990. Overlay: streamlines (black arrows) valid at 0300 UTC, 3 October 1990.

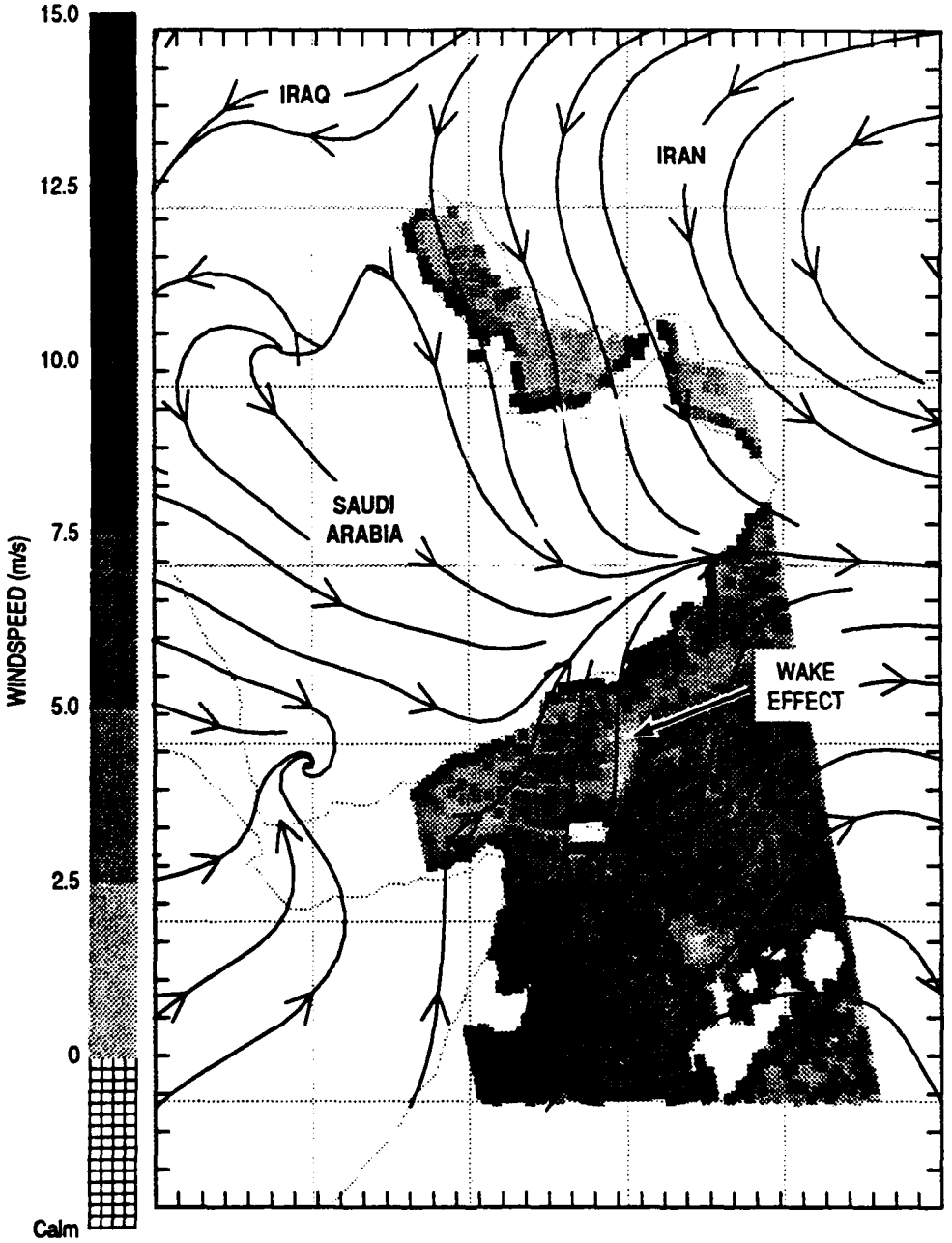
15.0
12.5
10.0
7.5
5.0
2.5
0
Calm
WINDSPEED (m/s)
IRAQ
IRAN
SAUDI
ARABIA
WAKE
EFFECT

Figure 55.
Grayshade display: SSM/I windspeed analysis for 1501 UTC, 3 October 1990. Overlay: streamlines (black arrows) valid at 1500 UTC, 3 October 1990.

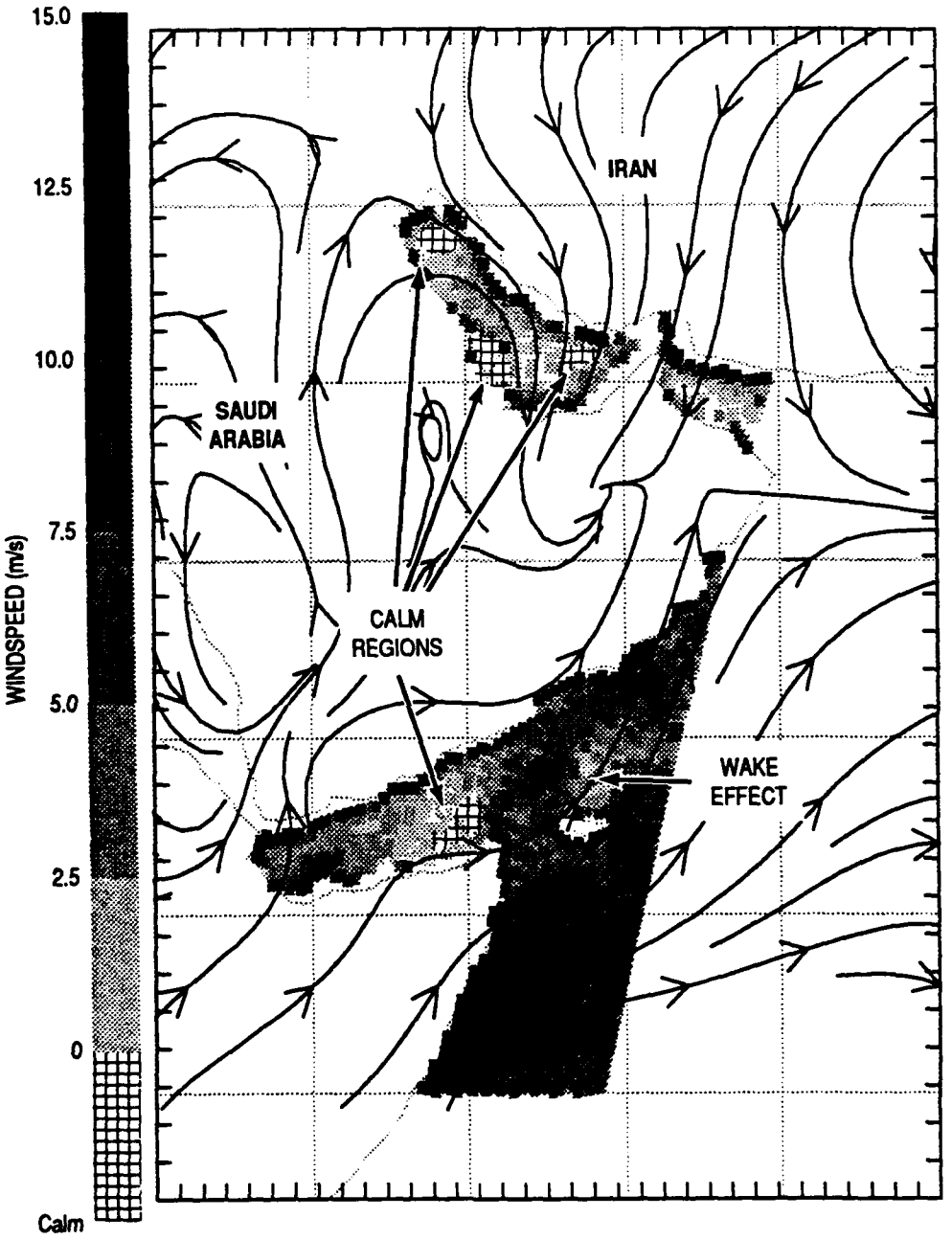
15.0
12.5
10.0
7.5
5.0
2.5
0
Calm
WINDSPEED (m/s)
IRAN
SAUDI ARABIA
CALM REGIONS
WAKE EFFECT

DISCLAIMER NOTICE

THIS DOCUMENT IS BEST QUALITY AVAILABLE. THE COPY FURNISHED TO DTIC CONTAINED A SIGNIFICANT NUMBER OF COLOR PAGES WHICH DO NOT REPRODUCE LEGIBLY ON BLACK AND WHITE MICROFICHE.